UNIVERSITY OF OSLO
Department of Geosciences

A tale of two damaging convective storms during the record-breaking Norwegian summer of 2014

Master thesis in Geosciences
Meteorology and oceanography

Charalampos Sarchosidis

2nd May 2017

Abstract

Two cases of severe thunderstorms that impacted the Oslo area have been investigated. The thunderstorms occurred during the summer of 2014, an extraordinary summer with record high temperatures, number of lightning strikes and amount of short-term precipitation. The thunderstorm on 26 June produced precipitation amounts of 44.5 mm in one hour and 72.8 mm in 24 hours, both records. It was short-lived in both time and space. The other thunderstorm on 4 August was part of a large organized convective system that traveled from southern Sweden to northern Norway, lasting 15 hours in total.

Even though both thunderstorms were intense, the dynamical processes leading to their formation and evolution were starkly different. The necessary ingredients for deep convection are sufficient moisture, conditional instability and a so-called triggering mechanism. An in-depth synoptic scale analysis utilizing maps of the large scale flow, Lagrangian backward trajectories and stability indices is conducted for both cases to better understand how these necessary ingredients were met and their respective roles in the observed deep convection.

The June case was characterized by large-scale persistent northerly flow associated with an occluding cyclone east of Norway and high pressure to the west. The flow pattern resulted in significant cold air advection and a suppressed tropopause (upper level cold anomaly). Meager amounts of moisture were found in this case, albeit with a local maximum in the thunderstorm region. Additionally, no synoptic scale triggering mechanism was present. The trajectory and stability index analyses indicate the primary cause of the thunderstorm was a steep vertical temperature lapse rate resulting from local surface heating and the large-scale upper-level cold anomaly. The surface heating on the day of the event was sufficient to create positively buoyant air parcels, thereby triggering the deep convection.

The August case provides a remarkable contrast. The large scale flow characterized by low pressure to the west and high pressure to the east of Norway resulted in significant warm, moist advection and an elevated tropopause. The trajectory analysis points to two moisture regions: the Atlantic ocean and over the Baltic. The combination of anomalously high surface temperatures and moisture content led to large values of conditional instability as evidenced in the stability index analysis. Associated with a low pressure center over Great Britain, a frontal boundary draped over western Norway on the day of the event providing a triggering mechanism. The large scale (in time and space) nature of the organized convective system can be tied to the presence of significant vertical wind shear associated with low-level baroclinicity (i.e. the front).

This study of two distinctly different cases of intense deep convection illustrates the utility of combining an understanding of the large scale flow pattern over the days prior to a convective event and the local scale conditions with respect to the necessary conditions for deep convection. Lagrangian analyses and stability indices were found to be valuable tools for the assessment of both

events, tools that are available in a forecast framework.

Acknowledgements

I want to thank Jón Egill Kristjánsson, first of all, for letting me actually *choose* a thesis within a subject I really love - thunderstorms. My wish was granted after he and Bjørn Røsting talked and came up with this thesis you are about to read. So many thanks to Bjørn as well.
Few months after being handed the master thesis subject, I discovered Richard Moore, who was about to teach the new amazing course "Weather Systems". I loved the course, so I had to ask and I am very thankful that he agreed to help me with my thesis. Both professors have been amazing to me.

I also want to thank Rich for being there for me after the tragic event that happened on August 2016. The loss of Jón Egill was a loss that affected not only us at MetOs, but the worldwide meteorological community. MetOs will never be the same without him. He showed his genuine love for the students and his passion for meteorology by passing along his own knowledge. What I loved the most about his way of teaching was that he never served a ready answer to a student's question. If someone asked "Why does this happen?" then he would fire back "Why do *you* think this happen?" and in the end get the student to answer their own question. Jón Egill will be dearly missed, but always remembered.

Another person that deserves many thanks is Anne Claire Fouilloux. She always manages to amaze me with her programming knowledge and has helped me with everything data related. She has gotten so many mails from me and has helped me so much that it would even seem appropriate to list her as a third supervisor. We, students would not be able to make it through our studies without her.

A big thank you to all of the people at the Norwegian Meteorological Institute that have helped me and provided me with lots of useful and fun data. I owe thanks to Laila Fodnes Sidselrud, Snorre Stavik Rønning, Trygve Aspenes, Morten Andreas Ødegaard Køltzow, Jan-Inge Hansen, Vibeke Wauters Thyness, Erling Bernhardsen and my friends at the climate division.

Lastly, thanks to everyone at MetOs. I am going to miss the friendly and family-like environment we have. Students and professors alike, have all been amazing.

And of course, I need to thank both my Greek and Norwegian family for supporting me.

Oslo, 2nd May 2017
Charalampos Sarchosidis

Contents

Chapter 1

Introduction

1.1 Summer 2014

Summer 2014: A summer that is remembered by all Norwegians as the perfect one. A record breaking season with both extremely high temperatures and amounts of precipitation.
Summer 2014 stands out as one of the hottest summers in Norway. It began with relatively warm and fair weather but the northern part of the country was experiencing snowfalls in early June. June was drier than normal, but during the last week of the month several events of a convective nature affected southern Norway accompanied with hail causing significant damages. The most notable events were multiple funnel clouds outside of Arendal on the 24th of June and the extreme precipitation recorded in Oslo on the 26th. The latter event represents one of the two cases analyzed in this thesis.

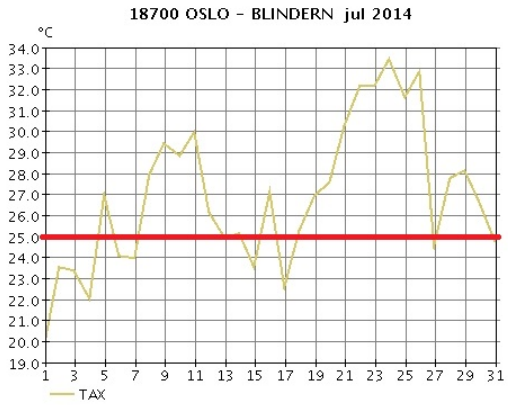

Figure 1.1: The maximum temperature observed by the weather station at Oslo - Blindern for July. A red line is drawn along the 25 °C value to showcase the large number of days with high maximum temperature.

July was the hottest month in the summer of 2014. The monthly mean temperature in Norway was 4.3 °C above normal. The highest temperature was measured in Gulsvik, Buskerud with 34.5 °C on July the 23th. Oslo - Blindern was close to reaching 34 °C the same day - 33.4 °C was measured which is a July record. Concomitant with the anomalously warm temperatures, afternoon thunderstorms were a common sight in eastern Norway. This was the case especially in the mainland of central and eastern Norway where weather stations observed monthly precipitation twice the average for July.
The warm weather continued throughout August, with convective systems dominating in South Norway. A specific event that received media attention was a severe convective system coming from Sweden on August the 4th, causing serious damage along its path. It lasted for many hours and survived all the way up to northern Norway. This is the other case that will be discussed in

this thesis.

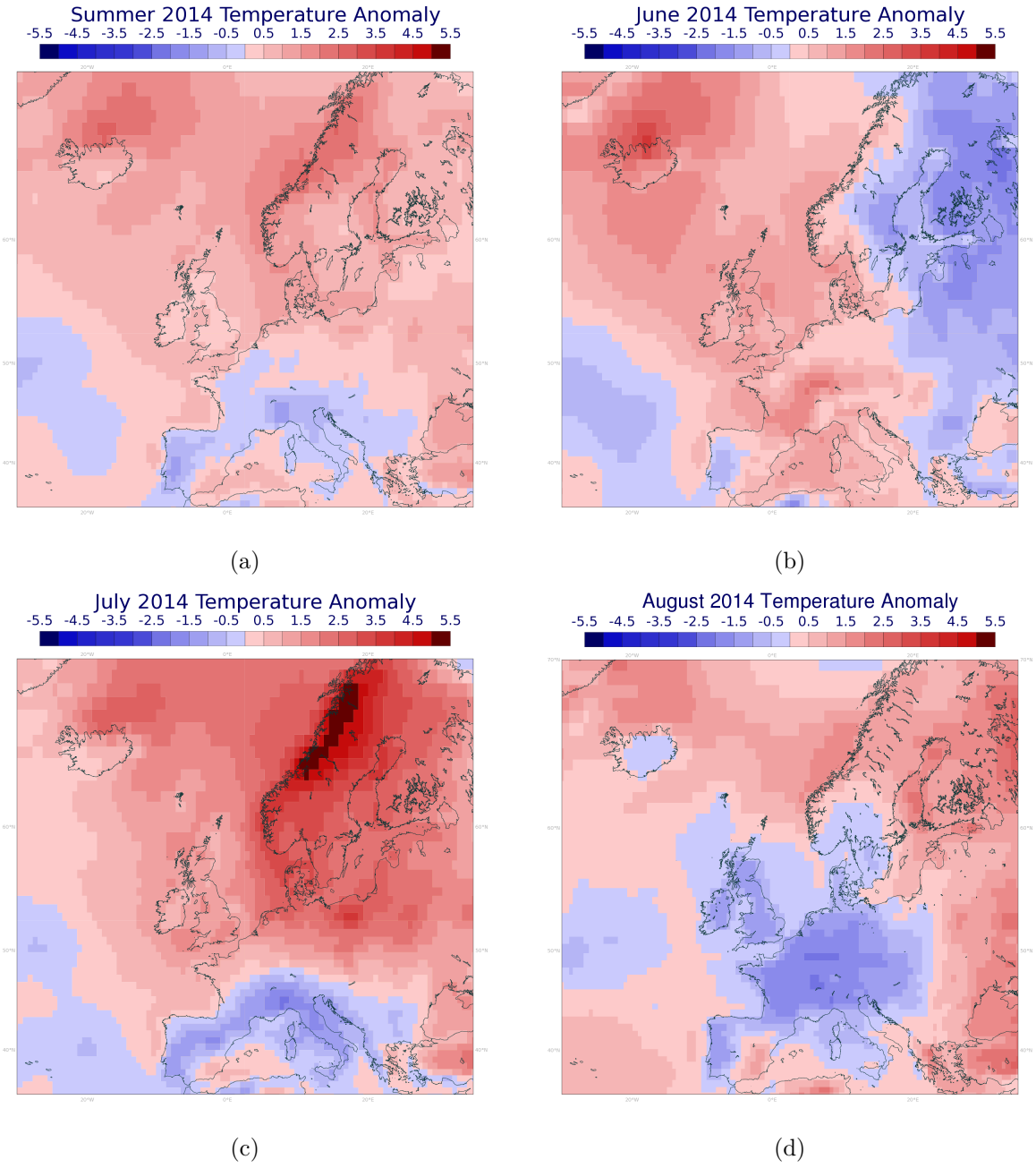

Figure 1.2: 2m temperature anomaly calculated with ERA-INTERIM for (a) all three summer months, (b) June, (c) July and (d) August compared to the average 2m temperature of the same months in the period of 1979 - 2015. The units are in °C.

A few more statistics follow to showcase the rarity of this warm summer, always based on the Norwegian Meteorological Institute's database. During the summer of 2014 at Oslo - Blindern, there were 69 days with temperature higher than 20°C and 31 days higher than 25 °C. The records are 78 days with T>20 °C in 2006 and 39 with T>25 °C in 1997. The whole summer of 2014 was 1.9 °C warmer than normal in entire Norway.

It was not just the precipitation and temperature that was impressive during the summer of 2014. It was a record-breaking year for electric activity as well. According to SINTEF, 2.7 million lightning strikes were registered between 1 January and 1 November. There were five times more lightning strikes registered in 2014 than in an average year (SINTEF, 2015). The maximum number of 24-hour lightning strikes, 178663, was recorded on 4 August, one of the two days that will be examined in this thesis (SINTEF, 2014). Another notable date in 2014 in regards to thunderstorms is the night of 9-10 October (Lindgren *et al.*, 2014). The whole coastline of South Norway from Fredrikshavn in the east to Stavanger in the west suffered from intense and consistent thunderstorms for several hours causing floods and damages. More than 10000 lightings strikes were registered, a phenomenon uncommon even for the summer season. So not only is the number of lightning strikes impressive, but also the longevity of that year's thunderstorm season. Perhaps the warm sea, after a hot summer, helped to extend the thunderstorm season of 2014 (Olsson & Stensholt, 2014).
Anomalous temperatures were recorded throughout Europe during the summer of 2014. Figure 1.2 shows the anomaly in 2m temperature for all summer months compared to the same summer months in the period of 1979-2015. A dipole structure is evident, with warm (cold) temperature anomalies in northern (southern) Europe. Cold anomalies in southern Europe exceeded 1 °C for the whole summer and 2.5 °C in July.

Figure 1.3: Photo taken by Alf J. Altenborg on 24 June 2014 near Arendal, showing three of the multiple waterspouts that formed out in the sea.

1.2 Overview of two convective events

1.2.1 June 26

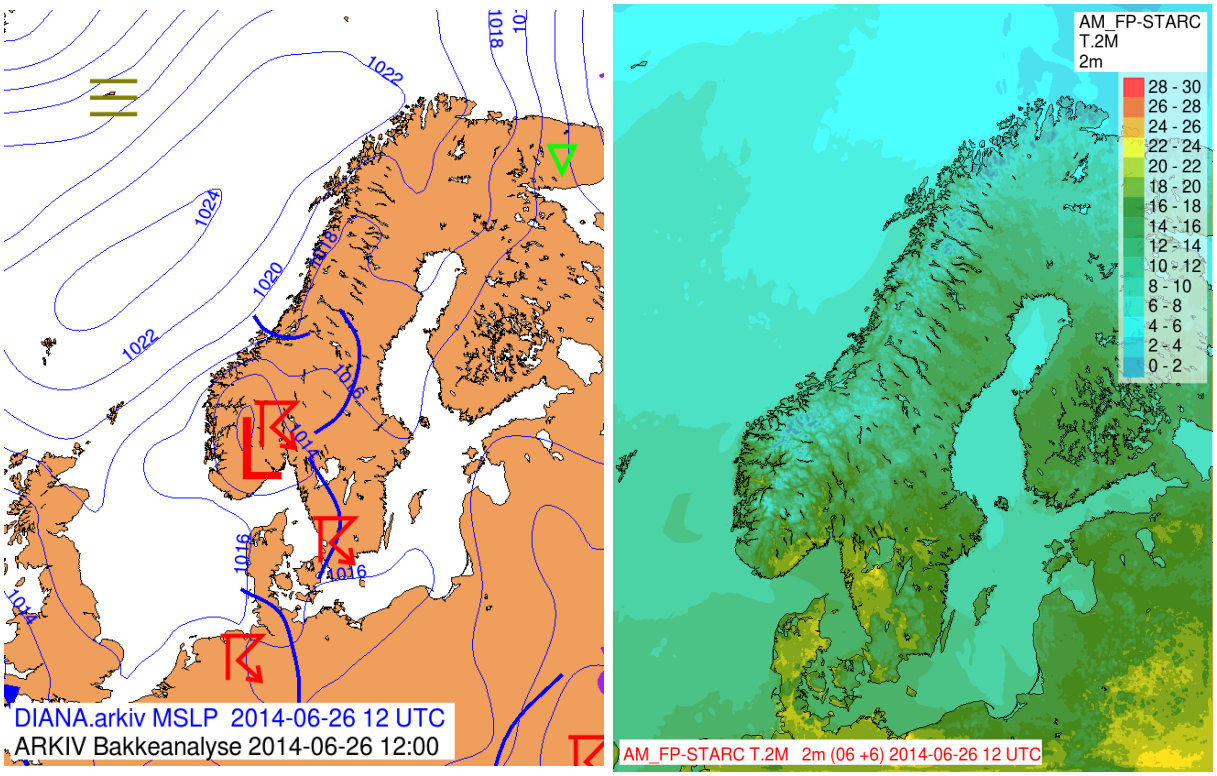

Figure 1.4: Figures showing a forecaster's subjective analysis map to the left and temperature at 2 meters (in °C) to the right for 26 June 2014 12 UTC. Bold blue lines in the analysis map indicate the presence of showers while the R-symbols indicate the presence of thunderstorms. Pressure systems, pressure fields and fronts are plotted as well.

June 26 began calm with scattered cumulus clouds and a normal temperature. The maximum temperature at Oslo - Blidern reached 19 °C, and 22 °C was recorded in southern and eastern Norway. As the day progressed, the scattered cumulus clouds developed into larger convective cells in Østlandet. In Figure 1.4 there are observations of thunderstorm activity at 12 UTC in eastern Norway and a local low pressure is positioned above South Norway according to the forecaster's analysis. A vigorous thunderstorm impacted Oslo. The extreme precipitation broke the record of both hourly and daily precipitation. Daily precipitation accumulation of 72.8 mm was measured at Oslo - Blindern, with 44.5 mm occurring in a single hour (between 14 and 15 UTC.) The average precipitation for June at Oslo-Blindern is 65 mm, and the total for June 2014 was 110.5 mm, 170% of the average. As such, the 24-hour accumulation on 26 June alone exceeded the average monthly precipitation.
The small-scale nature of the intense rainfall is also noteworthy. In Asker, 20 km west of Blindern, the precipitation for 26 June was 9.3 mm and the month's total was 66.1 mm. The 24-hour accumulated precipitation is presented in Figure 1.6. The precipitation pattern illustrates just how local the rainfall was and the large variability in precipitation amount in the Oslo area.

The convective cell dissipated quickly, with the intense rainfall transitioning to stratiform precipitation within an hour and a cessation of lightning activity. This autumn-like rainfall continued until midnight with lower temperatures.

Figure 1.5: Photo taken by Charalampos Sarchosidis at Ullevål looking southwards at 12:08 UTC. Old cells are seen in the background and new developing in the front.

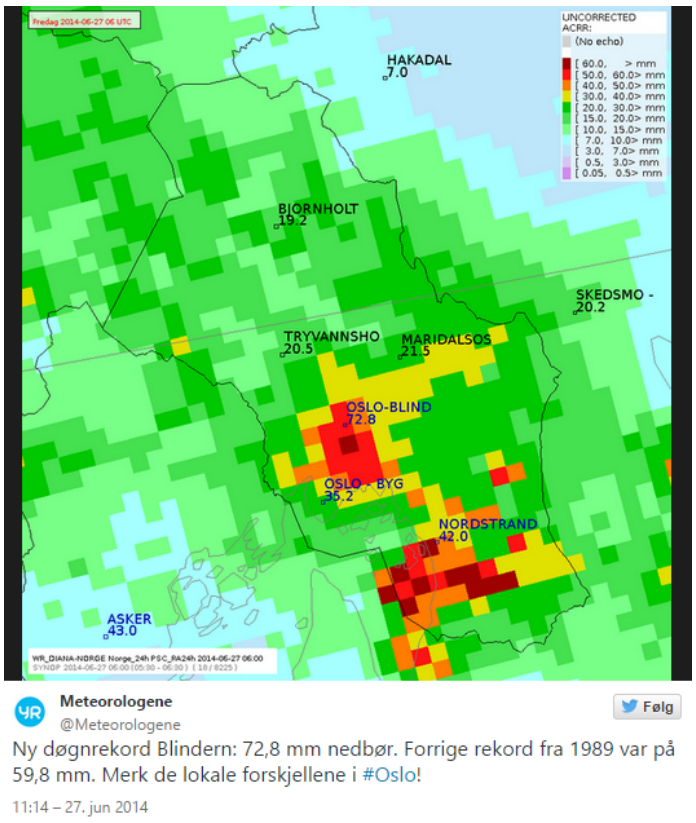

Meteorologene
@Meteorologene
Følg

Ny døgnrekord Blindern: 72,8 mm nedbør. Forrige rekord fra 1989 var på 59,8 mm. Merk de lokale forskjellene i #Oslo!

11:14 – 27. jun 2014

Figure 1.6: Picture from the Norwegian Meteorological Institute's twitter account showing the total precipitation accumulated between 26 June 06 UTC and 27 June 06 UTC over Oslo.

1.2.2 August 4

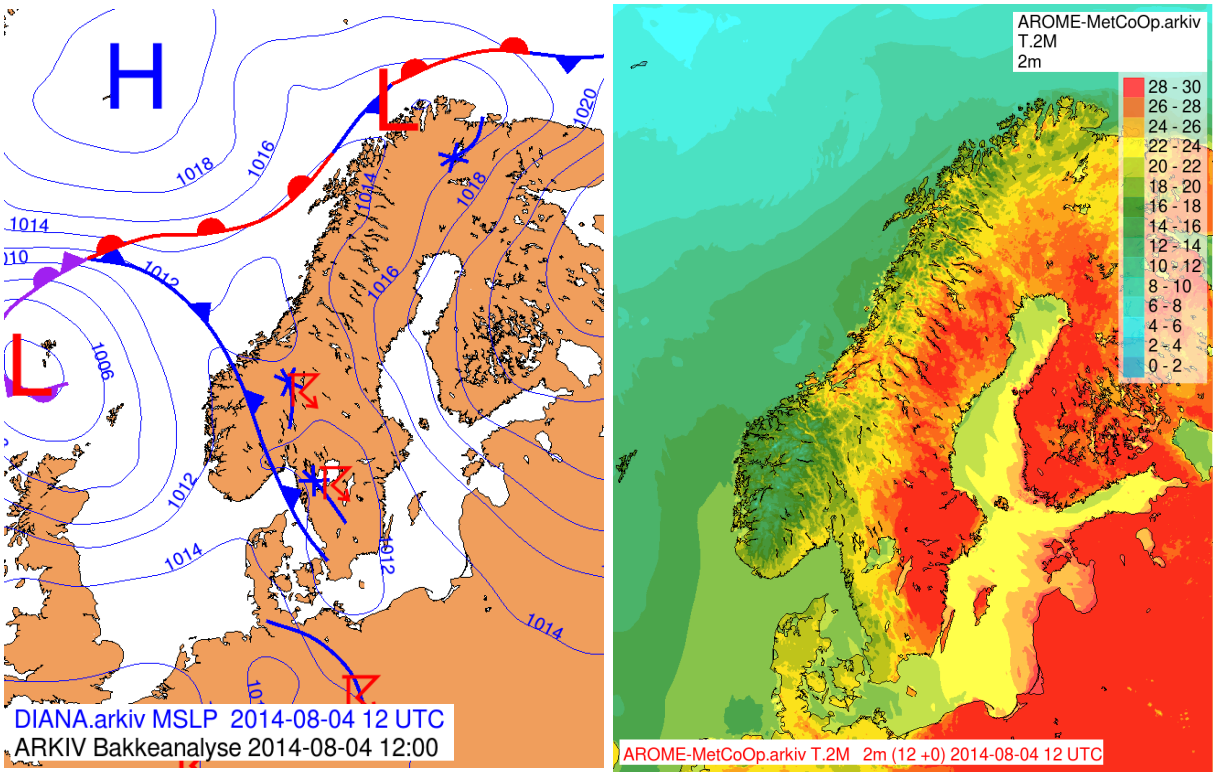

Figure 1.7: Figures showing a forecaster's subjective analysis map to the left and temperature at 2 meters (in °C) to the right for 4 August 2014 12 UTC. Bold blue lines in the analysis map indicate the presence of showers while the R-symbols indicate the presence of thunderstorms. Pressure systems, pressure fields and fronts are plotted as well.

After an anomalously warm July, the first days of August continued with temperatures above 20 °C in southern Norway. In association with a low pressure in the vicinity of Great Britain, many convective cells were observed over northern Europe. The date of interest for this thesis is 4 August 2014. In contrast to the 26 June case described above, the August event was of a much larger time and spatial scale. In the analysis map we can see the mentioned low pressure still being close to Great Britain at 12 UTC and its accompanying cold front destabilizing the atmosphere and creating in turn multiple thunderstorms in southern Scandinavia. The temperatures in eastern Scandinavia are worth mentioning, which reached around 35 °C at their maximum. In eastern Norway, the temperature did not reach such extreme values, but it was still warm with the temperature being at around 20-25 °C. It was as warm or even warmer in some areas far up in northern Norway and definitely warmer in central Norway Norway.

In contrast to the 26 June case, thunderstorm activity was observed during the night hours of 4 August in Denmark propagating northwards. In Oslo the morning started cloudy with drizzle and fog. The sun made brief appearances during the day and cumulus clouds formed during those periods, but did not develop into larger cumulonimbus clouds. The convective cells from Denmark propagated over southern Sweden in the morning hours. The organized convection reached the Oslo

area from the south at 15 UTC and continued to northern Norway before thunderstorm activity ceased the following day. The observed evolution was in stark contrast to the 26 June case wherein deep convection was isolated in both time and space.

1.3 General summer conditions in Norway

There is not much literature about the general conditions in Norway, let alone thunderstorms. However, according to the book "Været i Norge" by Harald Reitan, thunderstorms are common in Norway, but not as common or severe as farther south in Europe. They are most common in Agder, Telemark and Østlandet during the afternoon hours in the summer months. Thunderstorms are also found along the Norwegian coastline from Lindesnes in the south and all the way up to Finnmark during winter. July is considered to be the summer month with the best weather, hence the common holidays in Norway are set in July's last three weeks. August is usually the month with the most tropical nights (minimum temperature above 20 °C) because of the warm sea heating up the surrounding air masses. August is also warmer than June, but wetter as well (Reitan, 2005, p. 116, 125 and 144).
Cumulus clouds are usually seen during calm summer periods in eastern and southern Norway which can develop into cumulonimbus especially around elevated areas. Heavy convective events may also result from cumulonimbus clouds forming in Sweden, south and southeast of Norway, which then can affect the area of Oslofjord. Late in August when the temperature begins to decrease, the atmosphere stabilizes and thunderstorms become rarer (Danevig, 1969, p. 410).

1.4 Necessary ingredients for deep convection

The necessary ingredients for deep convection can be succinctly defines as: i) a sufficiently moist and deep layer in the low or mid atmosphere, ii) conditional instability, and iii) a triggering mechanism to raise air parcels to the level of free convection (the level where an air parcel becomes positively buoyant). For long-lived organized convection, it is necessary for the environment to contain large amounts of buoyancy (instability) and vertical wind shear (Johns & Doswell III, 1992). The former can be quantified in terms of the convective available potential energy (CAPE); a stability index providing information about the buoyancy and instability of a vertical column of air. Further details will be given in the next section. Large wind shear on the other hand is needed for the organization of the convective cells (Brooks, 2009).
The three mentioned ingredients influence the convective activity in different ways and their interaction determines the likelihood of a particular phenomenon occurring or not occurring. Information about moisture and instability can be provided by sounding data and observations, however that is not the case for triggering and lifting mechanisms. They are impossible to determine from sounding data alone, so mesoscale models are needed. Then based on the output of numerical models and the forecaster's interpretation of the data will lead to the identification of areas where lifting and triggering mechanisms are likely to occur (Sánchez *et al.*, 2009).
Those three required ingredients are more common in certain parts of Europe than others and they also vary with season. Also, Kaltenböck *et al.*, 2009 investigated numerous severe weather events related to thunderstorms in Europe and one of the main conclusions was that most of those events were associated with strong south-westerly flow at 500 hPa. This is because flow from this direction advects warm and moist air. Severe events occurred more frequently in summer (May/June

to August), with a pronounced diurnal cycle (Kaltenböck *et al.*, 2009).

1.5 Stability indices

In order to identify regions where thunderstorm development is likely to occur, several indices have been developed. Commonly used indices that will be examined herein are: the convective available potential energy (CAPE), the Showalter stability index, the K-index, the total totals (TT) and the Severe Weather Threat (SWEAT) index. They provide information about convective initiation, if vertical profiles are available from a sounding for example. However, the disadvantage is that we assume the physics of the atmosphere is the same regardless of the location or the time of the year (Brooks, 2009).
So even though the stability indices give a good indication of how unstable the atmosphere is, the location of the measurement is important. For example, in the United States (US) the lifting mechanisms are usually provided by the infusion of warm humid air from the Gulf of Mexico leading to thermodynamic processes (Graf *et al.*, 2011). Europe on the other hand, is farther north, the Atlantic Ocean sea surface temperature is considerably lower and the terrain is more complex. Therefore, synoptic systems, mesoscale effects and topography are the main reasons for thunderstorm initiation in Europe (Brooks, 2009). The environmental conditions in the US typically result in more extreme stability index values. When applied in Europe, values are often moderate by US standards when convective phenomena occur. European environments are similar to those seen in the cool season of south-eastern US and California with low lifting condensation level (LCL) heights and moderate CAPE (Kaltenböck *et al.*, 2009). It has been found that for Europe, stability indices are more valuable for forecasting when compared to the local, monthly climatological mean (Romero *et al.*, 2007).
Stability indices have considerable skill to predict thunderstorm probability (Kaltenböck *et al.*, 2009), however there are some limitations that must be taken into account by the forecaster (Doswell III & Schultz, 2006). No stability index functions well when on its own and may lead to contradictory results since the indices are not able to fully describe the state of the atmosphere (Schultz, 1989). This is because they do not take into account the lifting and triggering mechanisms, the third necessary ingredient, or the moisture supply, representing thus only the potential or latent instability of a layer in the atmosphere (Van Zomeren & Van Delden, 2007). For a better interpretation of the indices, they should be used in coordination with other variables for higher predictability accuracy (López *et al.*, 2001).
There have been various studies attempting to find which stability index is the best thunderstorm predictor. The best stability indices are found to be the ones based upon latent instability near the surface (Haklander & Van Delden, 2003). The advantage of CAPE, however, is that it is calculated by means of an integral of the vertical profile of the troposphere and lower stratosphere and is thus independent of particular atmospheric levels (López *et al.*, 2001). It is simply an indication of the atmosphere's buoyancy. Another study in Switzerland has showed that the Showalter Index has also proved to be a powerful predictor for thunderstorm initiation offering good results for soundings launched at both 00 UTC and 12 UTC (Huntrieser *et al.*, 1997). The SWEAT index, however, is superior in terms of severe weather forecasting. It is the only index of all mentioned that takes wind shear into account, which is necessary for rotating updrafts and organized, severe convective systems. However, it does not do as well for predicting weak thunderstorms, since large wind shear tends to be deleterious to cumulonimbus updraft longevity (Schultz, 1989).

1.5.1 Definitions

The stability indices analyzed in this thesis will be now defined and their threshold values will be presented based on MetEd, 2014. It should be reminded though that those values are based on the US atmospheric conditions.

CAPE and CIN

The convective available potential energy (CAPE) measures the vertically integrated positive buoyancy of a raised air parcel. It is given by

$$CAPE = R_d \int_{LFC}^{EL} (T'_v - T_v) dlnp \tag{1.1}$$

where T'_v and T_v are the air parcel and the environmental virtual temperature, respectively. Virtual temperature is the temperature that dry air would need to attain in order to have the same density as the moist air at the same pressure (Wallace & Hobbs, 2006, p. 67). The natural logarithm of pressure is integrated, as indicated by dlnp. LFC is the level of free convection and EL is the equilibrium level where the air parcel's temperature equals the environment's temperature and therefore stops rising. CAPE is often calculated from sounding data. CAPE is simply the area on the skew-T plot, extending from LFC to EL and bounded by the environmental temperature sounding on the left and a air parcel temperature on the right (Wallace & Hobbs, 2006, p. 345-346). Values between 1000-2500 J/kg indicate a moderately unstable atmosphere, 2500-3500 J/kg very unstable and above 3500, extremely unstable.

Often, another stability index called convective inhibition (CIN) is used together with CAPE. For deep convection to occur, an air parcel must reach the LFC and CIN defines the energy needed to forcibly lift an air parcel to the level where it becomes positively buoyant. Therefore, even if CAPE is large, high values of CIN may prohibit deep convection from occurring. CIN is defined as follows

$$CIN = R_d \int_{SFC}^{LFC} (T_v - T'_v) dlnp \tag{1.2}$$

The integral is between the surface (SFC) and the LFC. Both CAPE and CIN are measured in J kg^{-1} (Riemann-Campe *et al.*, 2009).
Additional indices are described in Peppler, 1988.

Showalter Stability Index

$$SSI = T_{500} - T'_{500} \quad \text{(Showalter, 1953)} \tag{1.3}$$

where T_{500} is the environment's temperature at 500 hPa and T'_{500} is the temperature an air parcel would achieve if it was lifted dry-adiabatically from 850 hPa to LFC and then moist-adiabatically to 500 hPa. This is also the disadvantage of this index. It does not take into account the layer below 850 hPa, which is also important for instability and moisture. This index estimates the existence of positive buoyant energy above LFC and the possibility of subsequent free convection. For SSI=+3 to +1, there is possibility of showers and thundershowers, for +1 to -2 thundershowers are likely and for values below -3 severe convective activity is to be expected.

K-Index

$$K - INDEX = (T_{850} - T_{500}) + T_{d,850} - (T_{700} - T_{d,700}) \quad \text{(George, 1960)} \tag{1.4}$$

where T_{850} and T_{700} are the air temperature at 850 hPa and 700 hPa, while $T_{d,850}$ and $T_{d,700}$ the dewpoint temperature at the same levels. By including both the temperature and the dewpoint temperature in the equation, this index provides information for the vertical distribution of both moisture and temperature. However, it has been found that K-index is not suitable for predicting severe thunderstorms and is rather used for identifying environments where heavy rainfall in general is likely to occur. Thunderstorm probability ranges from very low when KI<20 to a likelihood of widespread activity when KI>35.

Total Totals

$$TT = T_{850} + T_{d,850} - 2T_{500} \quad \text{(Miller, 1967)} \tag{1.5}$$

Total Totals (TT) is a simple equation with only three variables and two levels required. The higher the temperature and dewpoint temperature at 850 hPa and the lower the 500 hPa temperature, the bigger will the resulting TT value be. TT has been found to be a good predictor for 12-36 hour probability forecasts of thunderstorms and even better predictor for severe local storms. However, taking only two levels into account, this index is quite limited. Like the Showalter index, it does not include information about the atmospheric conditions below 850 hPa. For TT=44 thunderstorms are likely, for TT=50 severe thunderstorms are possible and for TT$\geq$55 severe thunderstorms are likely and possible tornadoes.

Severe Weather Index

$$SWEAT\ \ INDEX = 12T_{d,850} + 20(TT - 49) + 2f_{850} + f_{500} + 125[sin(d_{500} - d_{850}) + 0.2] \quad \text{(Miller } \textit{et al.}\text{, 1971)} \tag{1.6}$$

where f_{850} and f_{500} are the wind speeds at 850 and 500 hPa, d_{850} and d_{500} are the wind directions at 850 and 500 hPa and TT is the total totals index. In contrast to all the other indices mentioned, this index includes the effect of wind shear, a very important factor for thunderstorm development. For SWEAT=150 to 300 there is a slight potential for severe weather. For 300-400 severe weather is possible, while values above 400 indicate a tornadic environment. These threshold values are of course set for the Unites States and are therefore expected to be lower in Europe as is the case with all stability indices. Because of the inclusion of wind shear in the SWEAT index, it should rather be used for predicting severe thunderstorms than ordinary thunderstorms.

Chapter 2

Model and methods

2.1 ERA-Interim and IFS

There are several anomaly maps used in this thesis and ERA-Interim is the model that was used for their creation. Figures of the 2m temperature anomaly were shown in the Introduction and in Section 3.3 there are figures of the specific humidity mean, the specific humidity anomaly and CAPE anomaly. For the temperature, analysis from 00, 06, 12 and 18 UTC were taken into account and then each month was compared to the same month in the period of 1979-2015. Unfortunately, the CAPE parameter had some limitations. First of all, CAPE is available as a forecasted parameter only. It is available in 3 hourly steps, so the closest to our preferred times, would then be 03 UTC and 15 UTC. But, values for those times have been unavailable as well. A data error in ERA-Interim has caused these values to be zero, so there has been no other option than to use the 6 hour forecasted values for 06 UTC and 18 UTC to calculate the CAPE anomaly[1]. This means that the results must be treated with care. In order to calculate the anomaly, the CAPE of 26 June 2014 and 4 August 2014 was compared to the CAPE climatology, a period that was chosen to be from 15 days prior to 15 days after the event for the years 1979-2015. This method was also used by Graf *et al.*, 2011. The specific humidity anomaly was calculated in the same way, however in contrast to CAPE, analysis data of all four time steps (00, 06, 12, 18 UTC) of 26 June 2014 and 4 August 2014 are available.
ERA-Interim was also used to generate the files required to calculate backward trajectories with LAGRANTO, a Lagrangian trajectory model described in the next section.
The three different figures that were produced for the large scale circulation and the calculation of SWEAT index used data from the ECMWF operational analysis. ERA-Interim and the ECMWF operational analysis are based on the Integrated Forecasting System (IFS). A short description of ERA-Interim and IFS will now follow based on Dee *et al.*, 2011, where more details about the model can be found.
ERA-Interim is a global atmospheric reanalysis covering the period from 1979 until today and is being extended and updated continuously in near-real time. It is produced by the European Centre for Medium-Range Weather Forecasts (ECMWF) and is a replacement of ERA-40, an older reanalysis which was complete in 2002. Production of ERA-Interim, from 1989 onwards, began in summer 2006 and the period from 1979 to 1988 was added later in 2011 (Berrisford *et al.*, 2011).
The ERA-Interim produces reanalyzed data using the IFS 2006 release CY31R2, short for cycle 31

[1] https://software.ecmwf.int/wiki/display/CKB/Convective+Available+Potential+Energy+%28CAPE%29+values+are+erroneously+zero

and release 2 from this cycle. The fixed version ensures that no spurious trends are caused by an evolving NWP system. IFS incorporates a forecast model with three fully coupled components for the atmosphere, land surface and ocean waves. The spectral resolution of ERA-Interim is T255, which corresponds to approximately 79 km, whereas the vertical resolution consists of 60 levels from the surface at 1000 hPa to the top of the atmosphere at 0.1 hPa.

2.1.1 Calculating the SWEAT Index

The ECMWF operational analysis was used to calculate the SWEAT index, since it unfortunately is not an available parameter in AROME-MetCoOp (details on AROME-MetCoOp will be discussed later), the model behind all other stability indices presented in the next chapter. The equation, which has been already explained in Section 1.5, is as follows

$$SWEAT\ \ INDEX = 12T_{d,850} + 20(TT - 49) + 2f_{850} + f_{500} + 125[sin(d_{500} - d_{850}) + 0.2] \quad (2.1)$$

where $TT = T_{850} + T_{d,850} - 2T_{500}$. All parameters are available in the operational model except for the dewpoint temperature. The dewpoint temperature does not have a standard equation. The most common and simplest combines the air temperature and relative humidity:

$$T_d = T - \left(\frac{100 - RH}{5}\right) \quad (2.2)$$

This approximation can be simply interpreted as a decrease of the dewpoint temperature by 1 °C for every 5% decrease in relative humidity. However, this approximation is only valid for RH>50%, which is not the case when the dewpoint temperature we need for the SWEAT index is for the height of 850 hPa. The relative humidity can be well below 50% at that height. So another, more complex equation needs to be used to find the dewpoint temperature, which again combines temperature and relative humidity, but adds also some coefficients

$$T_d = \frac{B_1\left[\ln\left(\frac{RH}{100}\right) + \frac{A_1 T}{B_1 + T}\right]}{A_1 - \ln\left(\frac{RH}{100}\right) - \frac{A_1 T}{B_1 + T}} \quad (2.3)$$

where $A_1 = 17.625$ and $B_1 = 243.04$°C. This is a far more accurate calculation of the dewpoint temperature, when RH is defined as $RH = e/e_s$, which it is in IFS, and is valid for all values of RH (Lawrence, 2005).
Finally, one last important thing when calculating the SWEAT index is that if any term of the equation is negative, then it is set to zero.

2.2 LAGRANTO

LAGRANTO (Lagrangian Analysis Tool) is a Lagrangian trajectory model, much alike FLEXPART, that has the ability to track particles either forwards or backwards in time. Those trajectories will be useful in identifying the origins of the unstable and humid air masses that created those severe weather situations in our case. More information about the starting area and the dates are given in Subsection 2.2.2.

2.2.1 Description of LAGRANTO model

The Lagrangian trajectories calculated with the LAGRANTO model are based on parameters and values from the ERA-Interim model. Therefore parameters like potential temperature, specific humidity and pressure can be tracked along the paths of the parcels.
Since ERA-INTERIM was the model used to generate the needed files for the LAGRANTO trajectory calculations, the resolution is the same as the model's.
The rest of the subsection is based on Sprenger & Wernli, 2015, where further details can be found.
LAGRANTO, like all other trajectory models, solves numerically the trajectory equation: $D\mathbf{x}/Dt = \mathbf{u}(\mathbf{x})$, where $\mathbf{x} = (\lambda, \phi, p)$ is the position vector in geographical coordinates and $\mathbf{u} = (u, v, \omega)$ the 3-D wind vector. The trajectories are calculated by using wind fields from realanyses or model simulations.
Trajectories have been used for investigating different types of atmospheric flow phenomena, including extratropical cyclones, stratosphere-troposphere exchange and transport and mixing in the stratosphere. Other popular applications are tracking pollution plumes and the spreading of volcanic ashes.
LAGRANTO was developed as a versatile tool for the Lagrangian analysis of weather systems and their dynamics. It was first used to identify objectively coherent airstreams in case studies of extratropical cyclones, in particular warm conveyor belts, dry intrusions and later also stream jets and cold conveyor belts. Another important research area for the application of LAGRANTO is among others the quantitative analysis of moisture sources and transport which is the main reason for using it in our two cases.
LAGRANTO calculations are based on netCDF files that contain 3D wind fields on a regular longitude–latitude grid. In the vertical, different level types are supported: (i) ECMWF hybrid sigma-p level type, (ii) constant pressure levels, and (iii) isentropic levels. In this thesis ECMWF hybrid sigma-p level type is chosen. All fields must be horizontally and vertically unstaggered; in particular, the vertical wind must be provided at the same grid points as the horizontal wind components. LAGRANTO uses two types of files to calculate trajectories. The one type of files are the P-files (primary) and the other the S-files (secondary). The zonal wind U (m s^{-1}), the meridional wind V (m s^{-1}) and the vertical wind OMEGA (in Pa s^{-1}) are all available in the P-files for the trajectory calculation alongside with the surface pressure (PS) in order to identify the topography and whether there is intersection with the air parcels. Temperature and specific humidity are also parameters stored in the P-files. Further parameters are stored in the S-files, but some of them, like RH, need to be calculated.

2.2.2 Trajectory calculation

A trajectory, $\mathbf{x}(t)$, is obtained by integrating $D\mathbf{x}/Dt = \mathbf{u}(\mathbf{x})$ numerically. If we start at the position $\mathbf{x}$ at time t, the first iteration of the new position $\boldsymbol{x}^*$ is obtained from the following "forward" time step:

$$\boldsymbol{x}^{(*)} = \boldsymbol{x} + \boldsymbol{u}(\boldsymbol{x}, t) \cdot \Delta t, \tag{2.4}$$

where $\boldsymbol{u}(\boldsymbol{x}, t)$ is the wind at position $\mathbf{x}$ and Δt the time step. Whereas the first iteration only uses wind information at the starting position, the next iterations average the wind vector between the starting position and the previously estimated ending position, i.e.,

$$\boldsymbol{u}^{(*)} = 1/2[\boldsymbol{u}(\boldsymbol{x}, t) + \boldsymbol{u}(\boldsymbol{x}^{(*)}, t + \Delta t)] \tag{2.5}$$

and the second iteration of the new position then reads

$$\boldsymbol{x}^{(**)} = \boldsymbol{x} + \boldsymbol{u}^{(*)} \cdot \Delta t. \tag{2.6}$$

This process is shown schematically in Figure 2.1. LAGRANTO's default for the number of iterations is three iterative steps and the time step Δt equals 1/12 of the data time interval. However, those values can be changed manually. A bilinear interpolation is used for the horizontal interpolation and a linear for the vertical.

2.2.3 Running LAGRANTO for this thesis

LAGRANTO version 2.5.r35 was used to produce the trajectories. After downloading the necessary netCDF files for the relevant dates, a date file must be created, which is accomplished with the following command:

```
> datelist stdout -create 20140626_12 20140620_00
```

Since we are interested in calculating a backwards trajectory, the later date (starting date) comes before the earlier date in the command. This command creates a text file including all dates starting from 26 June 2014 12 UTC and all the way back to 20 June 2014 00 UTC with a time step of 6 hours, since it is the time step of the available netCDF files.
After having created this file, a region file can be created including the boundary coordinates of the region we want to have as a starting region. However, there are multiple ways of doing this and in this thesis the coordinates of Blindern, Oslo were set as a central point and then four points were chosen around it in each direction. Two points 1.5°to the west and east and 0.9°north and south of Blidnern, Oslo. The height and vertical distribution of the starting points can also be defined in various ways with plenty of options available. In our case we have chosen to divide the results into two layers, one layer from 1000 hPa up to 850 hPa, as shown in the command below, and one layer from 850 hPa up to 500 hPa. No starting points higher than that have been chosen since it is not expected that there is enough moisture so high up to affect the thunderstorm development. All grid points within those layers are chosen. The starting points are then written in the file called startf.2 with starting date 26 June 2014 12 UTC. The corresponding command is as follows:

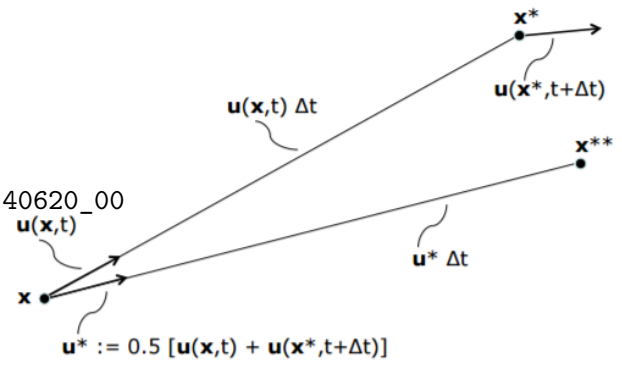

Figure 2.1: Schematic representation of the iterative Eulerian time step used in LAGRANTO. The air parcel's position at time t is given as $\boldsymbol{x}$. The velocity field at this position is $\boldsymbol{u}(\boldsymbol{x})$. Based on the position, the velocity and the time step, a new air parcel position can be calculated with a simple Euler forward step: $\boldsymbol{x}^* = \boldsymbol{x} + \Delta t \cdot \boldsymbol{u}(\boldsymbol{x}, t)$. However, a simple Euler forward step is not numerically accurate. Therefore, in a next iteration a new velocity $\boldsymbol{u}^*$ is computed as the average of the velocities at the initial position and at the forward projected position. A new air parcel position $\boldsymbol{x}^*$ is then calculated based on this refined guess of the velocity. In LAGRANTO, three such iterative steps are repeated to obtain the final new position of the air parcel (Figure 3 from Sprenger & Wernli, 2015).

```
> create_startf 20140626_12 startf850.2 'shift(10.721,59.943,1.5,0.9)  ...
                    ... @ grid(850,1000) @ hPa' -changet
```

The next program is called caltra and is the command that initiates the calculation of the trajectories. With the starting points defined in startf.2, the program will calculate the trajectories from 26 June 2014 12 UTC and back to 00 UTC 20 June 2014. The output is then written in a file called traj.4 after caltra has completed its run:

```
> caltra 20140626_12 20140620_00 startf.2 traj.4 -j -o 60
```

The -j flag is set to allow trajectories to be lifted and move along if they run into the ground. By adding -o 60, we set an hourly output interval of the air parcel positions. Those positions are then calculated each hour based on forecasts made by the available P-files. The traj.4 file is in netCDF format, but can be converted in a ASCII file if desired.
Then after having generated an output file that includes all the trajectory data, a program called "trace" can be used to choose parameters available from ERA-Interim to trace them. Additionally, new parameters that are not found in ERA-Interim can be calculated based on the variables already available. In this thesis specific humidity and pressure, which are available in ERA-Interim, were traced along the trajectories and so was potential temperature, but it had to be calculated beforehand.
The same procedure was followed for the August case with 4 August 2014 12 UTC as the starting date and 29 July 2014 00 UTC as the ending date.

2.3 AROME-MetCoOp

AROME-MetCoOp (Meteorological Cooperation on Operational Numerical Weather Prediction) is the result of a collaborative effort between the Swedish Meteorological and Hydrological Institute and the Norwegian Meteorological Institute. This model was put in operation in March 2014 and is based on Météo-France Applications of Research to Operations at Mesoscale (AROME). AROME-MetCoOp's weather forecasts are distributed in both Norway and Sweden. AROME-MetCoOp is a branch of the HIRLAM-ALADIN Research on Mesoscale Operational NWP in Euromed (HARMONIE) AROME model, version 38h1.2, which has been developed within the framework of the High Resolution Limited Area Model (HIRLAM) consortium, a research cooperation of 11 European meteorological institutes (Müller *et al.*, 2017).
AROME-MetCoOp covers the whole Scandinavia and the Baltic countries. The horizontal resolution is at 2.5 km and the horizontal grid (739 × 949 grid points) is defined by a Lambert projection with the center at 63.5°N and 15°E. The atmosphere is divided by a mass-based, terrain-following hybrid vertical discretization into 65 layers. This means that the vertical resolution closest to the ground is larger than the resolution higher up in the atmosphere, with the first layer having a 12.5 m height. The top layer is located at 33km. The model operates with a 3-hourly update cycling, where atmospheric and land surface variables are updated The AROME-MetCoOp model is forced by ECMWF at the lateral and upper boundaries (Müller *et al.*, 2017). An archive of NetCDF files is available at the Norwegian Meteorological Institute - four files for each day which include analysis and forecasts for 00, 06, 12 and 18 UTC. For the stability indices and specific humidity, the 12 UTC analysis of August the 4th is used, but no file exists for 26 June 12 UTC. So unfortunately, a 6 hour forecast at 06 UTC is used instead to obtain information about the weather situation at 12 UTC.
AROME-MetCoOp provides also vertical profiles of the atmosphere for certain locations. However,

they have not been included in this thesis. Unfortunately, no weather balloon launching takes place in Oslo or anywhere near, which is a shame. So even though a sounding would seem essential when analyzing a case with deep convection, a model generated vertical profile is not an ideal solution.

2.4 CMEMS

The Copernicus Marine Environment Monitoring Service (CMEMS) is run by the UK Met Office. CMEMS provides regular and systematic reference information on the physical state, variability and dynamics of the ocean and marine ecosystems for the global ocean and the European regional seas.
The SST data provided is a gap-free gridded product ('level 4'). This level 4 product is a satellite and in-situ foundation SST daily analysis on a 0.05° grid, produced by the Operational SST and Ice Analysis (OSTIA) system (Donlon *et al.*, 2012). Data is available back to 1st January 2007.
CMEMS was used in this thesis to create maps of daily SST anomalies relative to the Pathfinder V5.0 climatology. This dataset is on a lower resolution grid of 0.25°. The Pathfinder V5.0 climatology covers the period 1985-2001. So the SST anomaly for the dates chosen, is compared to the SST of the same date in the period 1985-2001 (Information, 2012).
Global estimated accuracy numbers are provided for 2012 based on a comparison with drifting buoy observations. The mean difference was found to be 0.06 K and the RMS difference 0.40 K (McLaren *et al.*, 2016).

2.5 Satellite images, radar images and lightning data

Satellite images, radar images and lightning registrations are kindly provided by the Norwegian Meteorological Institute.
Meteosat-10 is the satellite that provides the imagery for the Norwegian Meteorological Institute. Full disc imagery is provided every 15 minutes by the Meteosat-10 which was launched in 2012. It is the prime operational geostationary satellite, positioned at 0 degrees (EUMETSAT, 2015b).
The data is transmitted as High Rate transmissions in 12 spectral channels. Level 1.5 image data corresponds to the geolocated and radiometrically pre-processed image data, ready for further processing, e.g. the extraction of meteorological products. The images provided are on an infrared band centered on 10.8μm - Channel 9 (IR 10.8) (EUMETSAT, 2015a).

The lightning data includes detections of both intra-cloud (IC) cloud to ground (CG) lightnings. Lightning sensors detect approximately 70% of the CG lightning strikes and 30% of the IC lightnings. So if no strikes are detected, it does not mean that there has been no electric activity. Times of lighting strikes are in UTC.

2.6 Description of figures

To evaluate the synoptic scale evolution leading to both events, a number of characteristic weather charts are employed. A dynamic tropopause (DT) map represents the height of the tropopause by utilizing the characteristic that potential vorticity (PV) changes drastically from the troposperhere

to the sratosphere due the large change in vertical stability. The two PV unit surface is often chosen to represent this stark transition, where a PV unit is defined as being equal to 10^{-6} $m^2s^{-1}Kkg^{-1}$. Shading on DT maps is the potential temperature (PT) and low level vorticity (LLV) averaged in the 925 to 850 hPa levels is shown in black contours. In essence, the potential temperature defines the tropopause height: blue colors are equivalent to a suppressed tropopause and red colors to an elevated tropopaue. Via the hypsometric equtation, which equates the mean temperature of a layer of air to its thickness, the implication is that cold (warm) air masses result in a low and high tropopause, respectively. DT maps are also extremely useful in the identification of upper-level jet streams (where there is a large horizontal gradient of the PT). This also allows for the identification of Rossby waves along the DT (i.e. upper level troughs and ridges). The low-level vorticity is useful to an understanding of the three dimensional structure of the atmosphere, including but not limited to growing baroclinic waves and occluded extratropical cyclones. Both are relevant for the identification of triggering mechanisms for deep convection.
The second type of map presents the 1000-500 hPa thickness, sea level pressure (SLP) and winds larger than 35 ms^{-1} at 250 hPa level (jet streams). The blue and red contours correspond to low and high thickness values which, again via the hypsometric equation, relate to cold and warm air mass, respectively. SLP is presented in black contours and 250 hPa winds in shading. The relative structure of the thickness field and low level flow associated with the SLP patten is used to infer regions of temperature advection.
To examine moisture advection, the total column water vapor (TCWV) and wind vectors at 925 hPa are presented. TCWV (shading) represents the vertically integrated moisture content.
These maps help to identify where the necessary ingredients for thunderstorm formation, like moisture and warm air masses, originate. For simplicity, they hereafter be referred to as DT, SLP and TCWV maps, respectively.

Chapter 3

Results and discussion

3.1 June

3.1.1 Large scale circulation

DT and SLP maps for 12 UTC 20 June are presented in Figure 3.1 while in Figure 3.2 includes the TCWV map on top and IR satellite image at the bottom. The blue colors in the DT map for June the 20th indicate a suppressed tropopause over the northern parts. It is co-located with a maximum in the LLV field and minima in SLP and 1000-500 hPa thickness. These data represent a 'vertically-stacked' system indicative of an extratropical cyclone undergoing the occlusion process. The SLP map identifies a strong pressure gradient force associated with the SLP minimum previously mentioned, a second low pressure system to the northeast and a high pressure center between Greenland and Iceland. Given the observed thermal structure and strong northerly winds to the west of the low pressure systems (see Figure 3.2), cold air advection is predicted at this time and location. The TCWV map does not identify large values of moisture. Despite this fact, clouds are found over Scandinavia as seen in the IR image associated with the occluding cyclone.

Forty eight hours later (Figures 3.3 and 3.4), the impact of the cold air advection can be observed, as the suppressed tropopause has moved southward. The low pressure associated with the occluded cyclone has weakened considerable, as would be expected from an equivalent barotropic cyclone, and moved southward as well. An enhanced 1000-500 hPa gradient associated with 250 hPa winds speeds are found to the south of Scandinavian over mainland Europe. However, the thermal structure as evidenced in the 1000-500 hPa and the low-level flow remain conducive for continued cold air advection over western Norway. A relative lack of large amounts of TCWV is observed and clouds and small convective cells remain present in the IR imagery.

For 24 June (Figures 3.5 and 3.6) and 26 June (Figures 3.7 and 3.8) not much have changed. According to the top panels of Figure 3.5 and 3.7, the tropopause is still at a low height in the wider area of northeastern Europe and the pattern with high pressure to the west and low pressure to the northeast has remained unchanged. The northerly winds keep the cold pool over the same region and there is a general lack of cloudiness over Norway with the exception of the convective cells visible on the latter date. On 26 June a small low pressure system has formed in southern Norway, as observed in Figure 1.4, associated with a weak maximum in the 1000-500 hPa thickness.

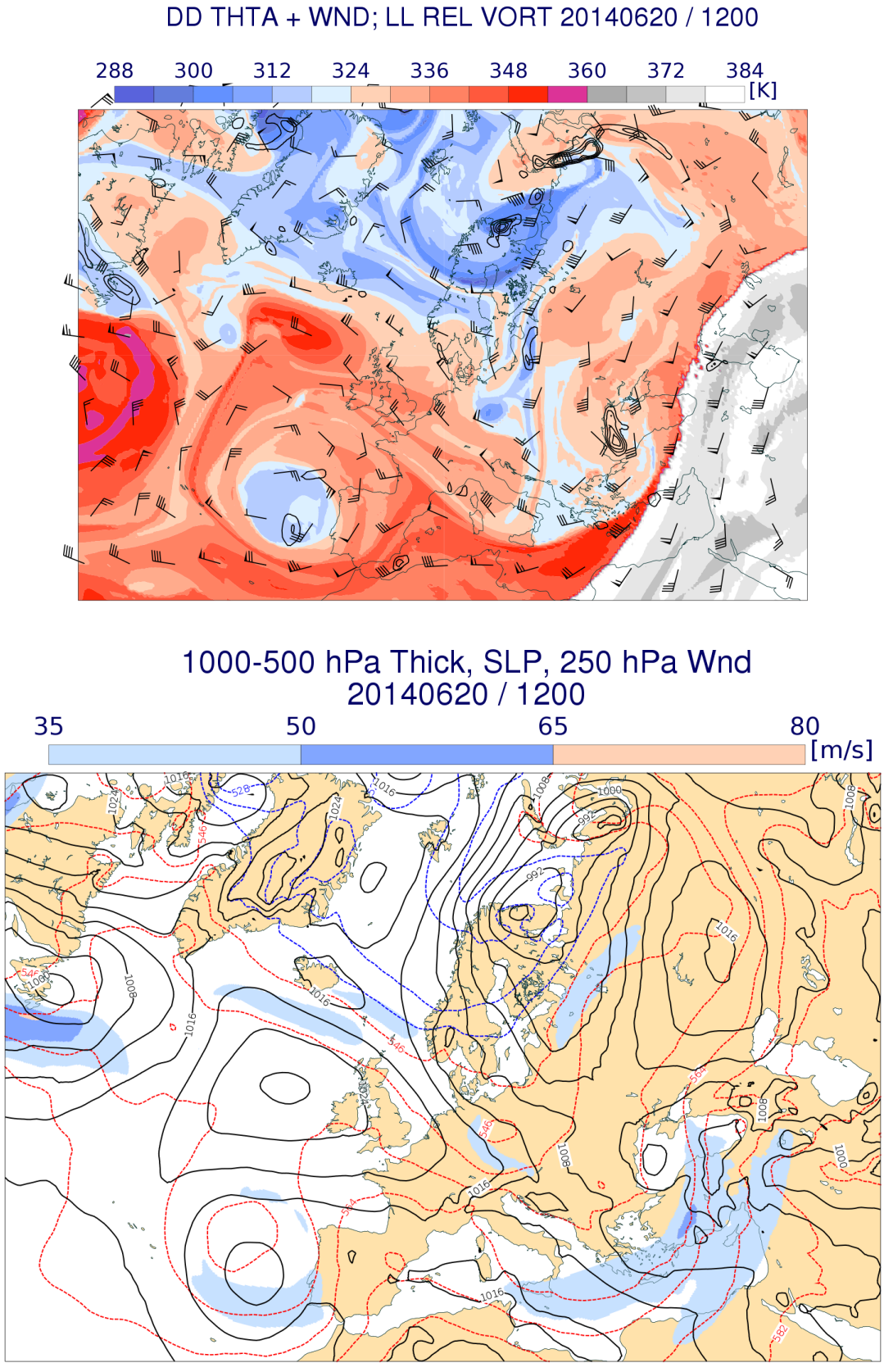

Figure 3.1: Weather maps for 12 UTC 20 June. Top panel: potential temperature (K, shading) and total wind speed (m/s, wind barbs) on the 2 potential vorticity unit surface, and the 925-850 hPa average low level relative vorticity (s^{-1}, black contours, only positive values greater than 10^{-4} shown with a contour interval of 0.5×10^{-4}). Bottom panel: 250 hPa wind speed (m/s, shading), mean sea level pressure (hPa, black contours, contour interval 4 hPa) and the 1000-500 hPa thickness (dm, dashed contours, contour interval of 6 dm). Data source is ECWMF operational analysis.

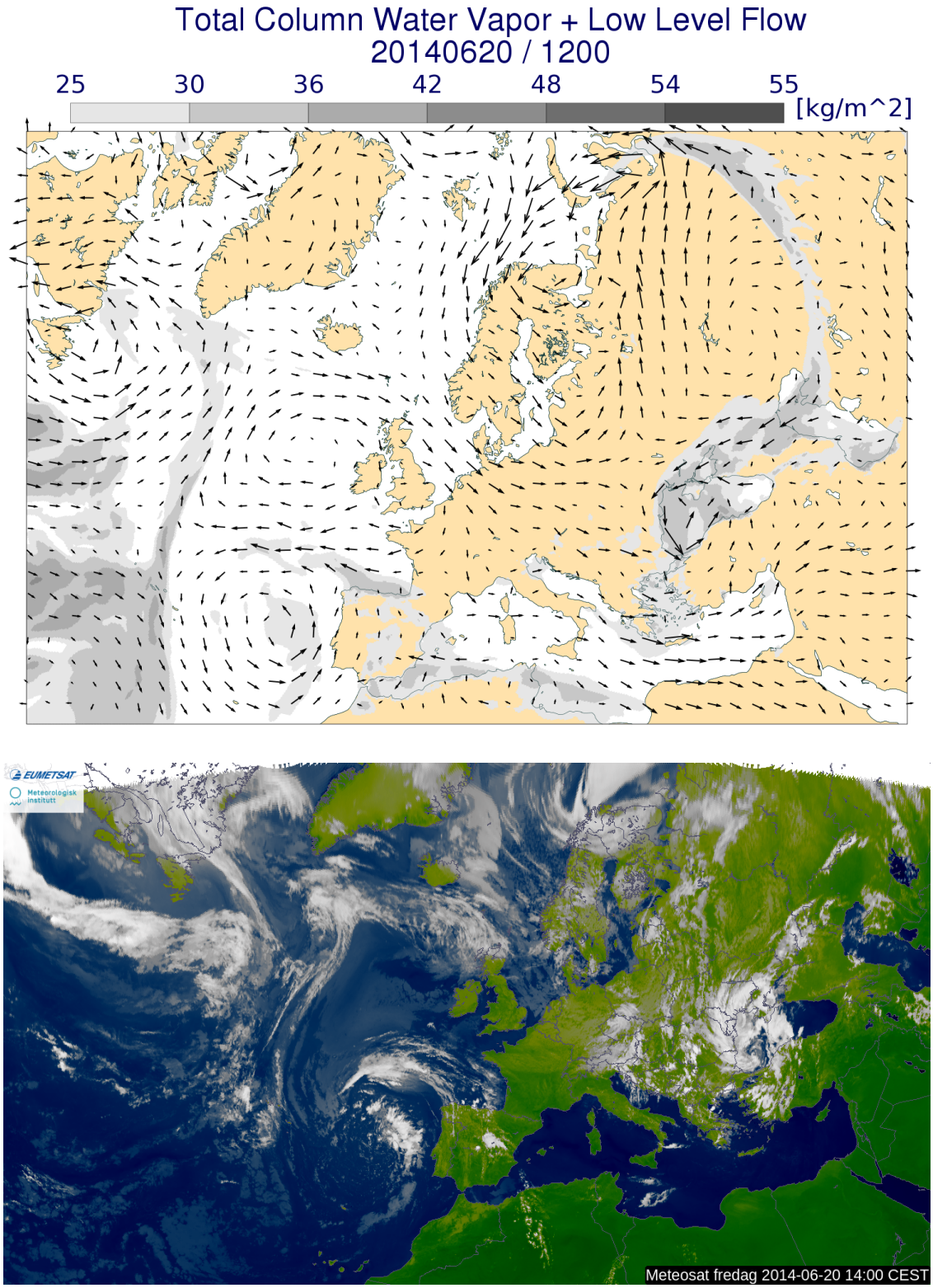

Figure 3.2: Weather maps for 12 UTC 20 June. Top panel: total column water vapor (kg/m^2, shading) showing the total water vapor integrated vertically and total wind speed (m/s, wind arrows) on the 925 hPa pressure surface. Bottom panel: IR satellite image based on the clouds' reflectivity. White colors indicate high clouds and gray/fade colors indicate low clouds.

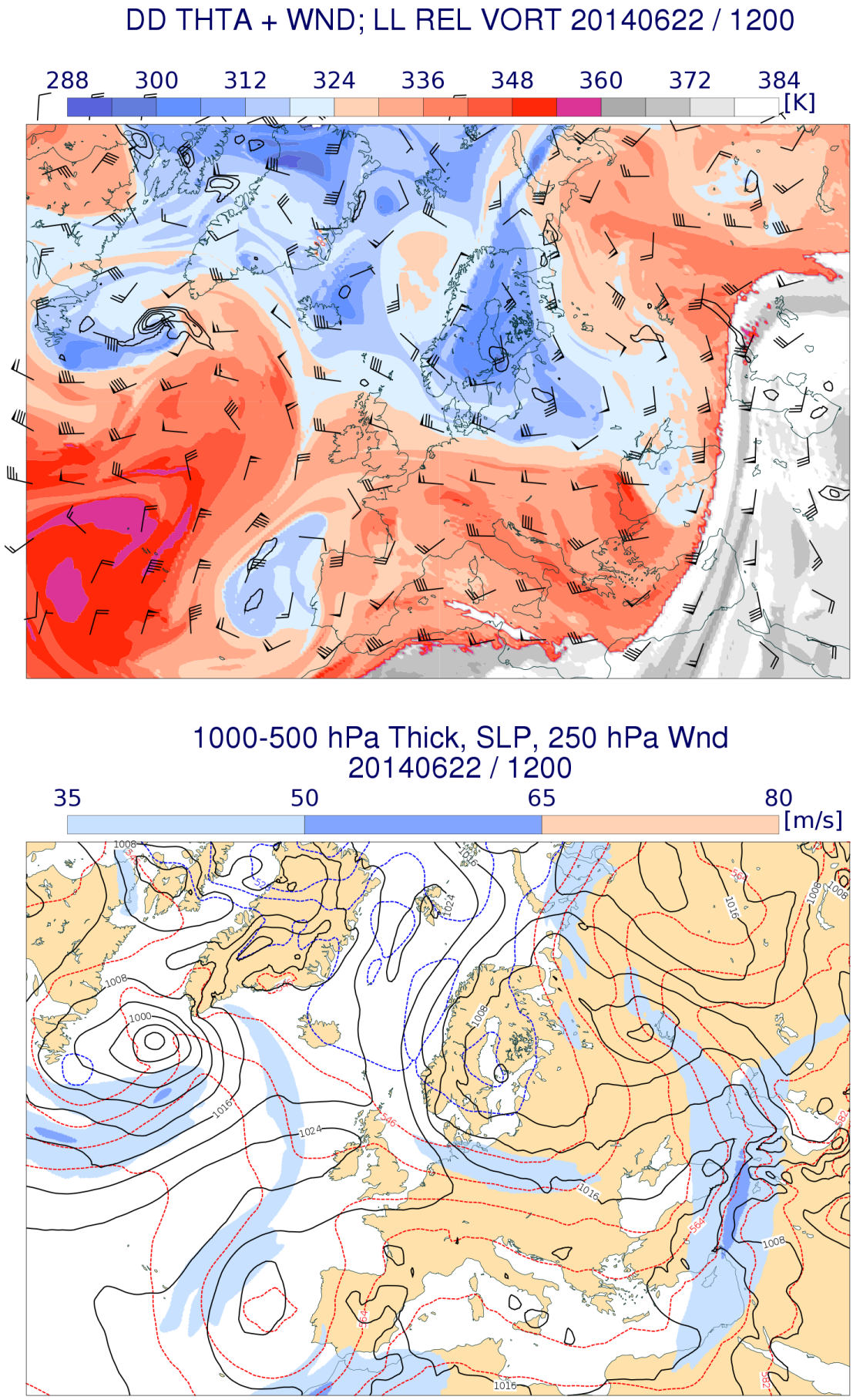

Figure 3.3: Same as Figure 3.1 except for for 12 UTC 22 June.

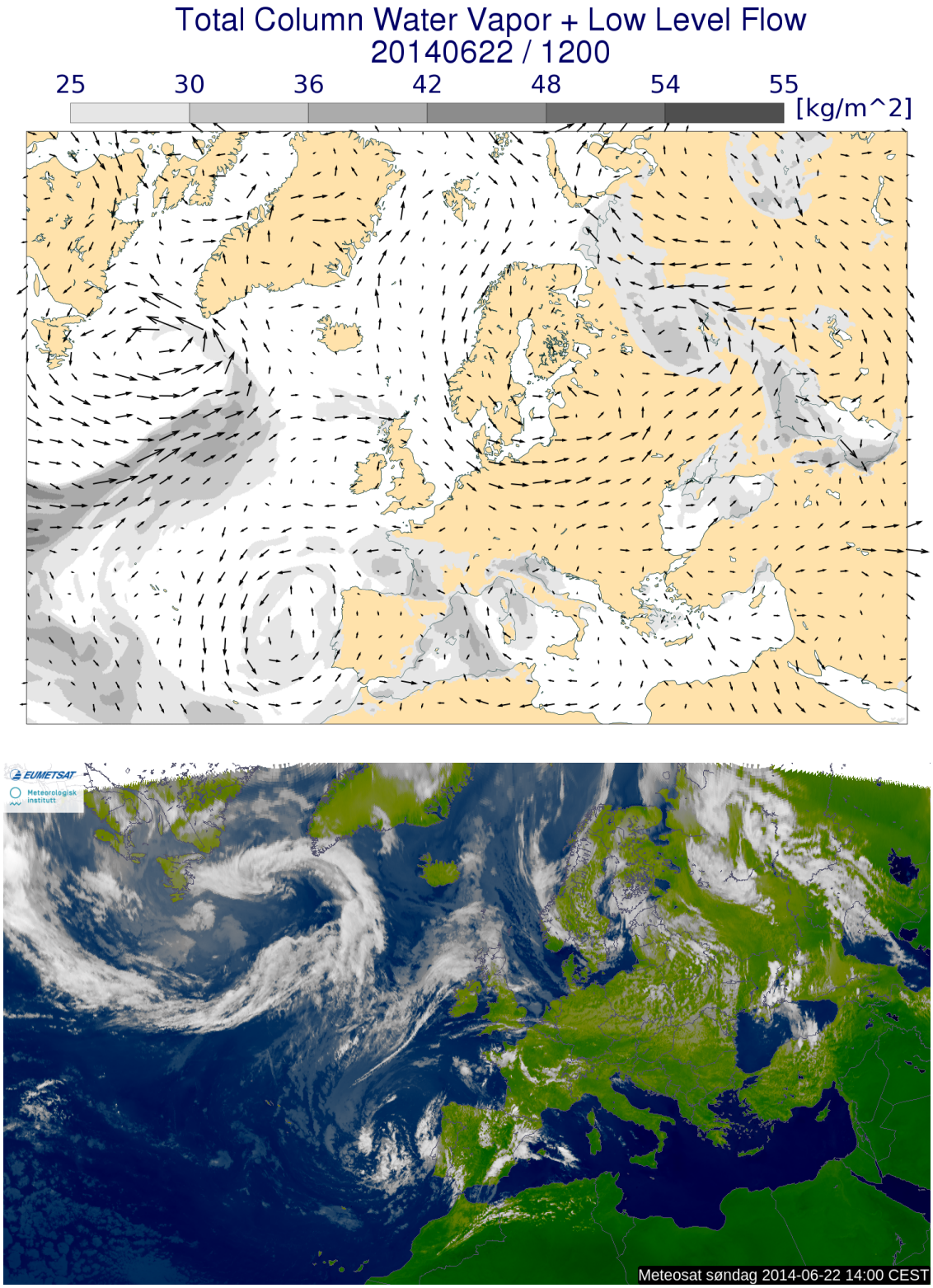

Figure 3.4: Same as Figure 3.2 except for for 12 UTC 22 June.

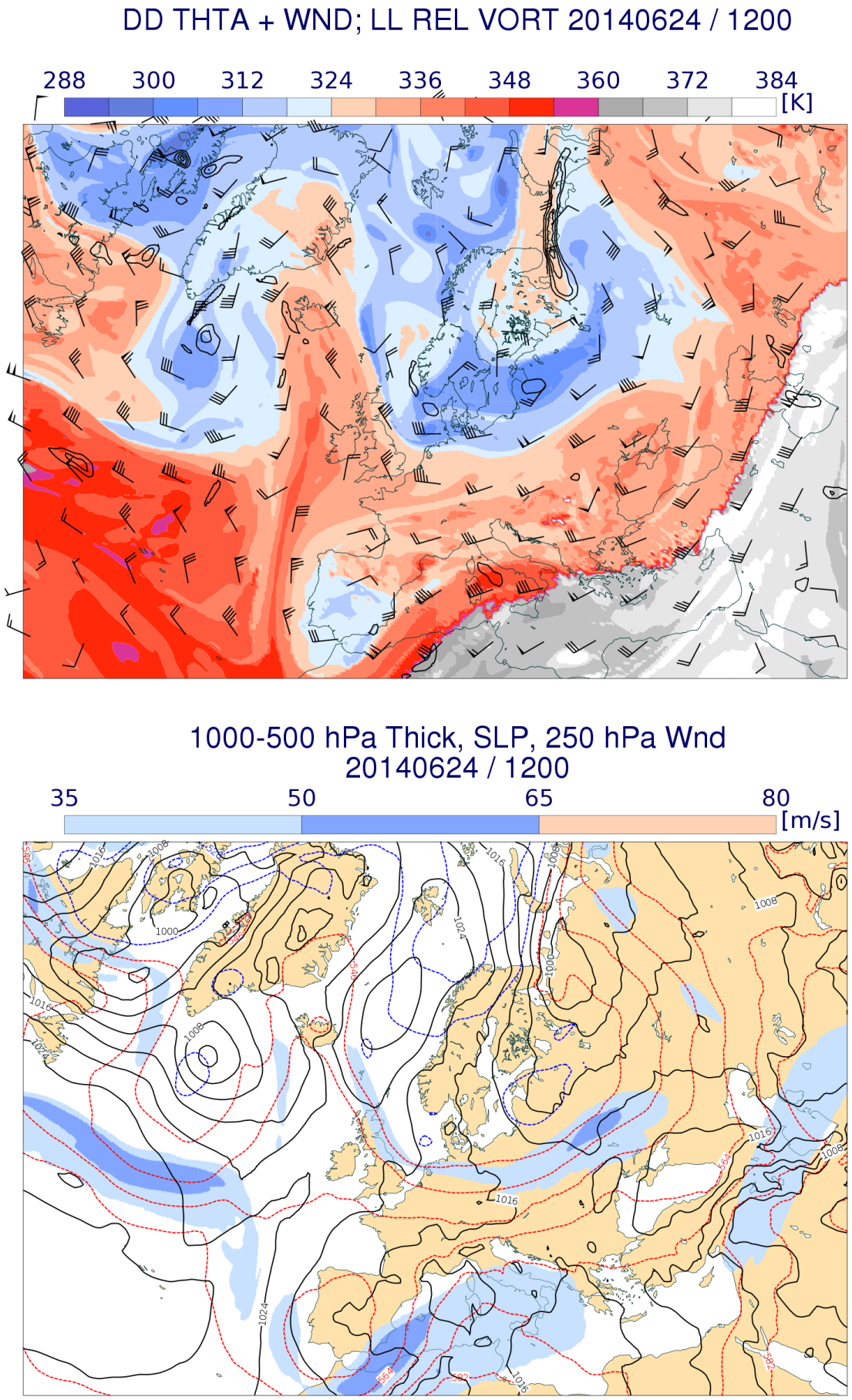

Figure 3.5: Same as Figure 3.1 except for for 12 UTC 24 June.

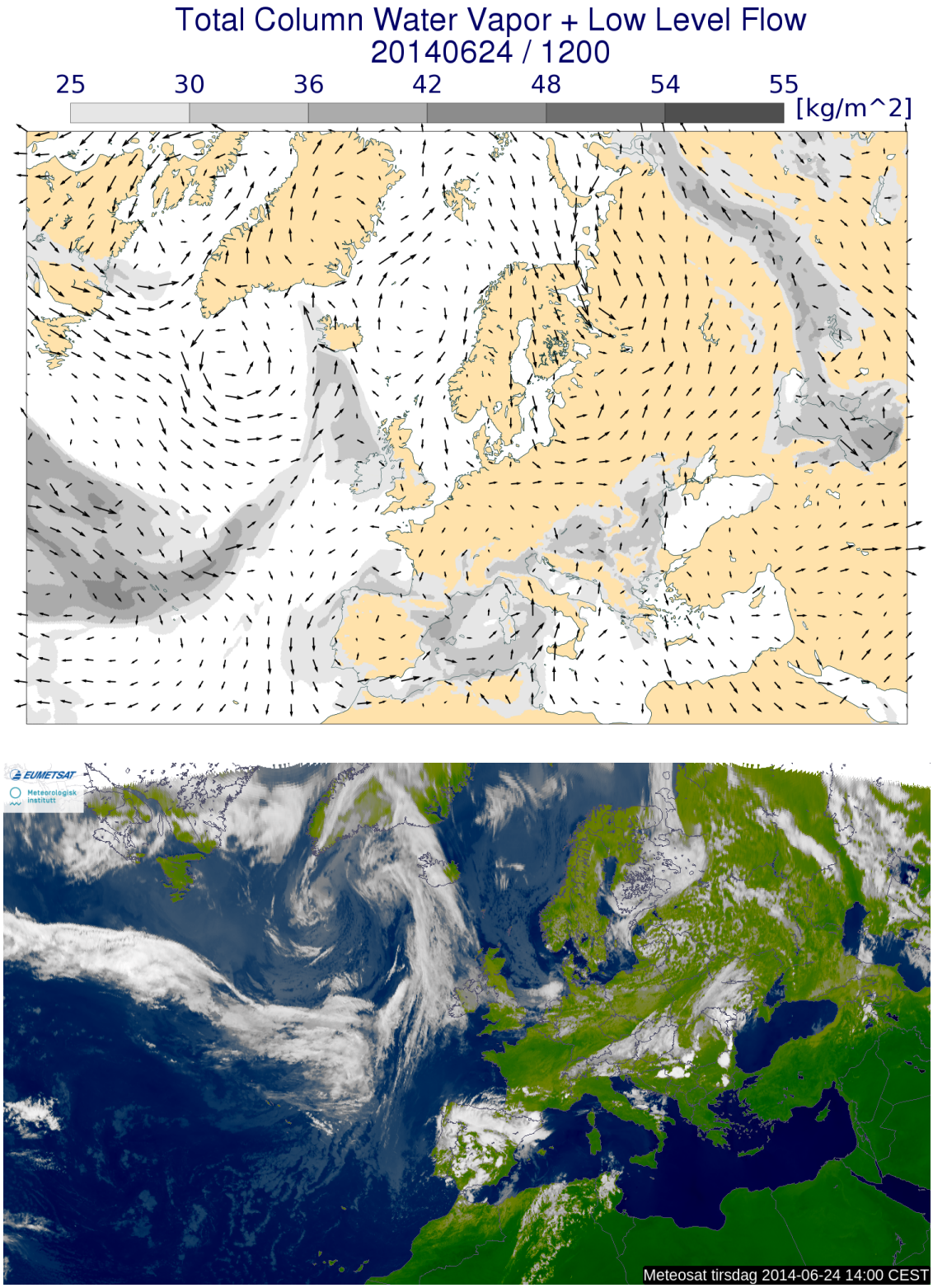

Figure 3.6: Same as Figure 3.2 except for for 12 UTC 24 June.

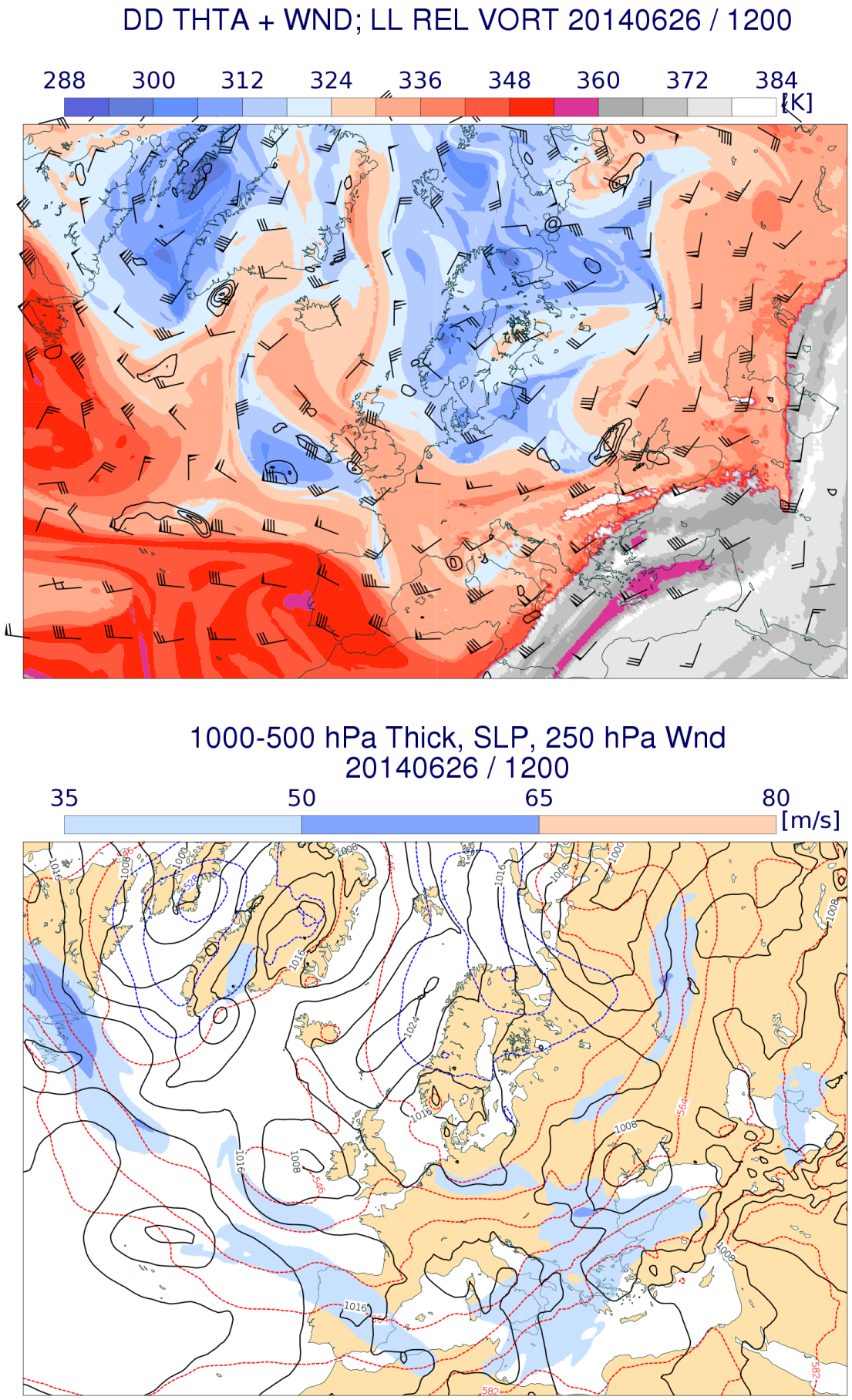

Figure 3.7: Same as Figure 3.1 except for for 12 UTC 26 June.

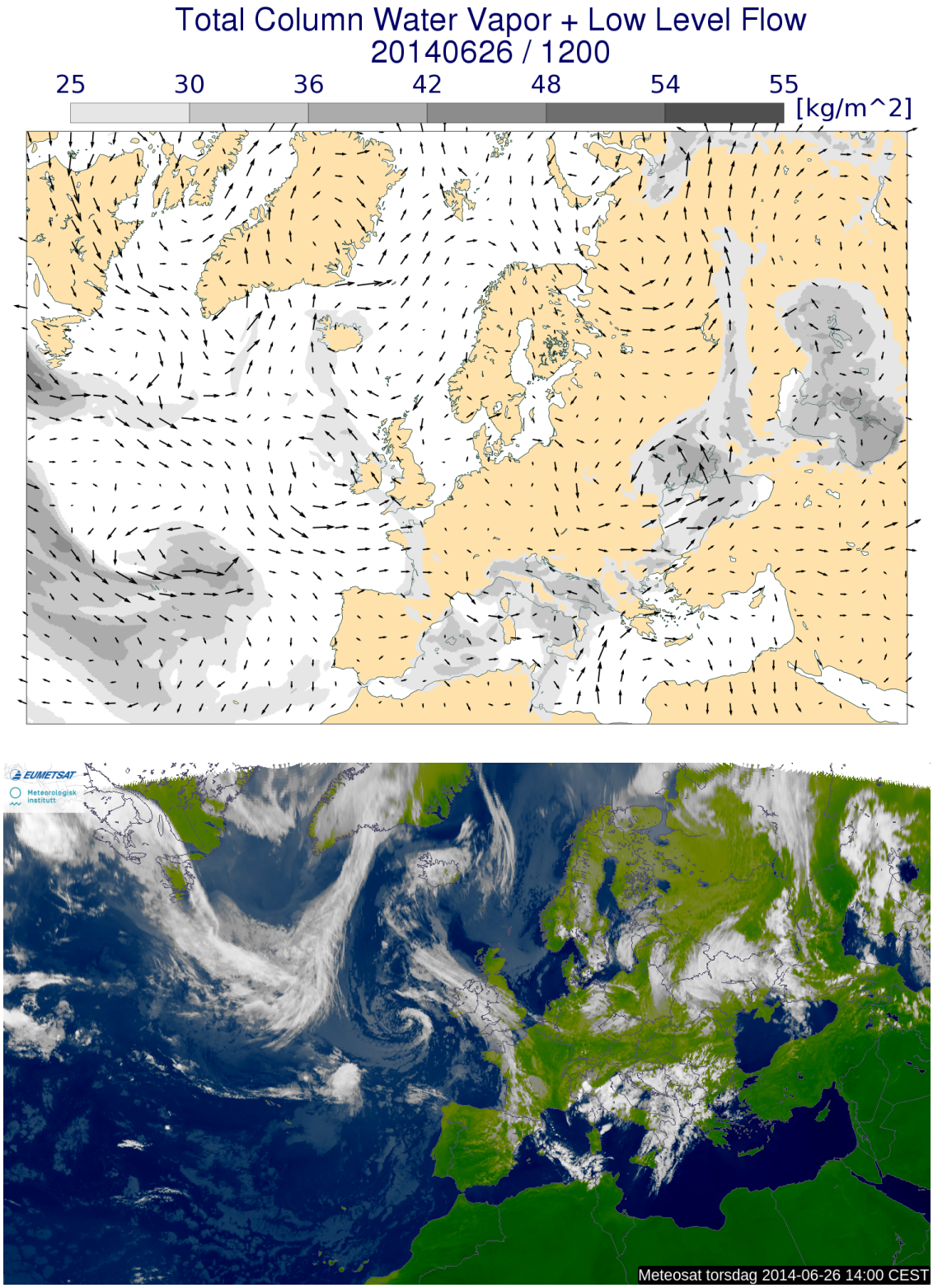

Figure 3.8: Same as Figure 3.2 except for for 12 UTC 26 June.

While a suppressed tropopause is evidence of a cold anomaly along the DT, it is hypothesized in this case that the depth of the anomaly is relatively small and near surface temperatures are not abnormally low. In the presence of surface heating, the two features represent an increased vertical temperature lapse rate, a situation that can be associated with positive buoyancy in a vertical column of air. The presence of deep convection in the observations and seen in the IR imagery lends credence to this theory. No values of impressive TCWV are seen anywhere in Scandinavia during the period prior to the day of our interest. However, cumulus clouds, showers and thunderstorms still made their appearance during this week. It should also be mentioned that the TCWV, although not high, was nonetheless higher than 20 kgm^2 in Oslo. It is also interesting that the wind direction at 925 hPa is not consistent. east of Oslo, at the Swedish border the wind has a direction from the northeast, while the wind on the west coast of Sweden and south coast of Norway the wind comes from the southwest. West of Oslo, the wind has a northwest direction. This is due to the low pressure located in southern Norway resulting in a cyclonic rotation.

3.1.2 LAGRANTO trajectories

The Lagrangian characteristics are described in terms of backward trajectory analysis from the 1000-850 and 850-500 hPa layers. In the June case, the entire number of trajectories in both the 1000-850 hPa and the 850-500 hPa layers are originated from the polar latitudes. The vast majority is coming from north of Svalbard with the exception of a few in the 850-500 hPa layer which go back even farther, west of Greenland and far east in Russia. This is in agreement with what was shown in the previous subsection. The low pressure systems to the east and the high pressure to the west led to the formation of strong northern winds throughout the whole troposphere bringing the cold air masses to southern Scandinavia.

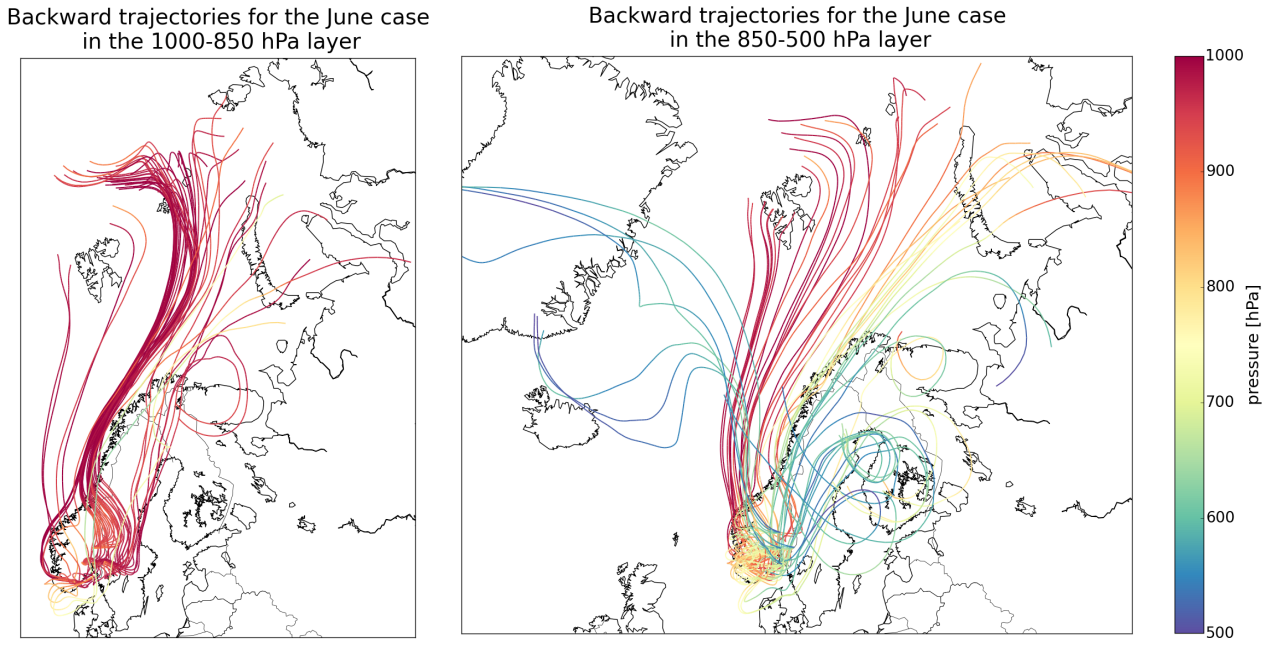

Figure 3.9: Lagrangian trajectories calculated backwards for 12 UTC 26 June - 00 UTC 20 June. The trajectories are colored by height for the layers of 1000-850 hPa to the left and 850-500 hPa to the right.

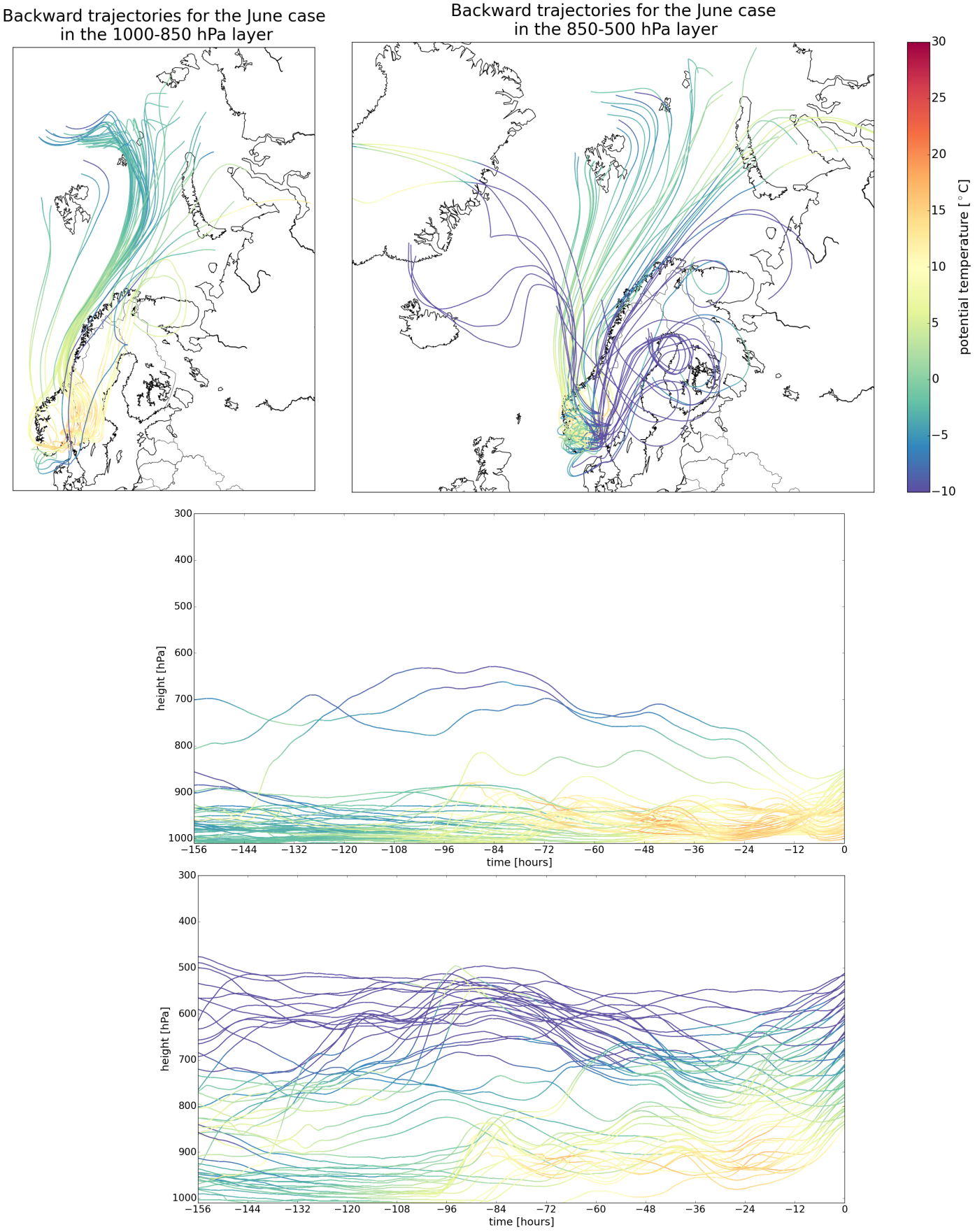

Figure 3.10: Lagrangian trajectories calculated backwards for 12 UTC 26 June - 00 UTC 20 June. The trajectories are colored by potential temperature (in °C) for the layers of 1000-850 hPa at the top left and 850-500 hPa at the top right. A vertical view of these trajectories are seen in the two bottom figures starting 156 hours prior to the event (00 UTC 20 June).

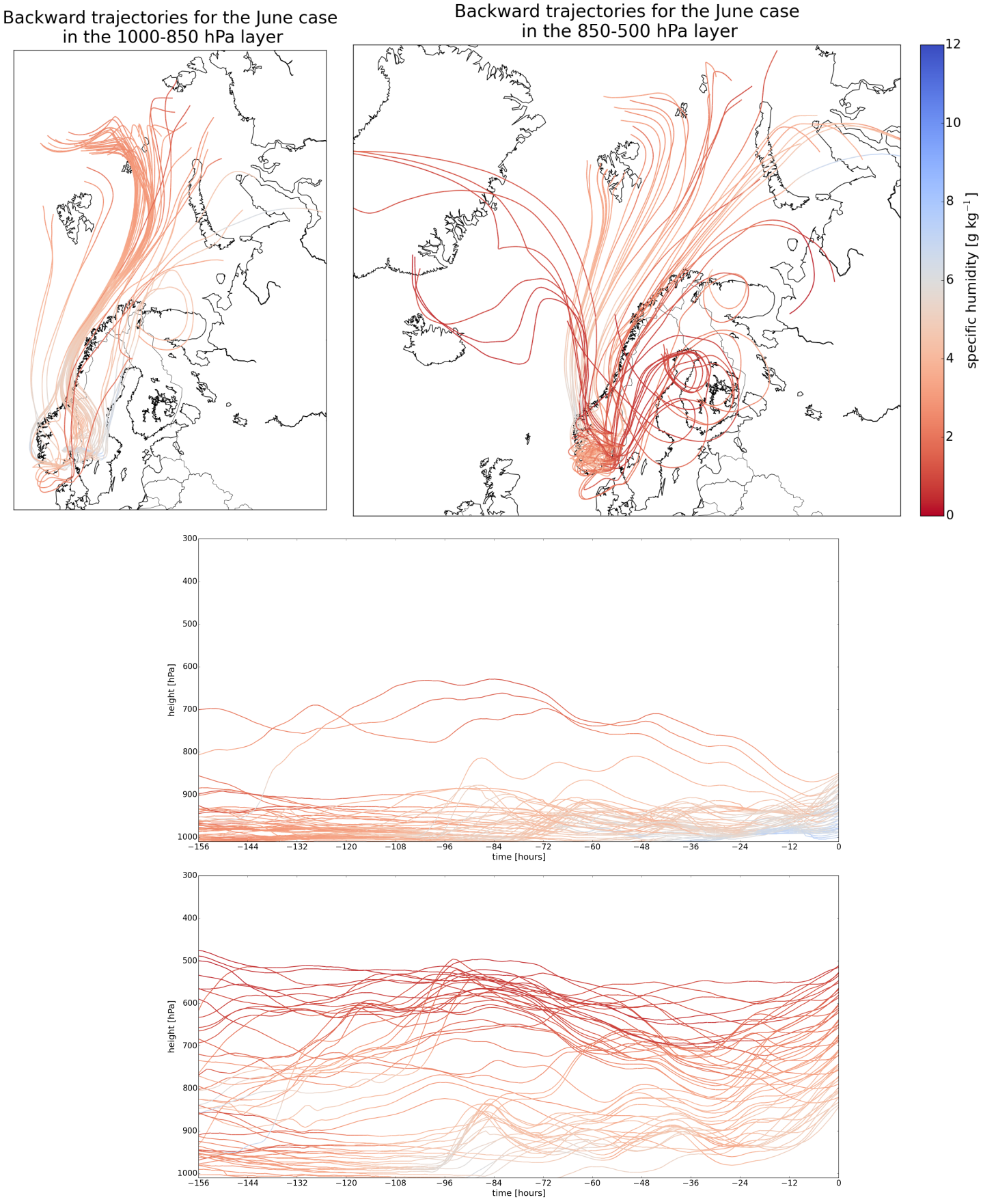

Figure 3.11: Lagrangian trajectories calculated backwards for 12 UTC 26 June - 00 UTC 20 June. The trajectories are colored by specific humidity (in g/kg) for the layers of 1000-850 hPa at the top left and 850-500 hPa at the top right. A vertical view of these trajectories are seen in the two bottom figures starting 156 hours prior to the event (00 UTC 20 June).

The cold air that is brought to southern Scandinavia can be seen in Figure 3.10 by tracking the potential temperature of the air parcels along their path. Backward trajectories in the 1000-850 hPa layer are found to be very instructive in this case. Along their journey, primarily remain low in the troposphere and undergo significant warming in the days before the event. The largest warming seems to take place after the trajectories have approached land and during the afternoon hours as indicated by the orange colors in the vertical view of the trajectories around 24 and 48 hours prior to the starting point, which is at 12:00 UTC. Giving the lack of a strong thermal gradient (as seen in the 1000-500 hPa thickness field), it appears that surface heating is the primary reason for the increase in temperature. In the 850-500 hPa layer, the highest trajectories have their potential temperature below 0 °C and their path appear separated from the Barents sea, which are much lower in altitude and warmer. Whereas most of these trajectories west of Norway remain low in the 850-500 hPa layer and get warmer when they reach the land, the trajectories to the east remain cold and high.
When it comes to specific humidity, it is seen in Figure 3.11 that there is very little moisture transported to Østlandet in the mid-troposphere. The figure is dominated by red and light red colors corresponding to dry air masses. For the lower layer, most trajectories remain relatively dry, but a number in the lowest levels undergo a moistening process over the final 24 hours. An increase in low-level moisture would also be considered a destabilization mechanism, as a raised air parcel would reach consideration lower in the atmosphere and continue to cool with ascent at the moist (as opposed to dry) adiabatic lapse rate; a process that maximizes buoyancy.

3.1.3 Radar images and lighting strikes

Radar images have been provided for the whole day of June the 26th, and five are listed below. In the radar images for the June case, stratiform precipitation is observed northwest of Oslo in the Hedmark county in the morning hours. The weather around the Oslo area was fair with few clouds, though some small convective cells are in development already at 08 UTC in Østfold. It does not take long till more cells form over the mountains in the counties of Buskerud and Vestfold, west of Oslo, and even more around the Moss area. Even though the rainfalls seem to propagate eastwards, the cells are forming and expanding to all directions. By 12 UTC almost the whole Østfold county is covered by rainfall and, as the white and purple reflectivities indicate, they are locally very intense. While the majority of the precipitation is moving to the east with a low speed, new cells are formed on the north side of the system in Moss, a few kilometers south of Oslo. At the same time the thunderstorms west of Oslo have grown larger and intensified and are also moving to the east. The convective cell that greatly affected Oslo formed over the city, although perhaps other thunderstorms nearby could have contributed to its formation with their outflow boundaries. Figure 3.12 shows the time of the heaviest precipitation in Oslo, at 14:52 UTC. The greatest precipitation amounts and the majority of the electric phenomena came between 14:00 and 15:00 UTC. Precipitation was very local in nature, with the amount varying greatly in the city. An enlarged image over Oslo showing the locality of this thunderstorm is shown in Figure 1.6.

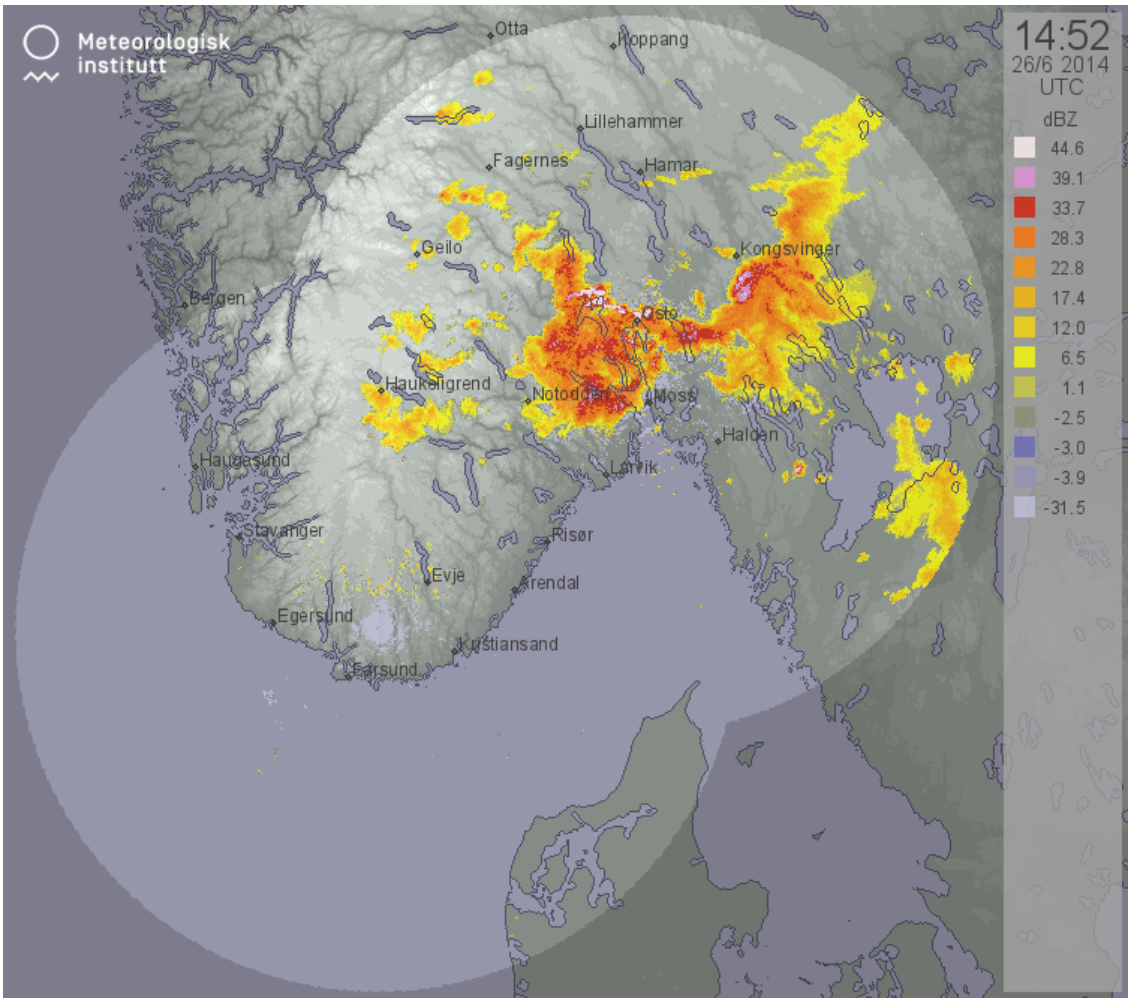

Figure 3.12: Radar image for southeastern Norway during the strongest rainfall in Oslo, at 14:52 UTC. The shadings represent rainfalls. Red, pink and white colors indicate high reflectivity, where the heaviest rainfall is found.

At 14:52 UTC it appears the thunderstorms west of Oslo and the thunderstorms south of Oslo have merged. However, soon after merging, the convective rainfall transformed into stratiform and the lightning activity ended at around 15:00 UTC. The rain continued until midnight and onwards, but with low intensity. So the thunderstorm itself was short-lived, but the damage caused by it was nonetheless great.
The direction and formation of the convective cells can also be seen by the location of the lightning strikes over the time. Figure 3.14 shows that the first lightning strikes appeared in the mountain region west of Oslo and south southeast of Oslo, in Østfold. As time progresses, the red crosses west of Oslo start propagating eastwards towards Oslo taking on an orange color (which is at around 14:00 UTC). At the same time lightnings are approaching Oslo from south southeast but only moments after lightning strikes appeared in the city of Oslo, all electric phenomena disappeared. There are no yellow crosses in the wider area of Østlandet meaning that all thunderstorm activity ceased by 15 UTC.

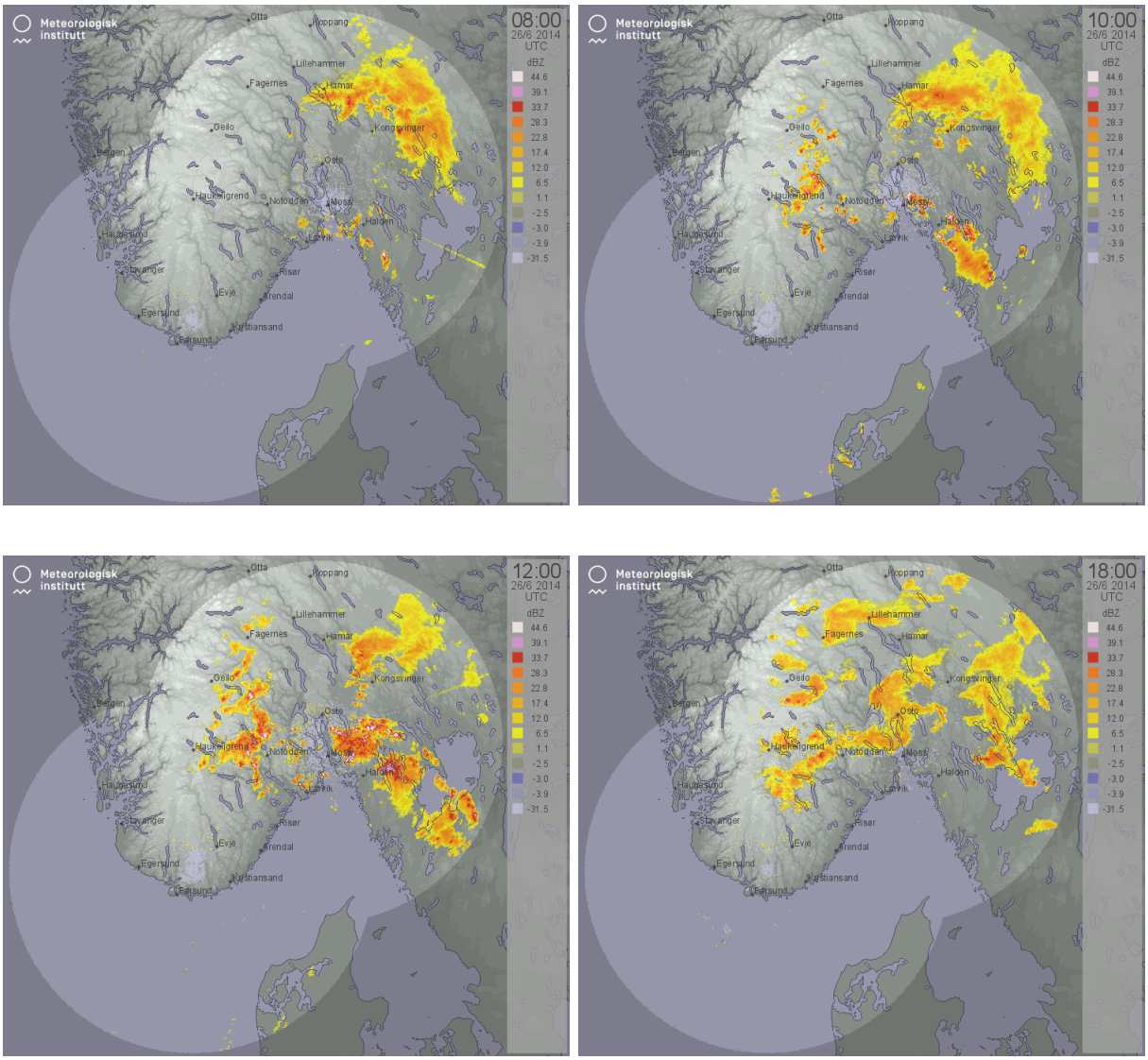

Figure 3.13: Radar images for southeastern Norway at 08:00, 10:00, 12:00 and 18:00 UTC. The shadings represent rainfalls. Red, pink and white colors indicate high reflectivity, where the heaviest rainfall is found.

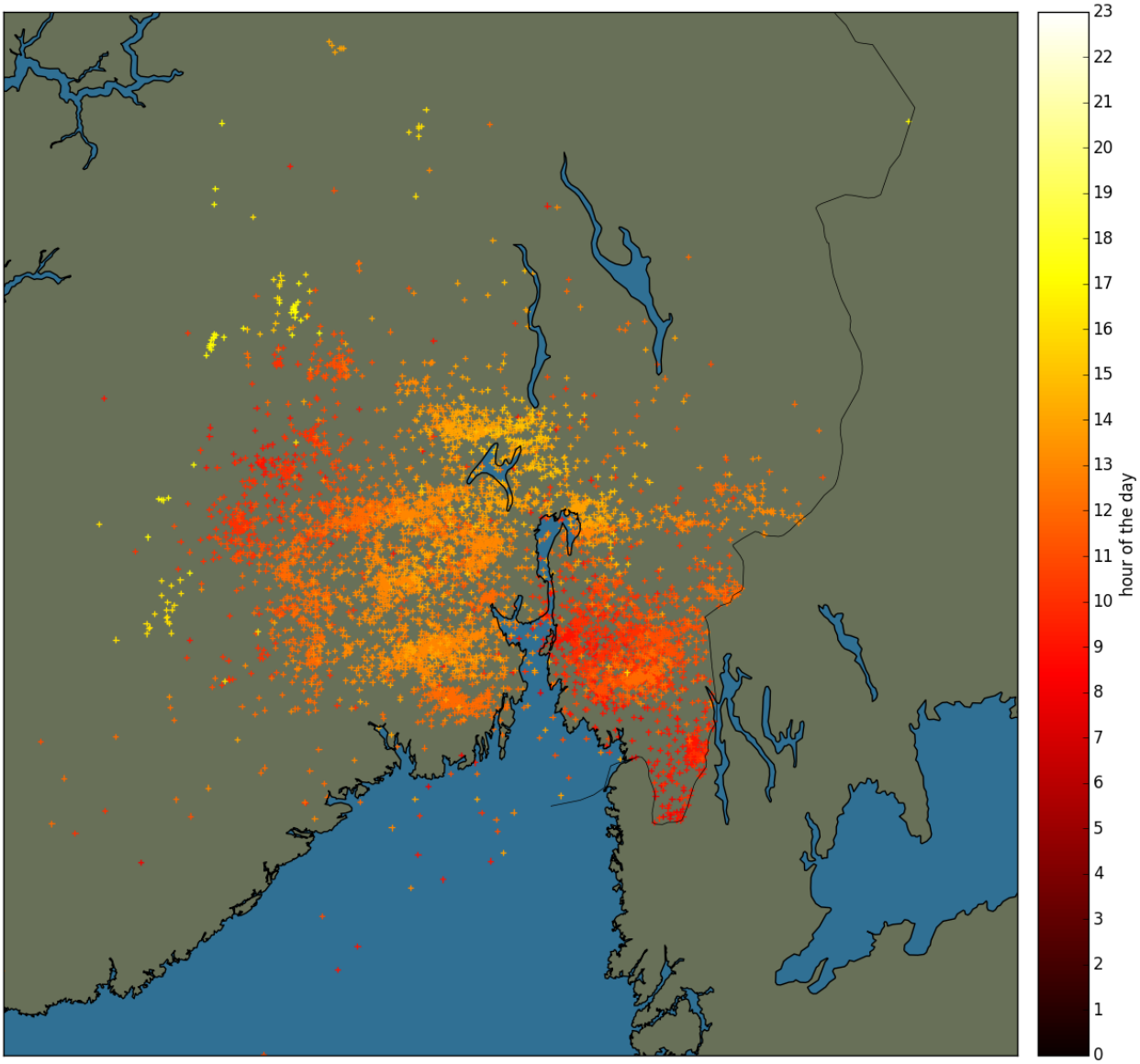

Figure 3.14: Lightning strikes for 26 June 2014. Lightning strikes are colored by hour of the day in UTC. Dark red crosses correspond to lighting strikes early in the day and yellow or white crosses are lightning strikes during the evening hours.

3.2 August

3.2.1 Large scale circulation

The August event provides a stark contrast to the situation in June. Starting from 29 July with Figures 3.15 and 3.16, the first obvious difference from the June case is how much warmer it is throughout the European continent: the values of the potential temperature on the DT are significantly larger on average and the cold air is concentrated farther to the north. Another significant difference is the amount of moisture in Europe. The atmosphere is much more humid than in June with high values of TCWV throughout most of continental Europe as well as over the Atlantic ocean (Figure 3.16 top). According to the satellite image, these warm and humid air masses are associated with thunderstorm activity in central, eastern and northeastern Europe (Figure 3.16 bottom).
One similarity with the June case is the presence of a significant cyclone and anticyclone pairing leading to strong low-level flow. However, given their locations between Iceland and Great Britain and over northeast Scandinavia respectively, flow with a southerly component is observed. By 31 July, in an association with the forming of a second low pressure system of west coast of Norway results in intense southerly flow, forming a river-like advection of warm and humid air from the Mediterranean area (Figure 3.17). A very apparent line of deep convection from the Balkan region and all the way up to Northern Scandinavia associated with this flow is observed in the IR imagery in Figure 3.18. At the same time, moisture approaches Norway from southwest with the help of a low pressure between Great Britain and Iceland.
A couple of days later, on 2 August, the low pressure center west of Norway has weakened, but another low center has formed over Great Britain and another southwest of Iceland. Both form along a baroclinic zone, as indicated by the 1000-500 hPa thickness gradient (see Figure 3.19). This is in contrast with the importance of the occluded cyclone in the June case. As pertains to moisture, the low-level flow pattern is conducive to moisture flow into southern Norway, with moisture being transported from both the Atlantic ocean and the Balkan region. The regions of moisture transport appear to merge at about this time. With strong temperature gradients in northwest Europe and high moisture content, as seen on August the 2nd, the possibility for deep convective activity was present and is confirmed via an examination of the IR imagery.

On 3 August, the pattern remains similar according to Figures 3.21 and 3.22 (low pressure to the west, high pressure to the east and strong warm moist advection into southern Scandinavia). Significant thunderstorm activity is observed in southern Scandinavia and convective cells are spotted in central Europe moving northwards.

The last four figures for our August case show the same surface pressure pattern as the day before. The southerlies are consistent throughout the whole troposphere and the advection of warm air can be seen by the elevated tropopause and the thick 1000-500 hPa layer. An elevated tropopause is observed over southern Scandinavia, once again in contrast to the June case. High in temperature and rich in moisture air masses are now dominating the entire region. The low pressure in Great Britain has now moved closer to Norway and slightly weakened. The presence of a front brought with this low is indicated by the strong LLV in southern Sweden. And with the help of the thickness contours showing colder air masses approaching west of Norway, it is indeed a cold front like shown in the analysis map in Figure 1.7 which can serve as a convergence zone to trigger deep convection. The severe thunderstorms that affected most of Norway are already formed at 12:00 UTC as seen in the satellite image.

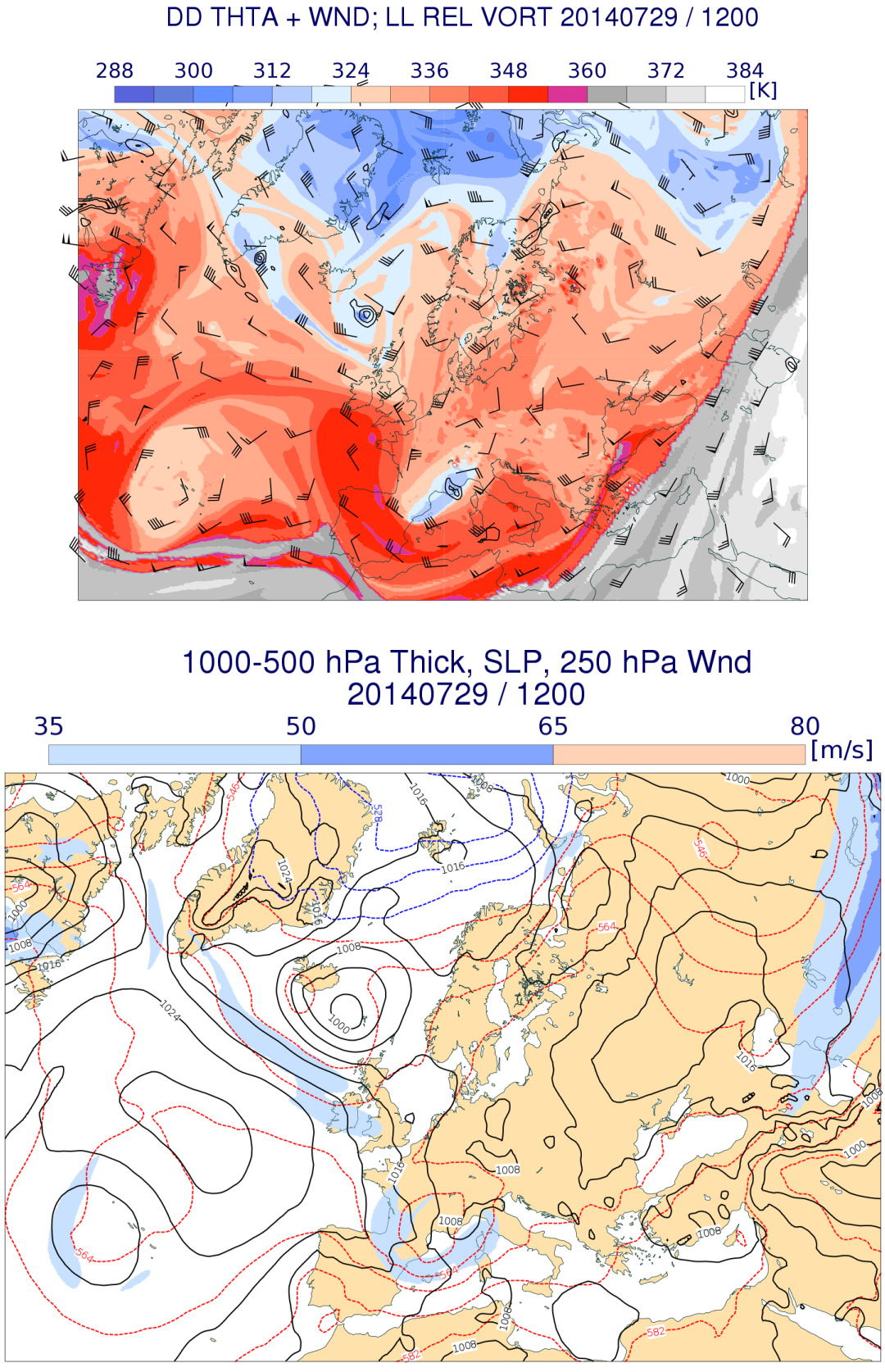

Figure 3.15: Weather maps for 12 UTC 29 July. Top panel: potential temperature (K, shading) and total wind speed (m/s, wind barbs) on the 2 potential vorticity unit surface, and the 925-850 hPa average low level relative vorticity (s^{-1}, black contours, only positive values greater than 10^{-4} shown with a contour interval of 0.5×10^{-4}). Bottom panel: 250 hPa wind speed (m/s, shading), mean sea level pressure (hPa, black contours, contour interval 4 hPa) and the 1000-500 hPa thickness (dm, dashed contours, contour interval of 6 dm). Data source is ECWMF operational analysis.

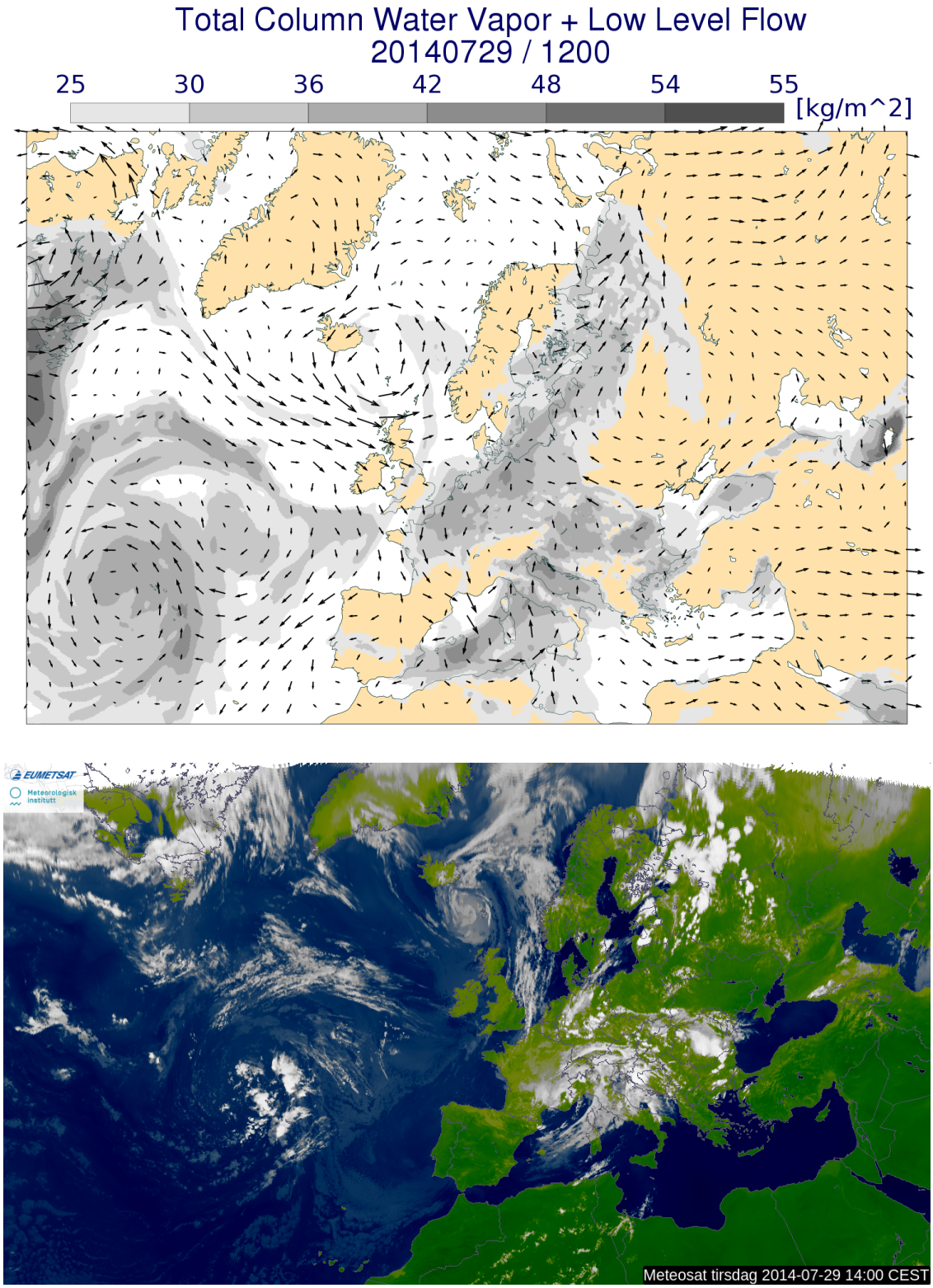

Figure 3.16: Weather maps for 12 UTC 29 July. Top panel: total column water vapor (kg/m^2, shading) showing the total water vapor integrated vertically and total wind speed (m/s, wind arrows) on the 925 hPa pressure surface. Bottom panel: IR satellite image based on the clouds' reflectivity. White colors indicate high clouds and gray/fade colors indicate low clouds.

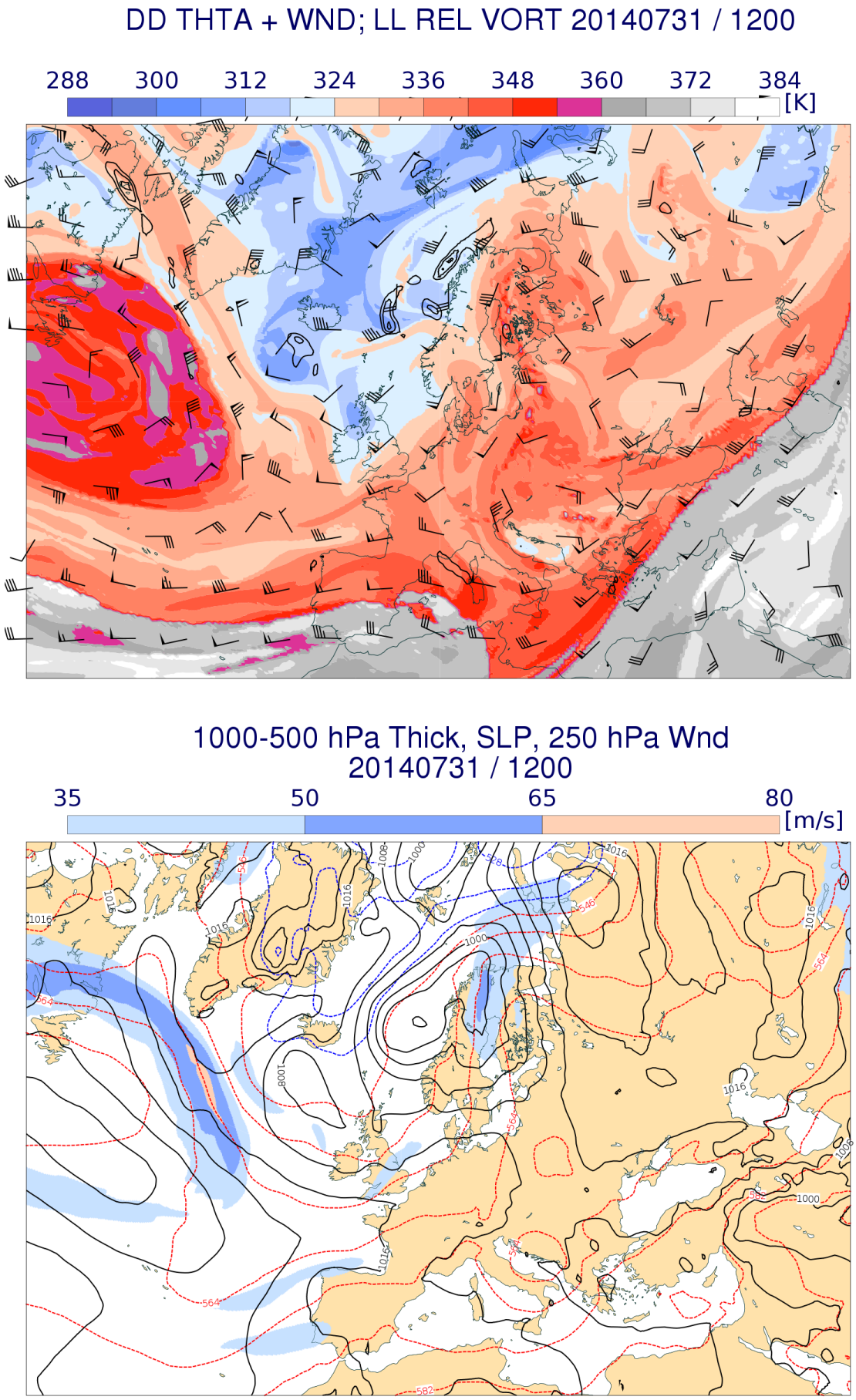

Figure 3.17: Same as Figure 3.15 except for for 12 UTC 31 July.

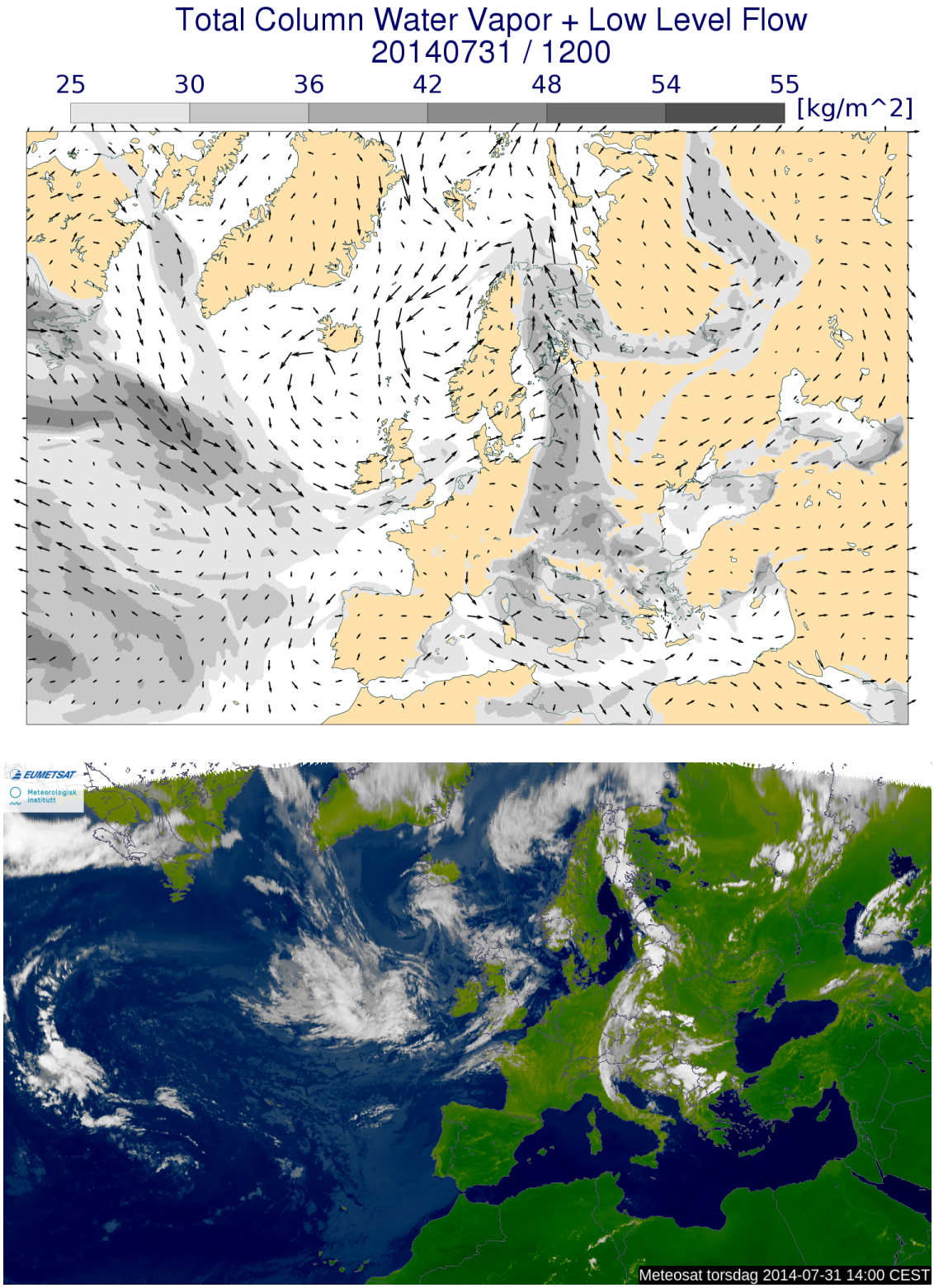

Figure 3.18: Same as Figure 3.16 except for for 12 UTC 31 July.

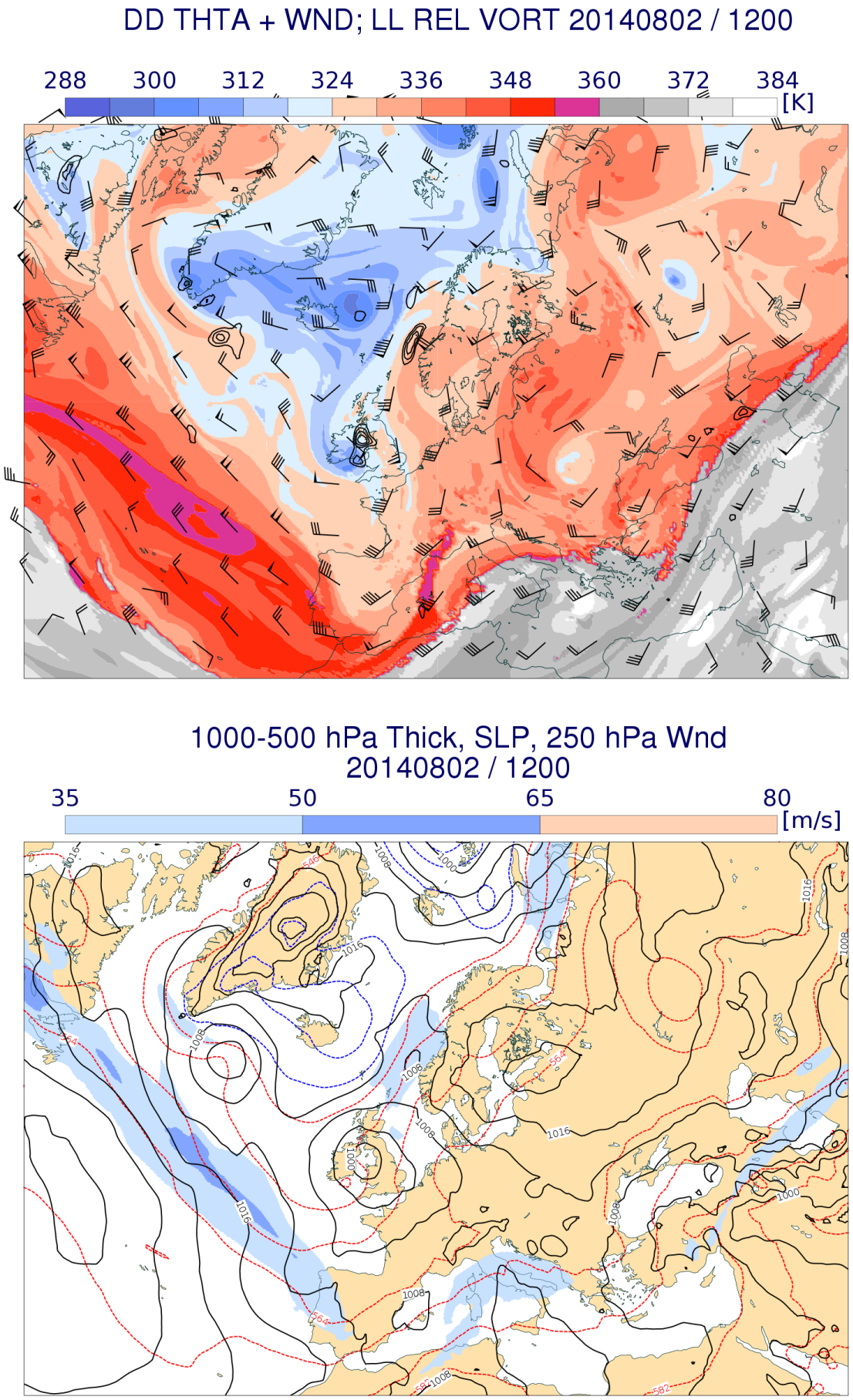

Figure 3.19: Same as Figure 3.15 except for for 12 UTC 2 August.

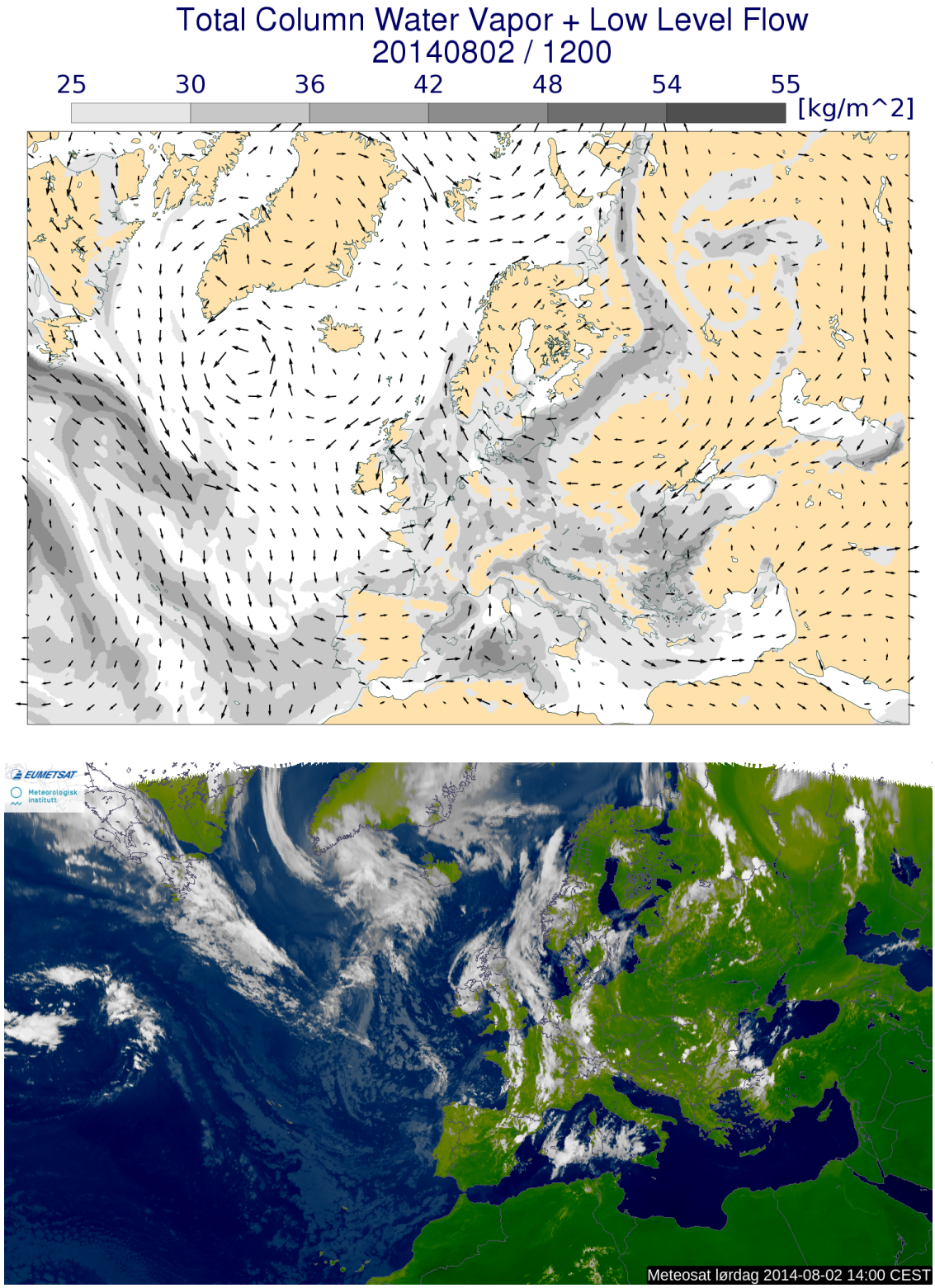

Figure 3.20: Same as Figure 3.16 except for for 12 UTC 2 August.

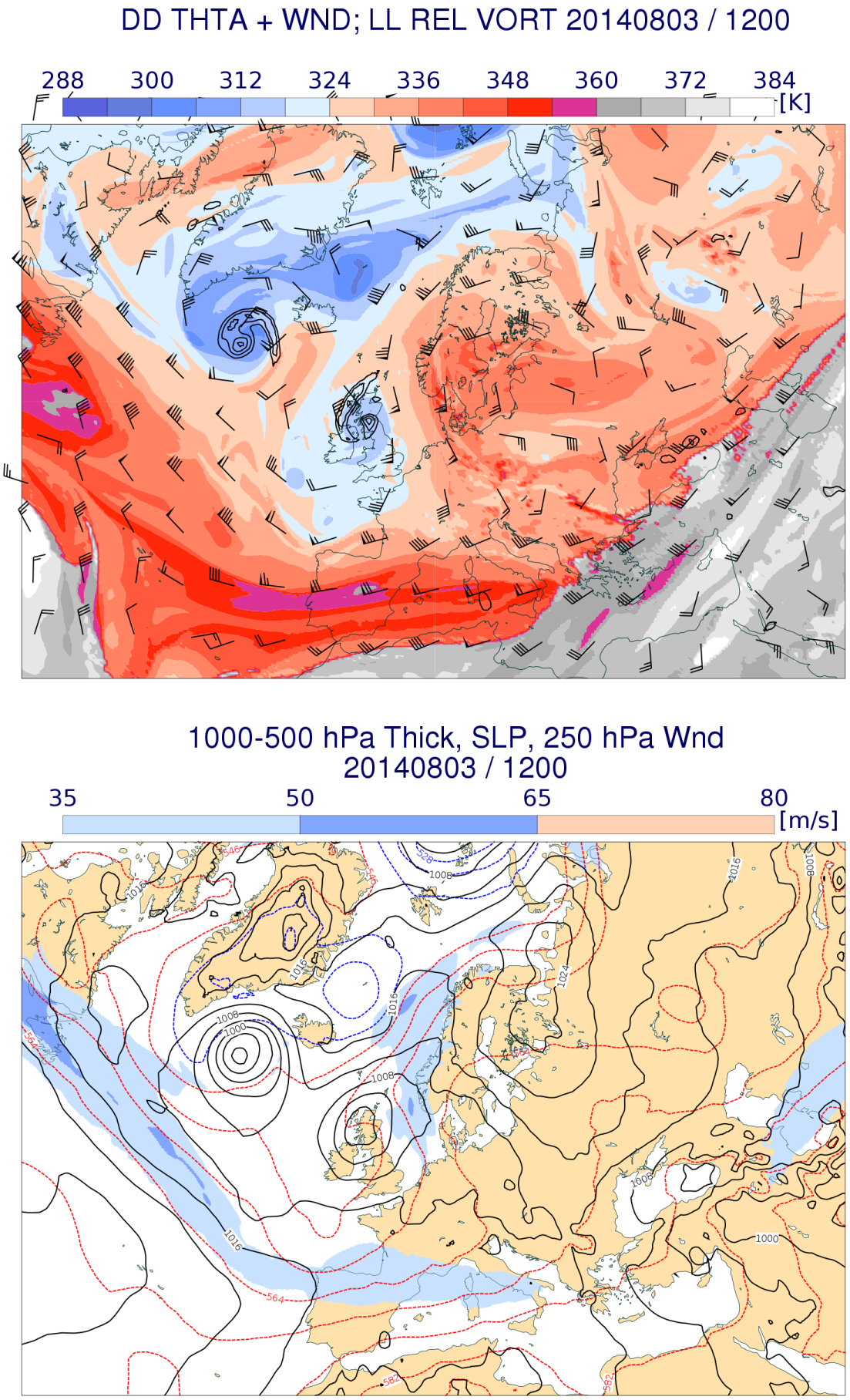

Figure 3.21: Same as Figure 3.15 except for for 12 UTC 3 August.

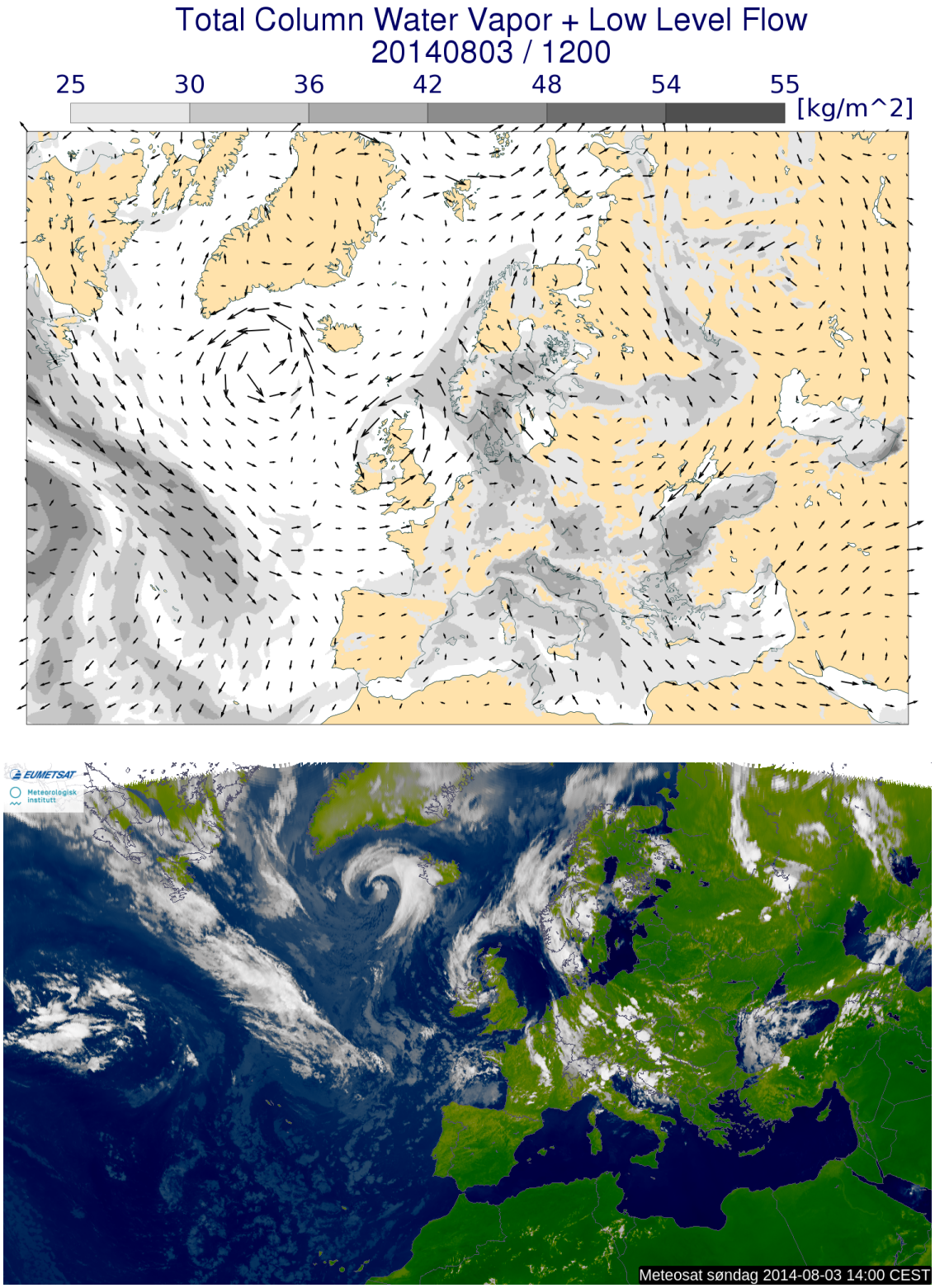

Figure 3.22: Same as Figure 3.16 except for for 12 UTC 3 August.

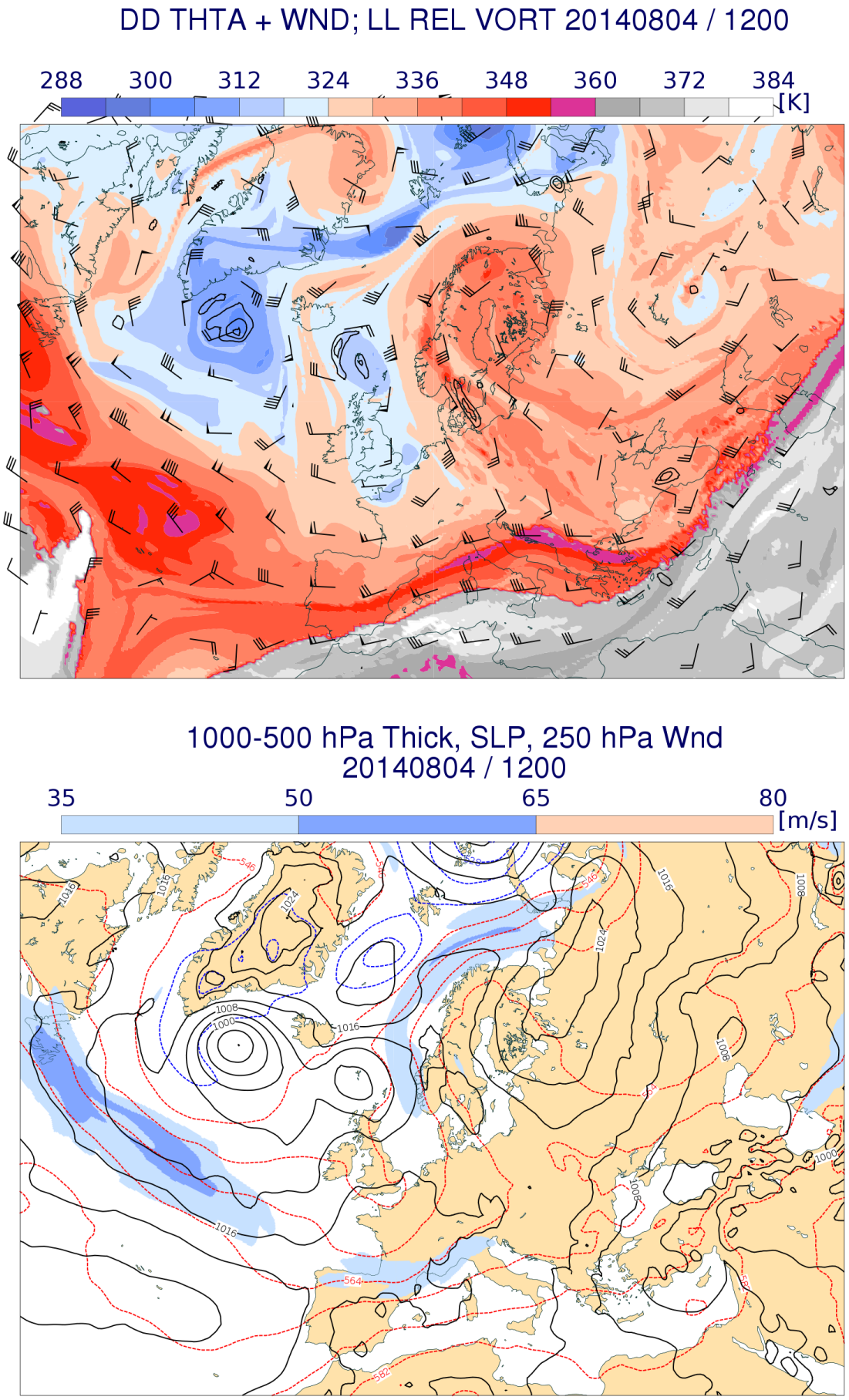

Figure 3.23: Same as Figure 3.15 except for for 12 UTC 4 August.

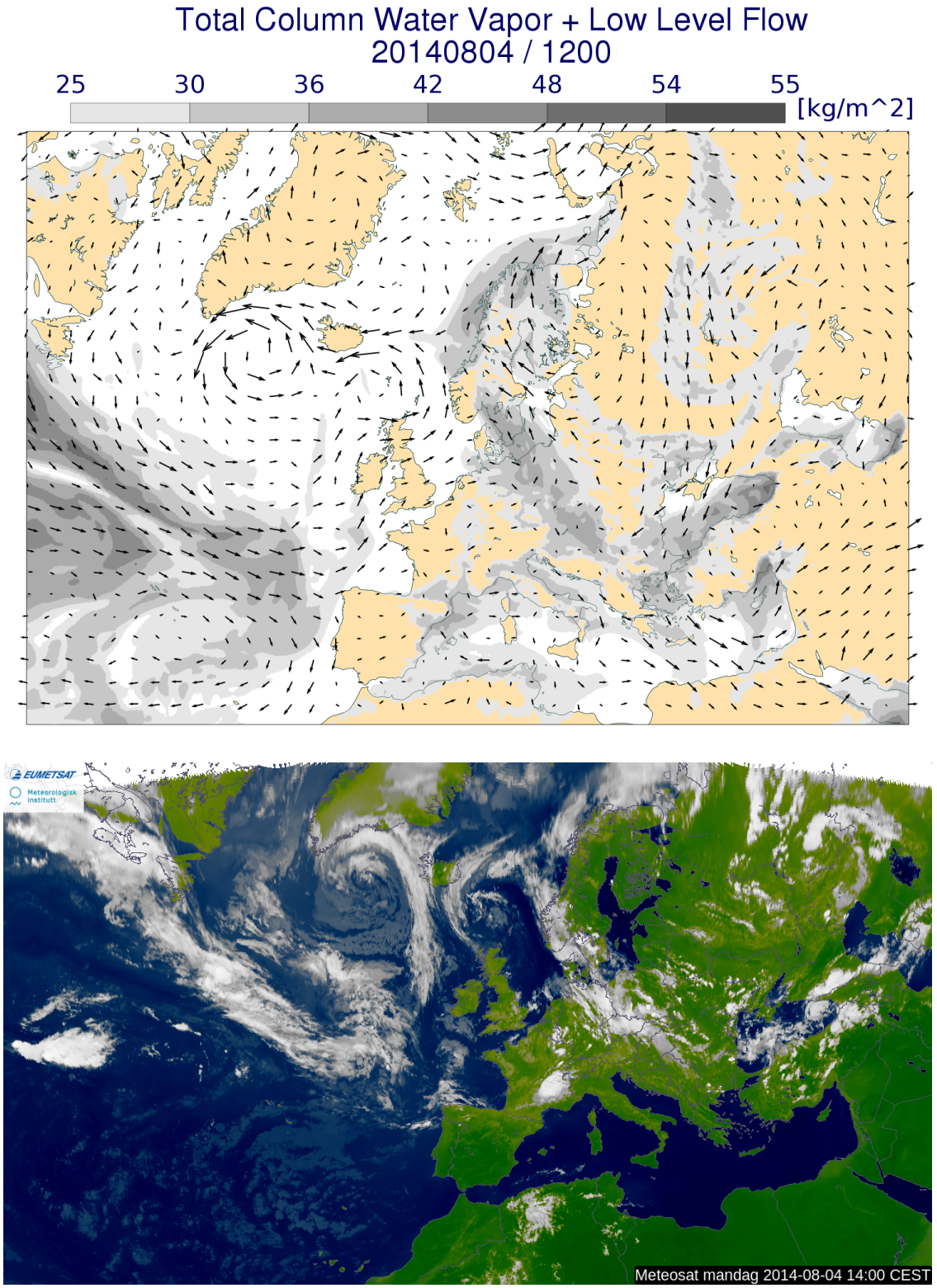

Figure 3.24: Same as Figure 3.16 except for for 12 UTC 4 August.

3.2.2 LAGRANTO trajectories

The trajectory paths for the August case are, like the large scale circulation, in contrast to those of the June case. No trajectories originate from north of Oslo, as anticipated from the the proceeding weather maps. In the bottom layer, the source regions are split to the west and east. The trajectories from the west have come from the Atlantic ocean, west of Great Britain and south of Iceland. The trajectories coming east of Oslo, have their source region in the Balkan region, most of them farther east to the north of the Caspian sea. More or less, the same source regions are seen for the 850-500 hPa layer. All trajectories in both layers are propagating in the lower troposphere except for some that originated just west of Ukraine at a height of 500 hPa which also remained at that height.

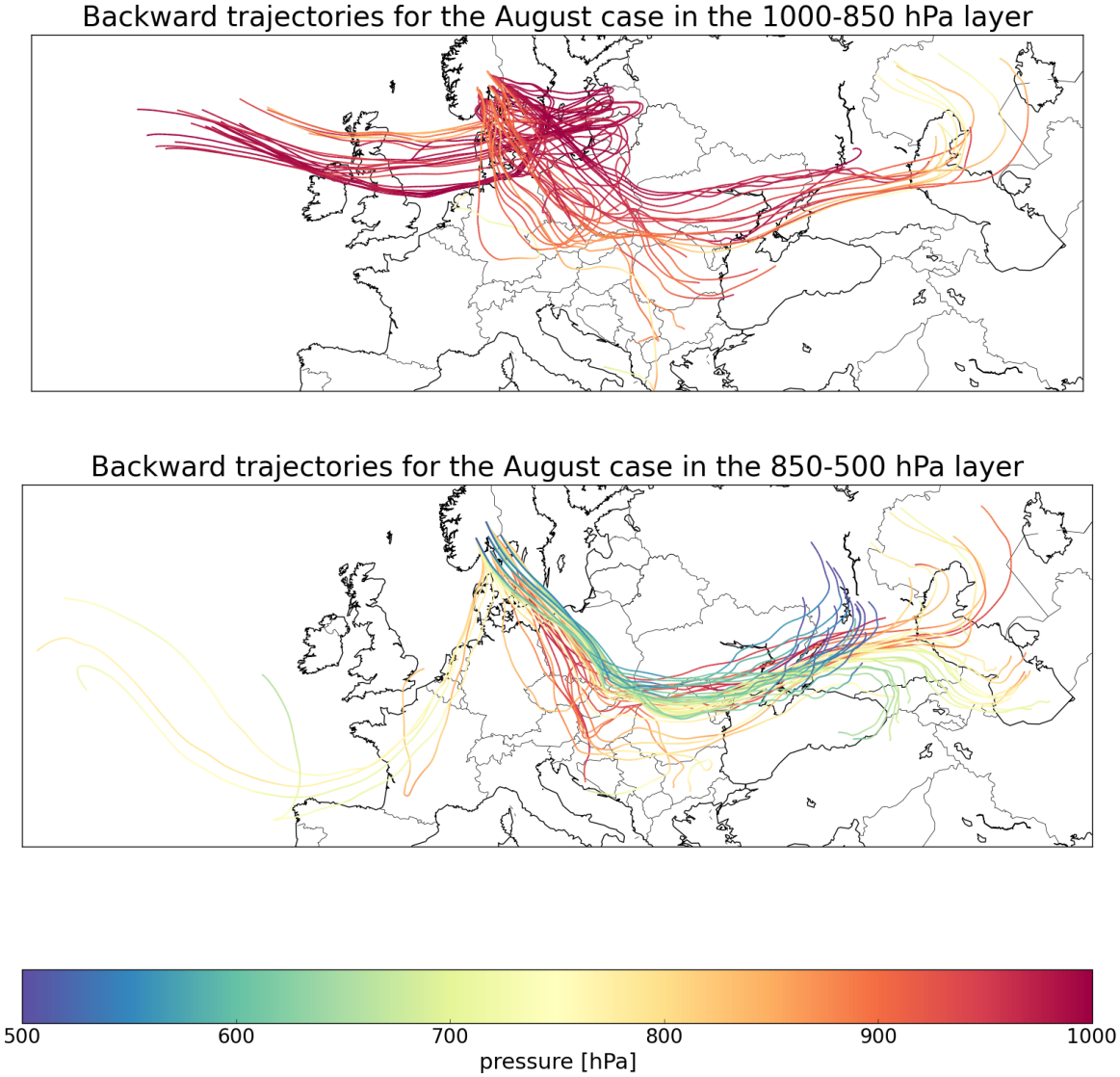

Figure 3.25: Lagrangian trajectories calculated backwards for 12 UTC 4 August - 00 UTC 29 July. The trajectories are colored by height for the layers of 1000-850 hPa at the top and 850-500 hPa at the bottom.

These trajectories are also the coldest ones with negative potential temperature all the way to southern Norway as seen on Figure 3.27. The rest of the trajectories in the 850-500 hPa layer have temperatures between 10 °C and 15 °C, which was the maximum temperature in the bottom layer for the June case. The mean potential temperature of the trajectories in the 1000-850 hPa layer

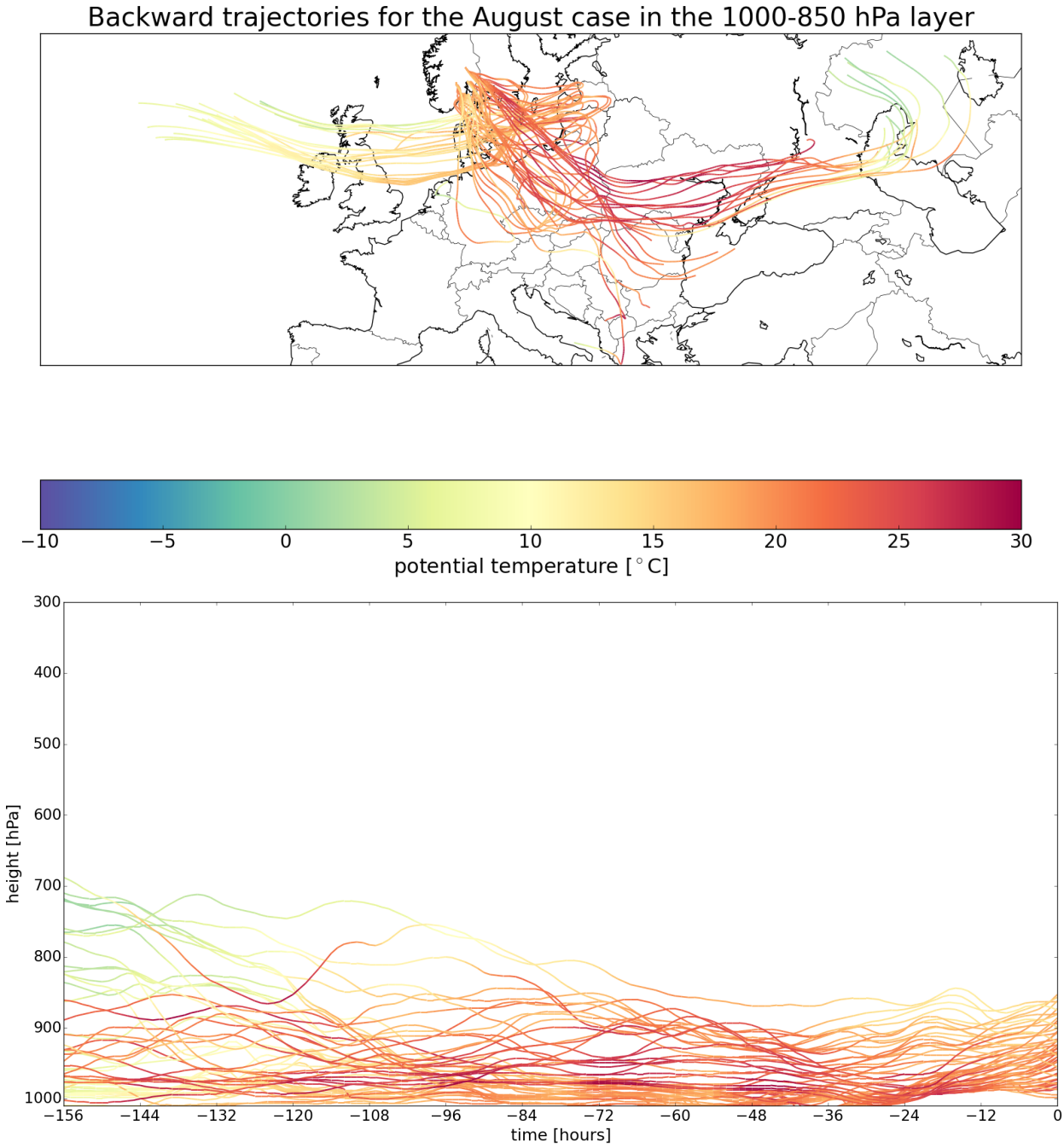

Figure 3.26: Lagrangian trajectories calculated backwards for 12 UTC 4 August - 00 UTC 29 July. The trajectories are colored by potential temperature (in °C) for the layer of 1000-850 hPa. A vertical view of these trajectories is seen at the bottom figure starting 156 hours prior to the event (00 UTC 29 July).

is above 20 °C and reach 30 °C in the bottom 100 hPa. The coldest trajectories in the 1000-850 hPa layer are the ones starting north of the Caspian sea, but eventually get warmer when they reach the European continent. As the trajectories approach Scandinavia, they are affected by surface heating as seen by those closest to the surface around 24, 48 and 72 hours prior to the event analyzed.

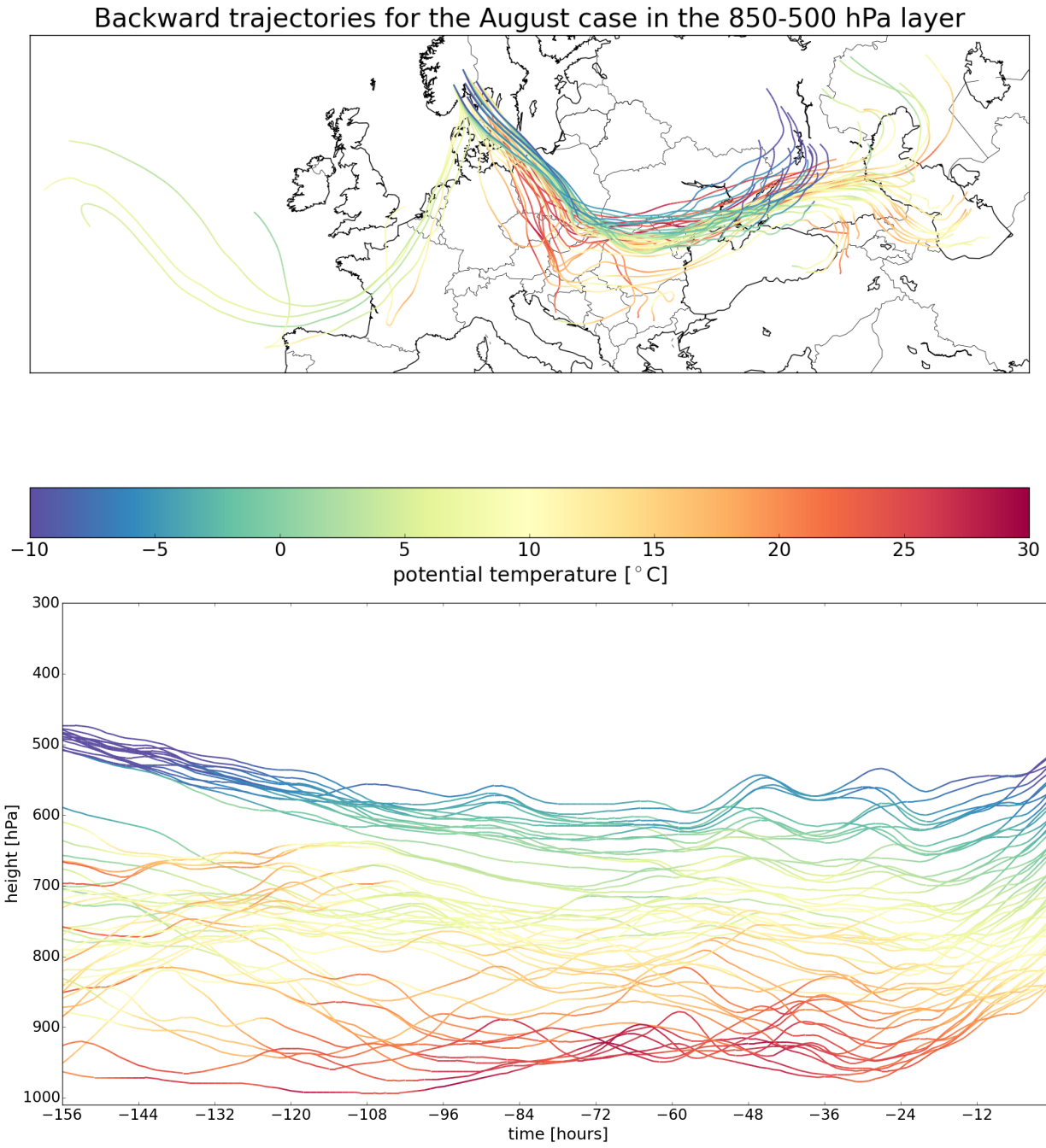

Figure 3.27: Lagrangian trajectories calculated backwards for 12 UTC 4 August - 00 UTC 29 July. The trajectories are colored by potential temperature (in °C) for the layer of 850-500 hPa. A vertical view of these trajectories is seen at the bottom figure starting 156 hours prior to the event (00 UTC 29 July).

When it comes to specific humidity the results are again in contrast to the June case. This is to be expected as the figures in the previous subsection showed large amounts of TCWV in the atmosphere throughout the European continent. Apart from the top of the 850-500 hPa layer, the rest of the layer is actually more humid than the bottom troposphere in the June case. And in the 1000-850 hPa layer, the values of specific humidity are approximately twice as large as the values in the same layer in June. The main source region of this moisture is the Balkans and although the air masses coming from far east are dry, this changes when they approach central Europe. The

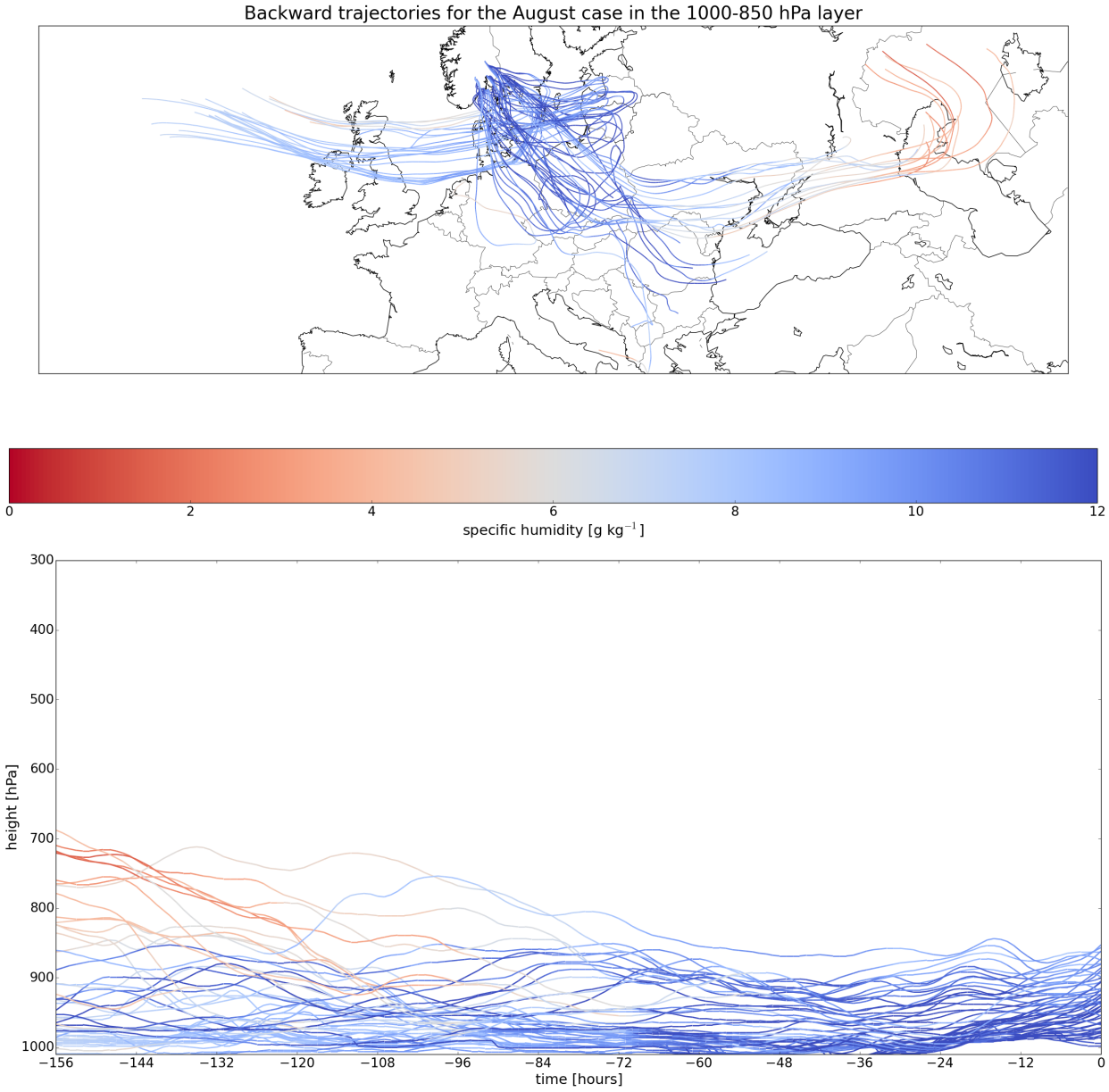

Figure 3.28: Lagrangian trajectories calculated backwards for 12 UTC 4 August - 00 UTC 29 July. The trajectories are colored by specific humidity (in g/kg) for the layer of 1000-850 hPa. A vertical view of these trajectories is seen at the bottom figure starting 156 hours prior to the event (00 UTC 29 July).

ocean air coming from the Atlantic is humid as well, but the maximum values are reached after performing a 'loop' over the Baltic countries.

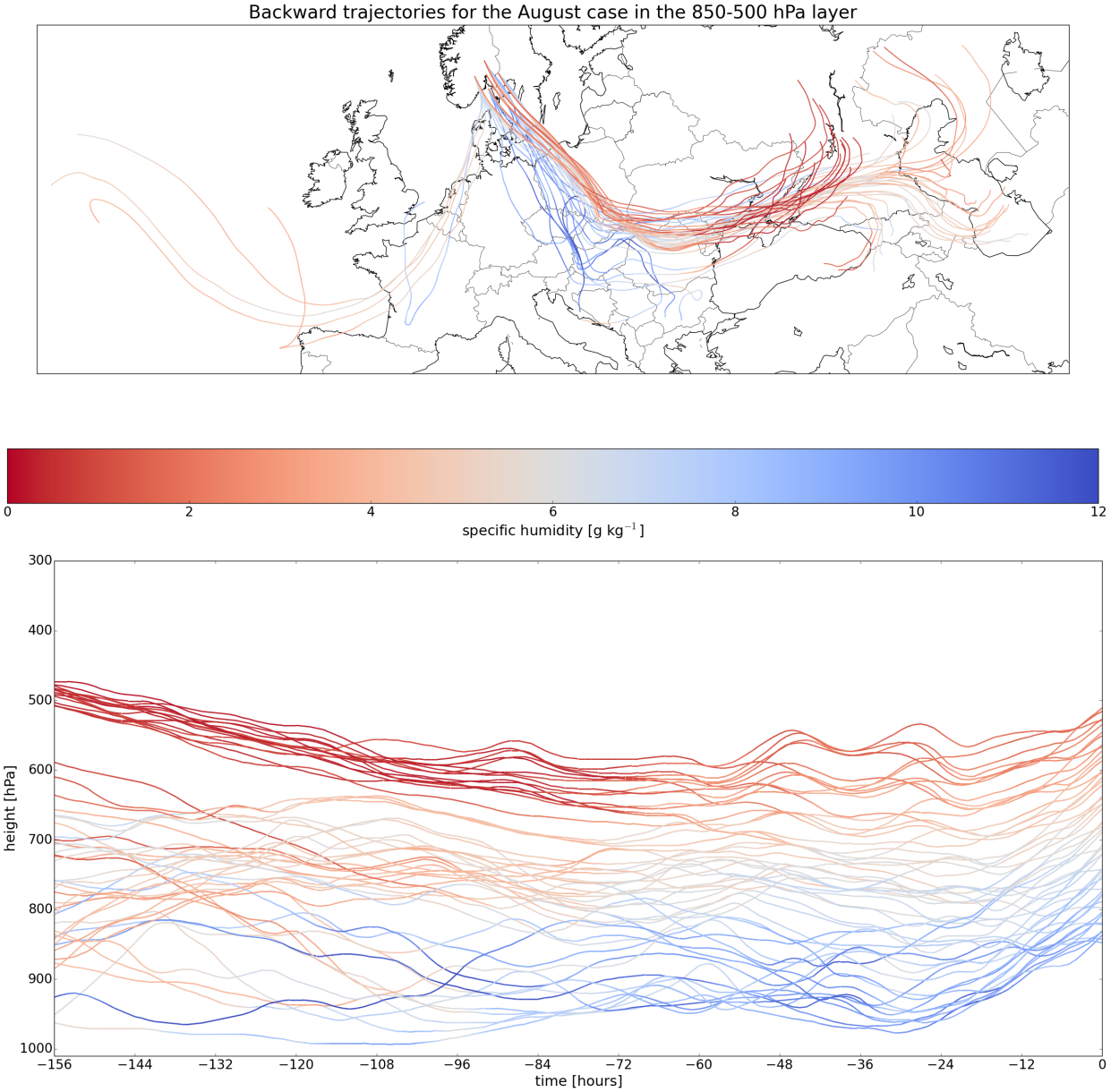

Figure 3.29: Lagrangian trajectories calculated backwards for 12 UTC 4 August - 00 UTC 29 July. The trajectories are colored by specific humidity (in g/kg) for the layer of 850-500 hPa. A vertical view of these trajectories is seen at the bottom figure starting 156 hours prior to the event (00 UTC 29 July).

3.2.3 Radar images and lighting strikes

On August the 4th, many convective cells are seen moving north northwest, in agreement with the flow observed in the weather maps in Figure 3.23 and 3.24 and the Lagrangian trajectory analysis.

Most of the southeastern part of Norway is affected and at 10 UTC the organized convective system being examined in this case is observed in the Radar imagery. The system is moving along the Swedish coastline and other intense well-organized thunderstorms are moving along the borders to Sweden. The convective system affected the Oslo area from approximately 15 UTC to 16:30 UTC and the eastern parts outside of Oslo received the heaviest precipitation. At 15:45 UTC the system has an interesting shape in the Radar imagery. It looks like a tail is stretching from Oslo and then bent all the way to the Swedish border. And then a dry spot with precipitation curled around it before it disappears moments later. In the animation of the radar images a slight rotation of the system is observed from 15 UTC till 18 UTC. After the thunderstorm's departure, the whole south of Norway is free of rainfall.

This system traveled much farther and lived much longer than the thunderstorm in June. The thunderstorm in June lived only a couple of hours and never left the area of Oslo.
Because of the low pressure located near Norway these days, the thunderstorm activity lasted for a couple of days and therefore there are provided figures for lightning strikes for 4 August, but also for 3 and 5 August 2014. On August 3rd, thunderstorm activity is spotted already at midnight hours over the sea, west of southern Norway. Those thunderstorms have a south to north direction, but at the same time all of them are advected northeastwards moving over the whole coastline before reaching the boarders to Sweden at the end of the day. Now the next day, the direction of the thunderstorm paths are different. The thunderstorms that formed in southern Sweden (the lightning data provided is only for Norway), entered Norwegian territory around noon and then propagated in a bow formation ending up in northern Norway after midnight (the same thunderstorms are depicted with the black colors as midnight had passed). As such the group of thunderstorms lasted for approximately 15 hours. Another long lasting group of thunderstorms is seen in northern Norway in the afternoon hours of August the 5th before dissipating over the ocean during the evening. This is rare for such high latitudes.

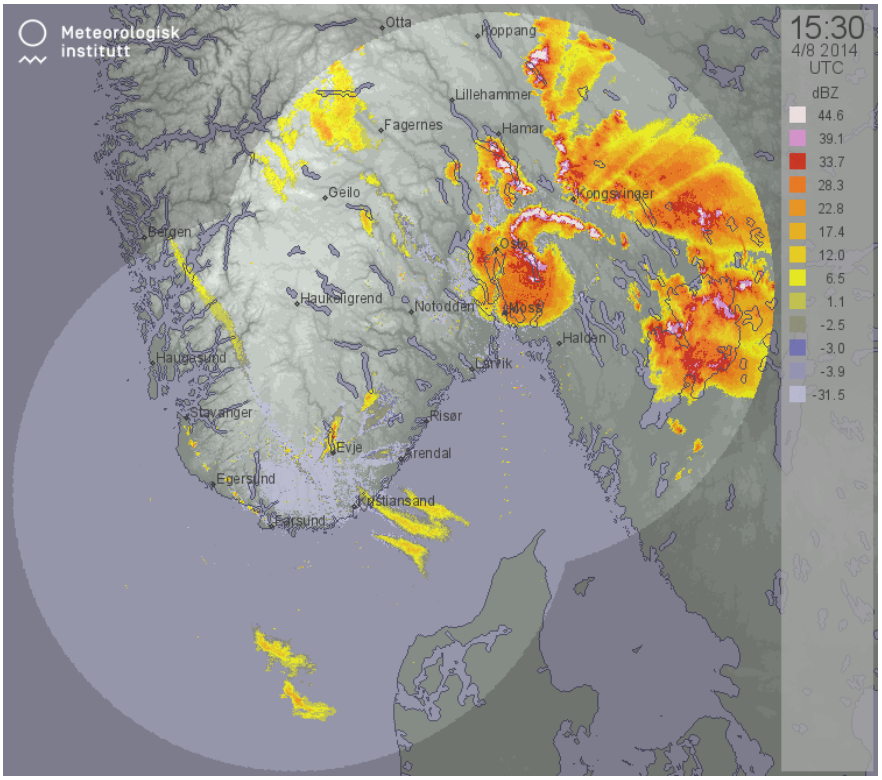

Figure 3.30: Radar image for Southeastern Norway showcasing the cell's "tail" at 15:30 UTC. The shadings represent rainfalls. Red, pink and white colors indicate high reflectivity, where the heaviest rainfall is found.

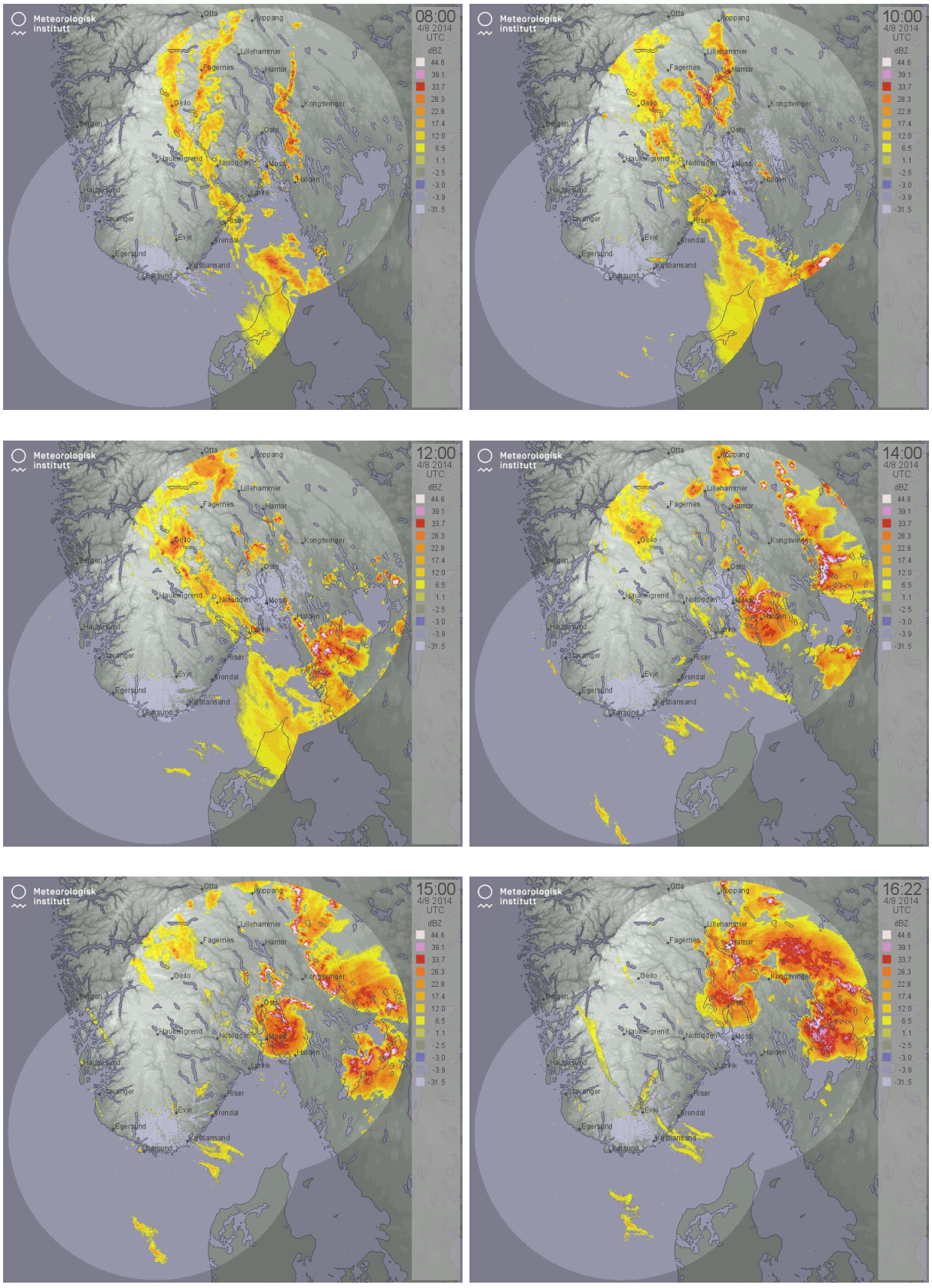

Figure 3.31: Radar images for Southeastern Norway at 08, 10, 12, 14, 15 and 16:22 UTC. The shadings represent rainfalls. Red, pink and white colors indicate high reflectivity, where the heaviest rainfall is found.

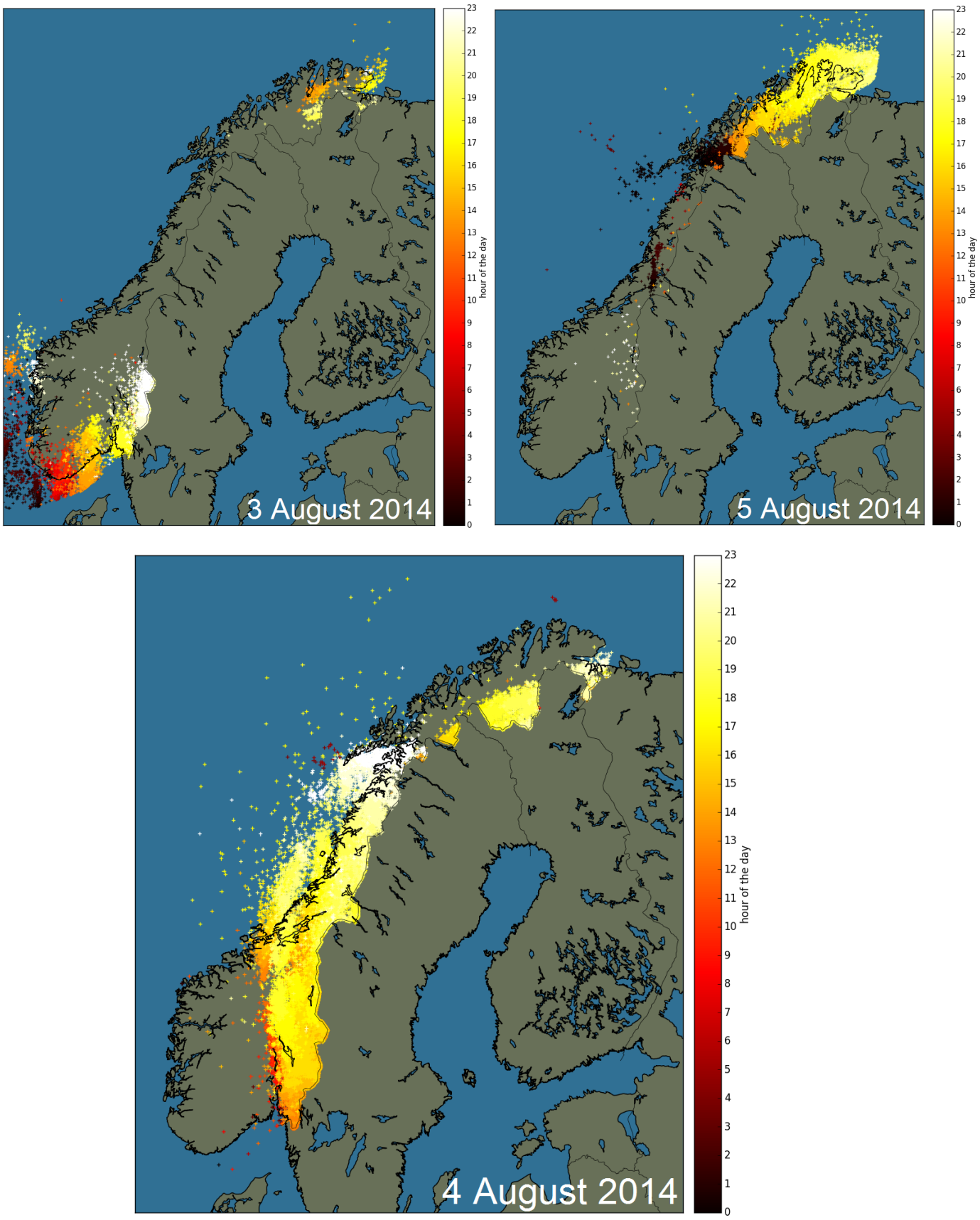

Figure 3.32: Lightning strikes for 3 August 2014 at the top left, 4 August 2014 at the bottom and 5 August 2014 at the top right. Lightning strikes are colored by hour of the day in local time. Dark red crosses correspond to lighting strikes early in the day and yellow or white crosses are lightning strikes during the evening hours.

3.3 Stability indices and moisture

The convective available potential energy (CAPE) is one of the most commonly used stability indices to determine the intensity of deep convection. When comparing the figures for the two cases, it might look as if the CAPE values are not noteworthy for the June case, but the fact is that the values for the August case are extremely high. The yellow colors for June the 26th indicate CAPE values as high as 2000 J/kg, which is unusually for high latitudes. August however, is an even more remarkable situation where the values of CAPE even surpass 3000 J/kg in large parts of central Scandinavia at 12 UTC. Such values are very rare and extreme for Scandinavia. Even early in the morning and in the evening the CAPE values are comparable to the values of the June case at 12 UTC which helps to explain why those thunderstorms had such a long lifespan and were able to travel so far north.
The rarity of these values are depicted in the figures of CAPE anomaly, where the the values have been compared to the period of 1979-2015. Again, we see that the August case is the one that stands out and the region with the highest anomalies is coinciding with the formation area and path of the severe thunderstorms during that day. The CAPE anomaly for the June case is not as impressive, but still reached 600 J/kg above normal where multiple convective cells formed. It is interesting and should be noted how the thunderstorms that formed did so only within the areas of positive anomaly. No thunderstorms were formed where there was no positive CAPE anomaly.
The K-index is related to the probability of occurrence of a thunderstorm. In most areas around Oslo, the K-index is at 25-30 with some faint yellow spots indicating values of 30-35. This implies that widely scattered/scattered thunderstorms are expected, which was the case that day. In the August case the map is filled with much more yellow and even orange colors. Those values indicate the probability of numerous thunderstorms. The Radar imagery identified many cells formed that day and that the highest values of the K-index are seen along their path. High values are observed throughout the whole day in both cases (not shown).
For the Showalter stability index (SSI) the warmer the particle is than its environment, the lower will the SSI value be (more severe thunderstorms). The lifted-index (LI), which is not available by Arome-MetCoOp and not shown in this thesis, is similar to SSI, with the only difference being that LI uses a near-surface parcel rather than a parcel at 850hPa. Already from the morning hours of June the 26th, values of -3 to -6 are observed in the Oslo area. These values are equivalent to severe thunderstorms in this area. At 12 UTC, the values are still as high. In the August case, it is not just Southern Scandinavia that is covered with low values of SSI, but the whole Scandinavia in general which is another example of how this case is much larger in scale. The values are between -3 and -6 here as well, but at 18 UTC the SSI values go even lower than -6 (not shown) in middle Norway meaning that even tornadoes are possible.
The maps of total totals (TT) are quite interestingly different from the previous stability indices. Now once again the whole Scandinavia is covered in large values in the August case case which indicates the possibility for severe thunderstorms. However when it comes to Southern Scandinavia, it is the case of 26th June that has the highest values of TT. Almost the whole region, a region larger than that in August, has values above 50.
Finally, out of all the indices, the SWEAT index will be the most interesting to look at because of the terms in its equation. As previously mentioned, this index includes information about temperature, humidity and the wind field. Of all the indices presented, this is the only one that takes the wind field into account, a really important ingredient for the development of well-organized, long-lasting severe thunderstorms. The highest values for the June case reach between 300 and 350 a bit south of Oslo. This is an area where plenty of cells formed at noon and later affected the area of Oslo.

No thunderstorms formed where the SWEAT index was below 150, the threshold for thunderstorm development, as seen in the radar images for southeastern Norway. Once again, the August case stands out. Almost the whole of Scandinavia has values exceeding 150 and a maximum above 350. The highest values at 12 UTC are found along the coastline of Sweden, south of Oslo, the same area where the most severe convective cells where located before passing Oslo. If the SWEAT index had exceeded 400, then tornadic thunderstorms would be expected, but this value is more relevant for the United States than Europe. After all, funnel clouds and severe winds were actually observed in Sweden (according to the European Severe Weather Database[1]).
For the figures of the specific humidity at 1000 hPa, the scale is not the same for both cases. This is because of the amount of moisture being so much larger in the August case. This is in agreement with what the trajectories and the TCWV values showed previously. Most of the moisture in the June case is concentrated along the east side of the mountains in central Norway, but there is moisture in the whole eastern Norway in general. Again, the area where the most moisture is concentrated is the area where the thunderstorms formed. In the August case, however, almost the whole country of Norway and Sweden is covered by values exceeding 0.017 kg/kg. The highest values are found along the border with Sweden.
Figure 3.39 shows the contrast in the humidity amount between the two cases, but is the specific moisture on 26th of June considered low just because it is lower than on 4th of August? To answer this question, the mean and the anomaly of the specific humidity is provided. According to Figure 3.41 the anomaly is almost the same in both cases for the area of Oslo - around 4-4.5 g/kg. But then why do the LAGRANTO figures show dry trajectories, and the TCWV maps show values much higher for the August case? The answer lies in the average of the period each date is compared to. The mean of 20 July to 19 August is approximately twice as high than the mean of 11 June to 11 July. As mentioned in the Introduction, August is wetter than June. So even though the anomaly is the almost the same in both cases, the air on June the 26th is still much drier. However, this higher than normal moisture amount on June the 26th was nonetheless crucial for the thunderstorm initiation.
Finally, based on the last six figures, it can be seen that the stability indices are highly affected by the moisture concentration. Most of the stability indices have their maxima at the same locations where the specific humidity maxima are found.

[1] http://www.eswd.eu/cgi-bin/eswd.cgi?lang=en_0\&lastquery=17383078164\&force_static_map=true;

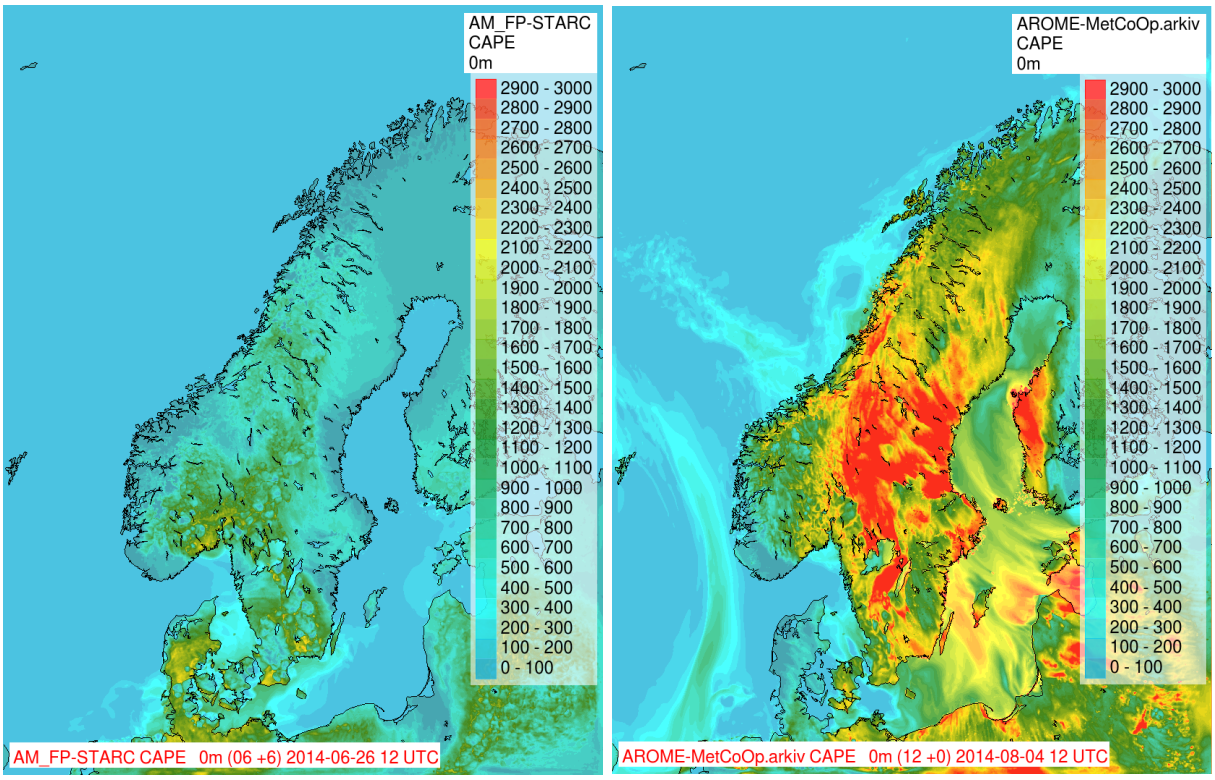

(a) 26th June 12 UTC (b) 04th August 12 UTC

Figure 3.33: Convective available potential energy

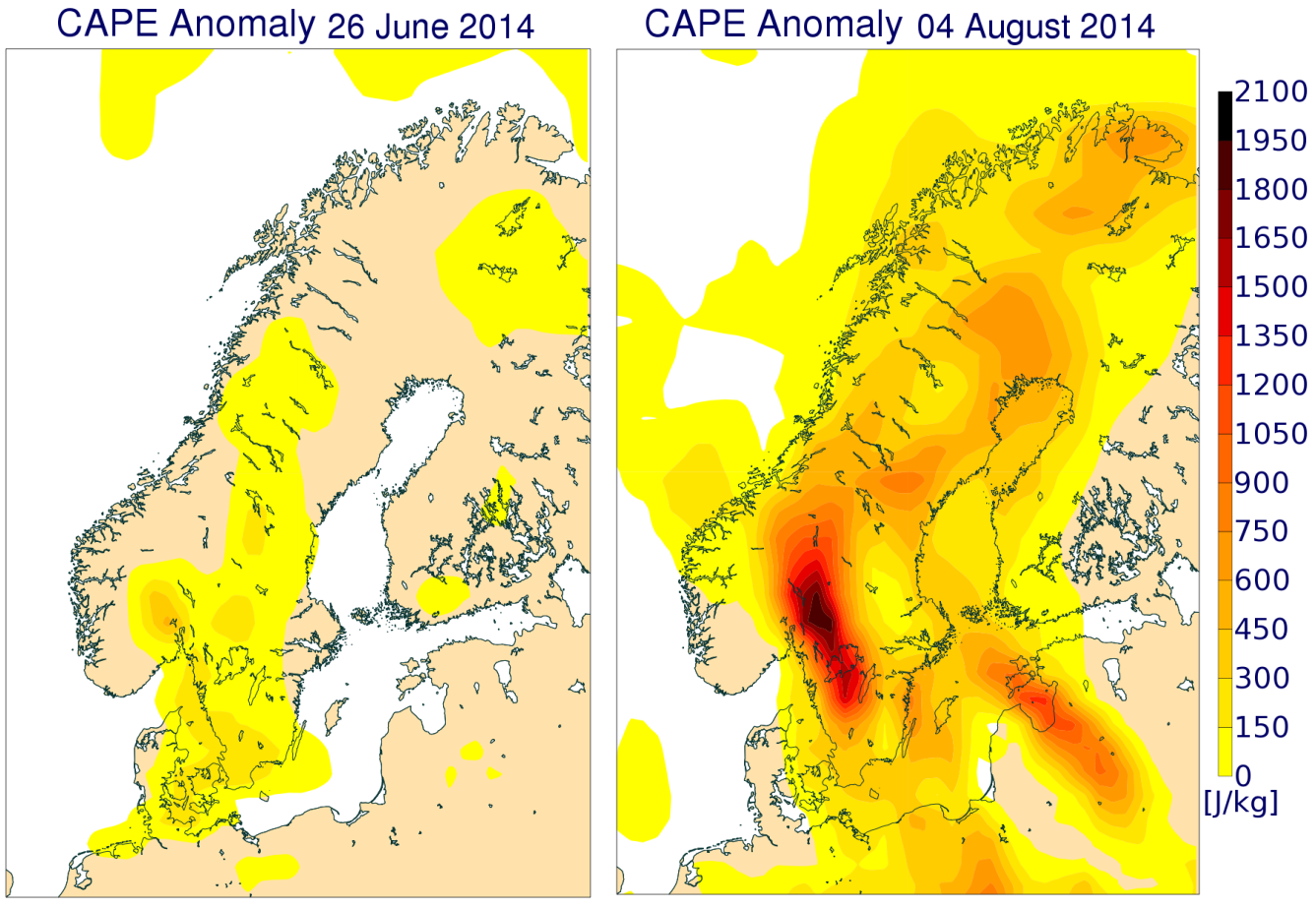

(a) 26 June 2014 06 & 18 UTC compared to 11 June - 11 July 1979-2015 (b) 4 August 2014 06 & 18 UTC compared to 20 July - 19 August 1979-2015

Figure 3.34: CAPE anomaly

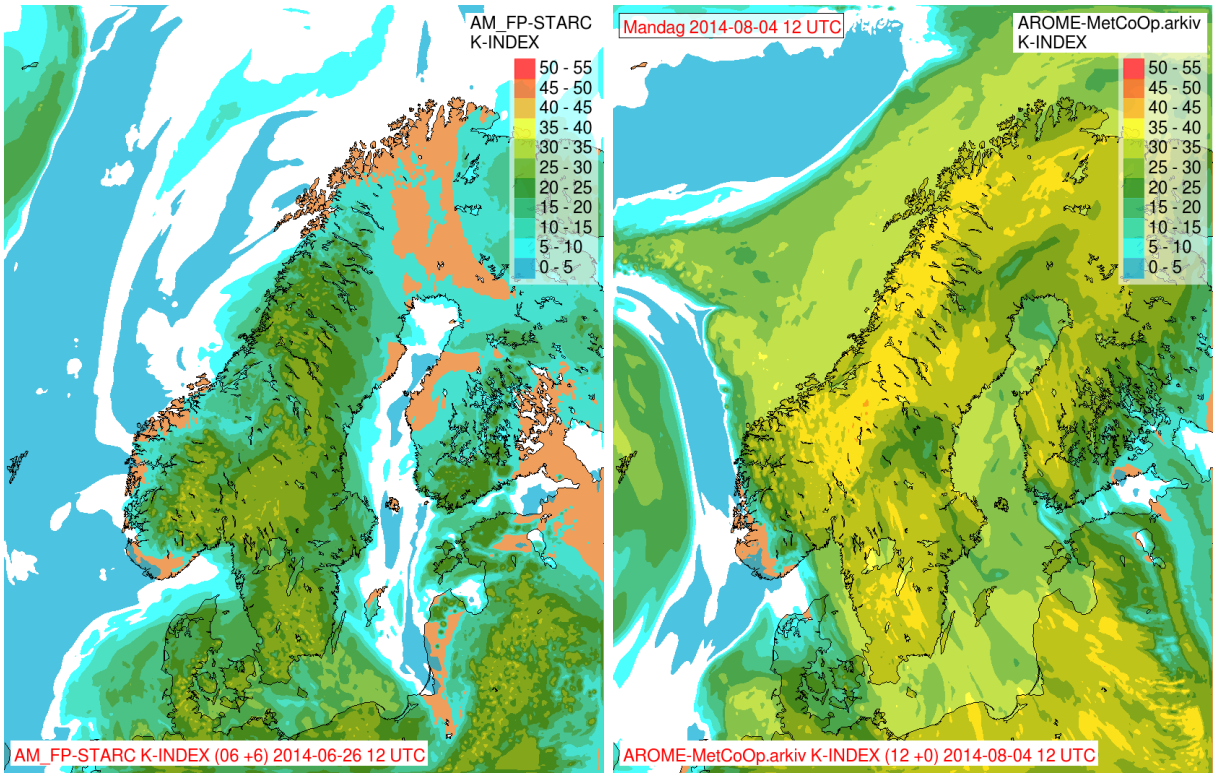

(a) 26th June 12 UTC (b) 04th August 12 UTC

Figure 3.35: K-index

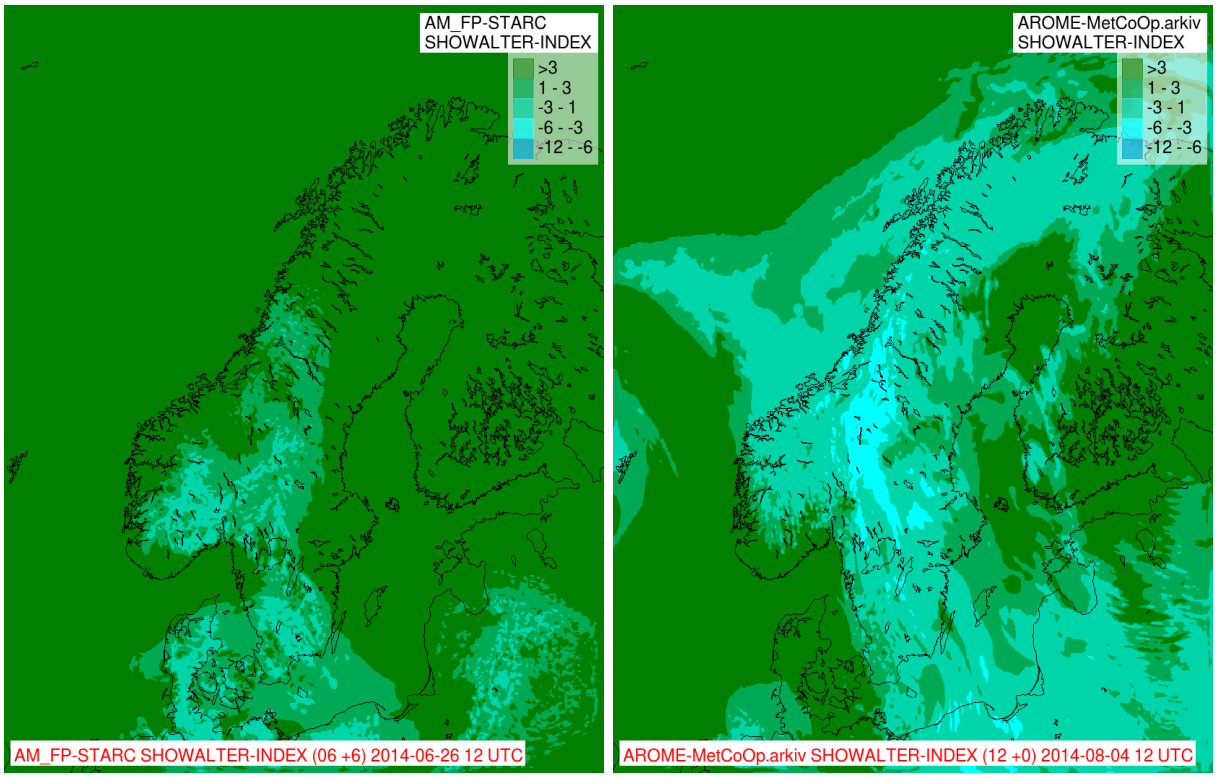

(a) 26th June 12 UTC (b) 04th August 12 UTC

Figure 3.36: Showalter stability index

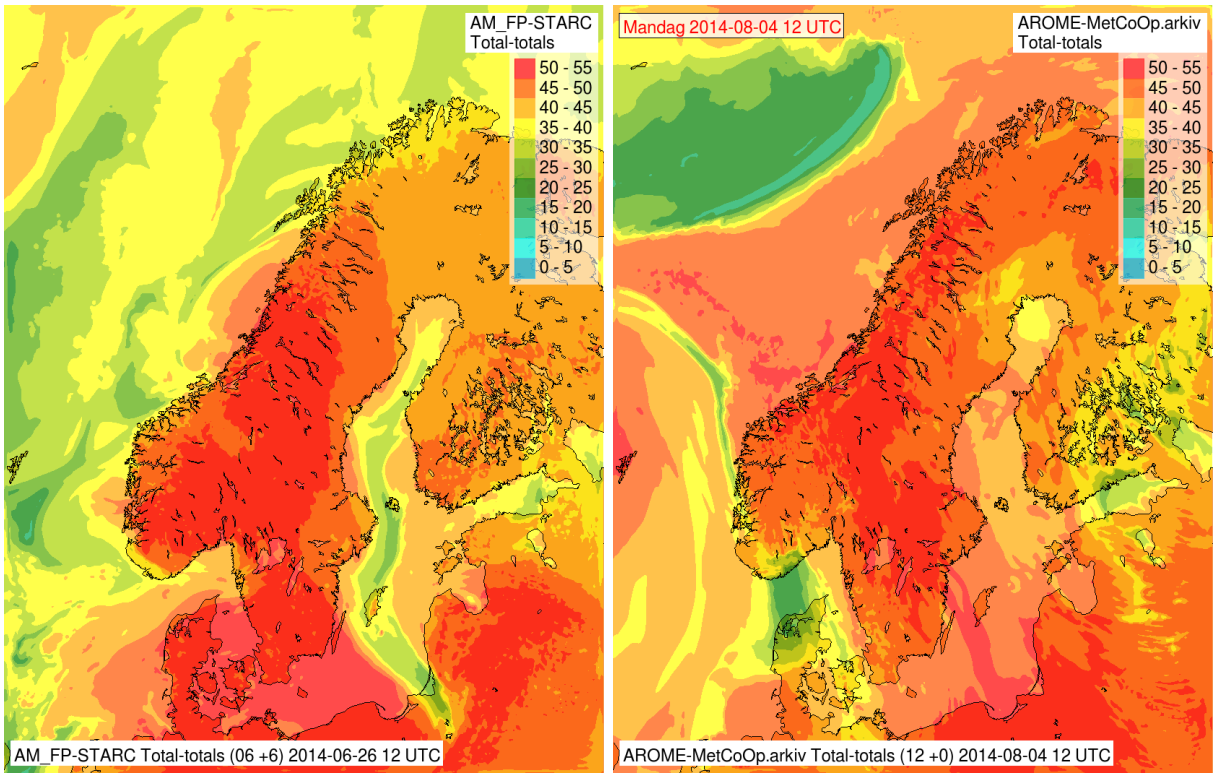

(a) 26th June 12 UTC (b) 04th August 12 UTC

Figure 3.37: Total totals

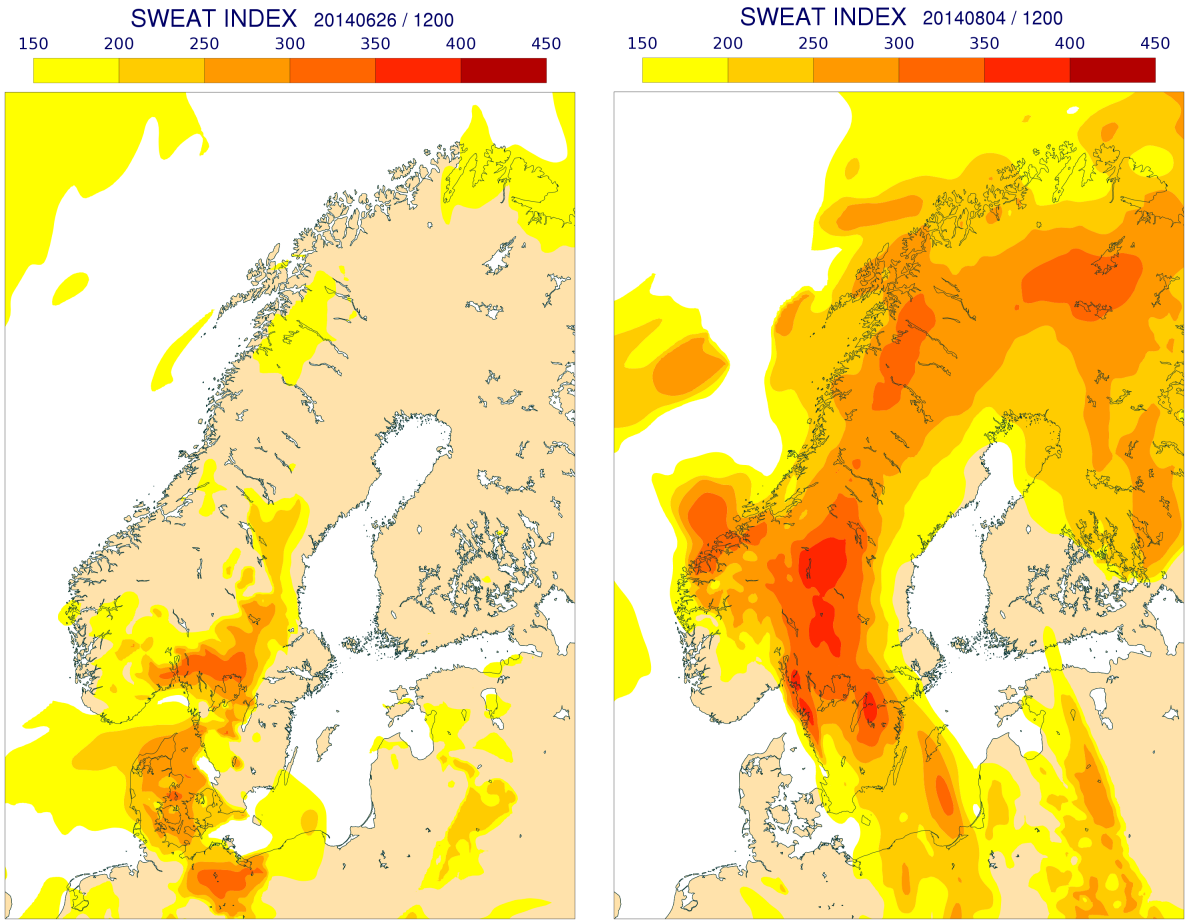

(a) 26th June 12 UTC (b) 04th August 12 UTC

Figure 3.38: Sweat Index

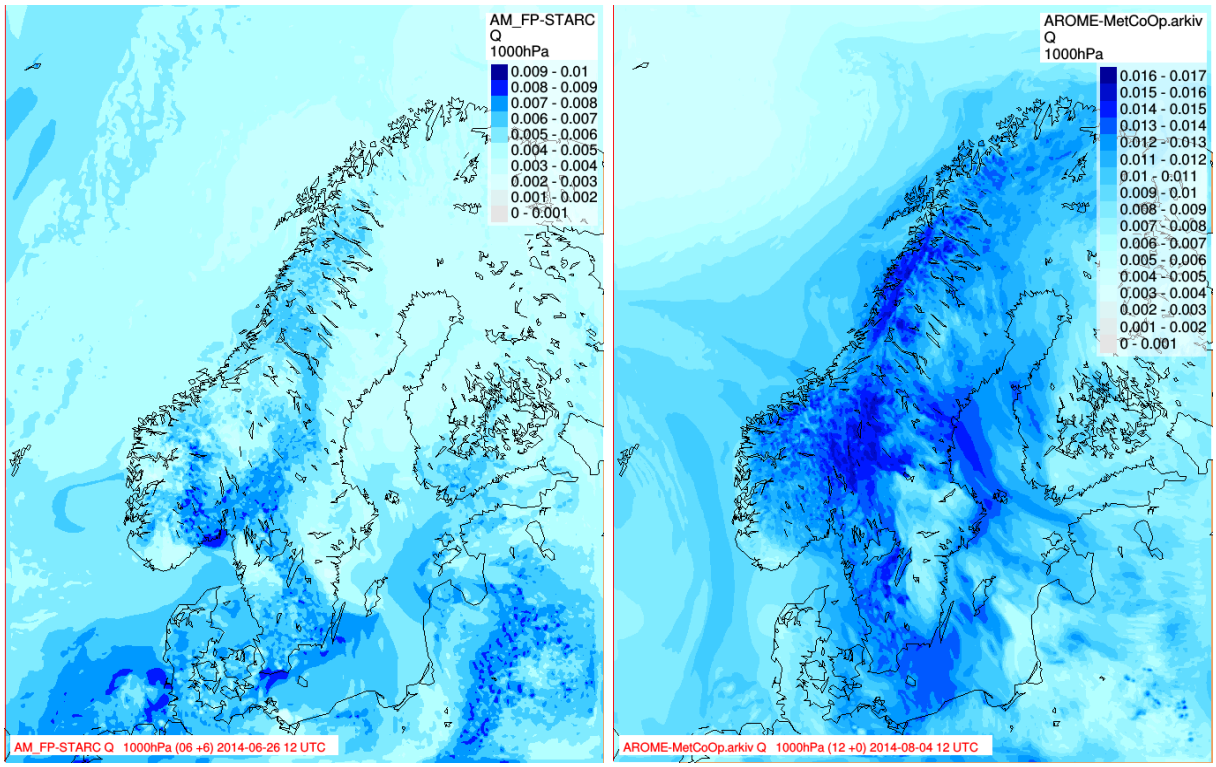

(a) 26th June 12 UTC (b) 04th August 12 UTC

Figure 3.39: Specific humidity at 1000 hPa. Units in kg/kg.

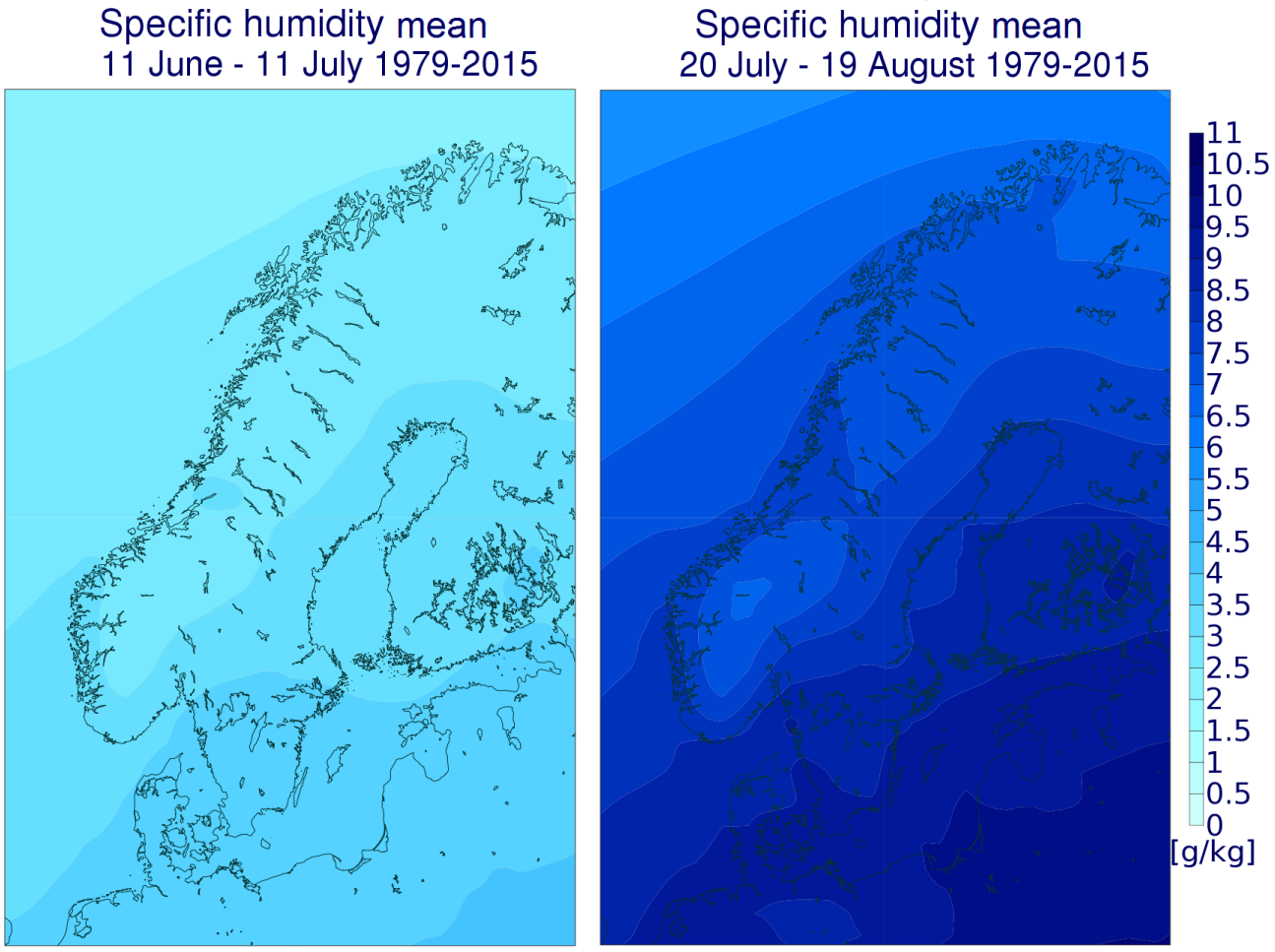

Figure 3.40: Specific humidity mean for 1979-2015 at 1000 hPa.

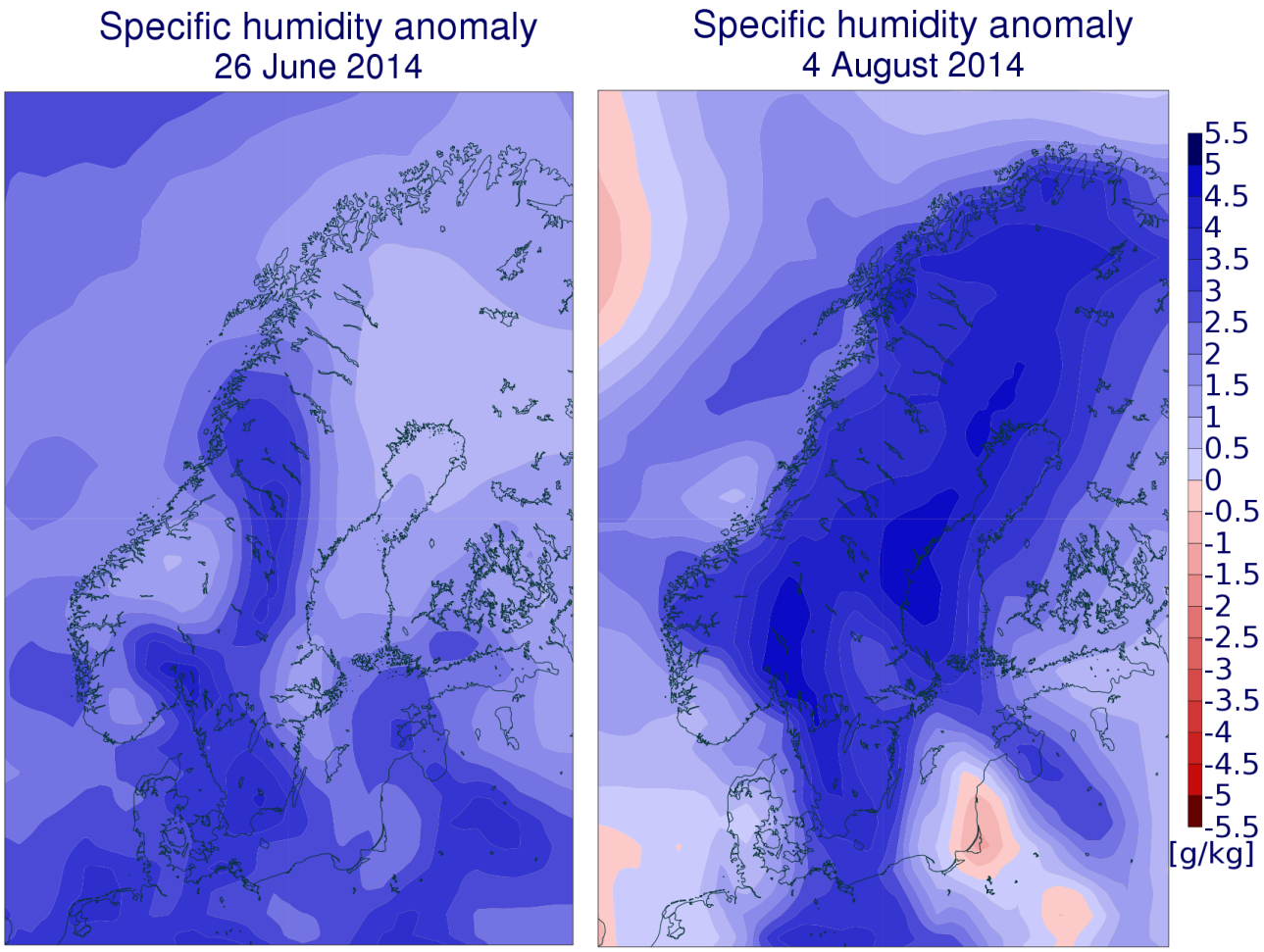

Figure 3.41: Specific humidity anomaly for 26 June and 4 August 2014 compared to 11 June-11 July and 20 July-19 August 1979-2015 respectively at 1000 hPa.

3.3.1 Analyzing the SWEAT Index

The SWEAT Index is, as already discussed, a stability index containing several parameters. So even though the SWEAT Index is larger in the August case that in June, the contributions to those values may come from different terms. Comparing the terms between the two cases may also explain the reason behind each thunderstorm formation.
The first term is 12 times dew point temperature at 850 hPa. For Figure 3.42a and 3.38b, the scale had to be different because of the values being so much larger in the August case. The values are expected. The cold troposphere in June resulted in low dewpoint temperature in contrast to the August case where the temperature was abnormally high and there was significant moisture advection into Scandinavia. However, the largest values in June are located in the areas where thunderstorms formed, so valuable information is provided in this case even with low values in general. For August, once again the largest values are seen where the most intense convection occurred.

The next term involves the TT index: $20(TT - 49)$ and the results are again expected based on

what we saw in Figure 3.37. The values of TT were bigger in June and this is again what is seen here in Figure 3.43. While TT values go up to 130 over Oslo in June, the values for August do not surpass 90 in Sweden. TT only reaches 30 closest to Oslo. The reason behind this, is the large temperature difference between the lower and and mid-troposphere, whereas in the August case the high temperatures reached high latitudes. The TT term is an indication of instability, so the atmosphere was much more unstable over eastern Norway in June (with the caveat that only two vertical levels are used to calculate TT).
The last two terms refer to the wind shear of the troposphere. The first term, $2f_{850} + f_{500}$, is the wind shear according to the speed change with height. However, the term is just the sum of the wind speed at 850 hPa and at 500 hPa, so it should be noted that it does not really tell us much about the vertical profile of the wind. However, it is known that the wind is always weaker in the boundary layer, so a large value of this term would mean an wind speed increase with height. This seems to be the case with August (see Figure 3.44b) due to the baroclinicity caused by the cold front. The lower values of Figure 3.44a are expected as it seems from the TCWV map in Figure 3.8 that the winds are quite weak and although stronger at 500 hPa (judging by the isobar width in Figure 3.7), they are still not strong enough to create large values of wind shear.

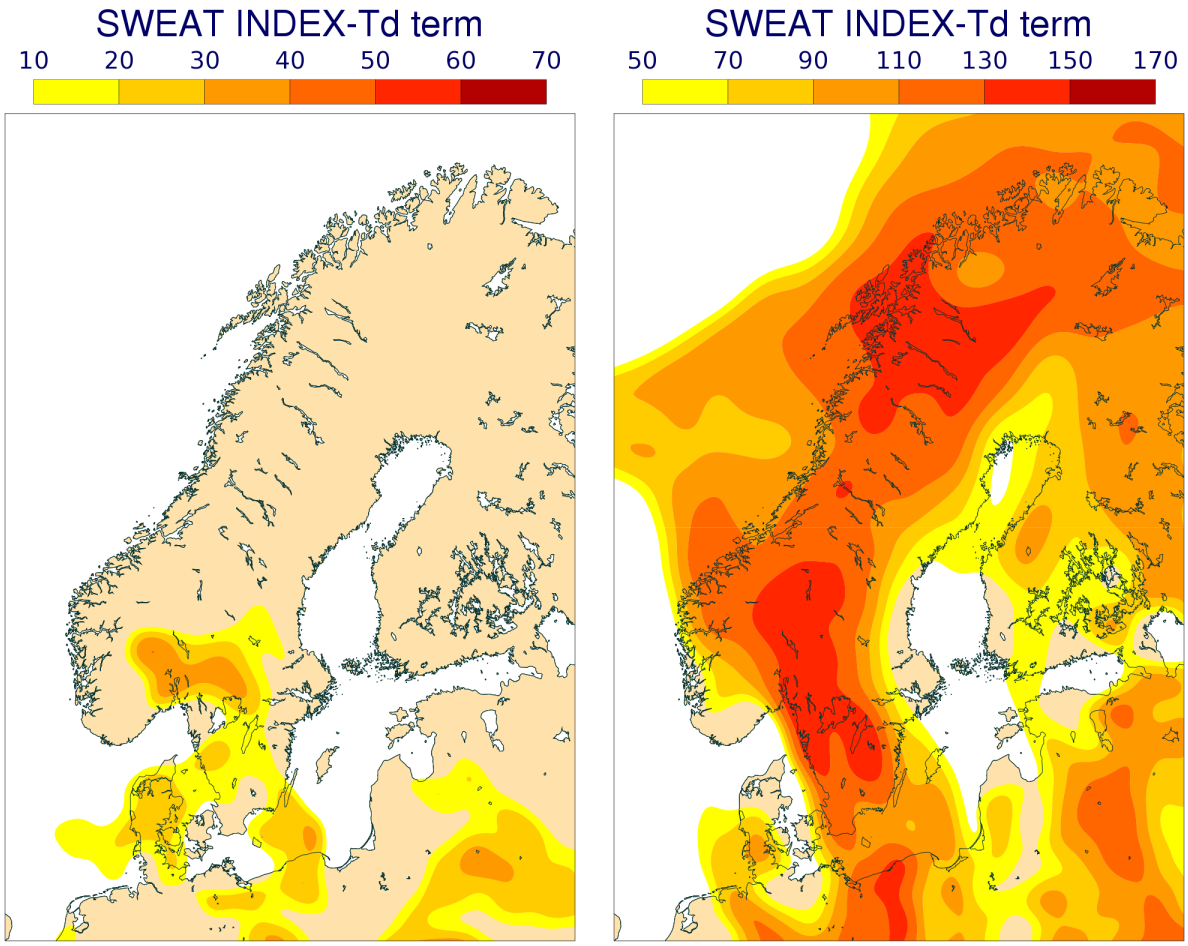

(a) 26th June 12UTC

(b) 04th August 12UTC

Figure 3.42: SWEAT Index - $12T_{d,850}$ (in °C), the term of the dewpoint temperature at 850 hPa providing information about moisture is plotted.

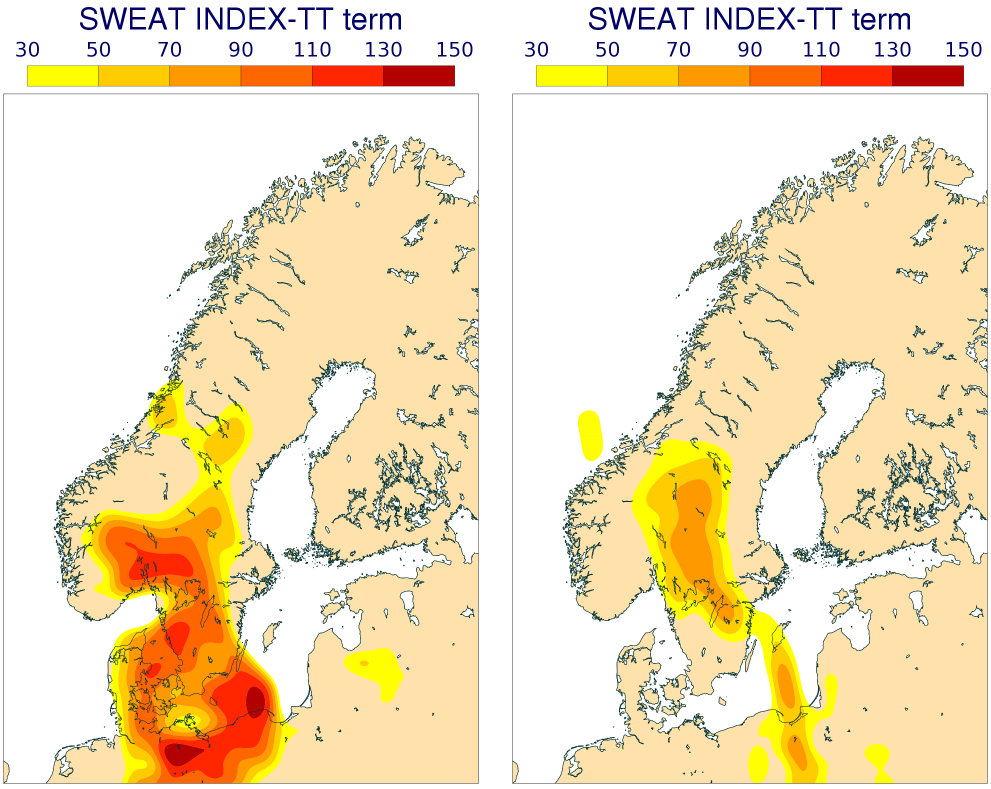

(a) 26th June 12UTC (b) 04th August 12UTC

Figure 3.43: SWEAT Index - $20(TT - 49)$ (in °C), the total totals-term providing information about the instability.

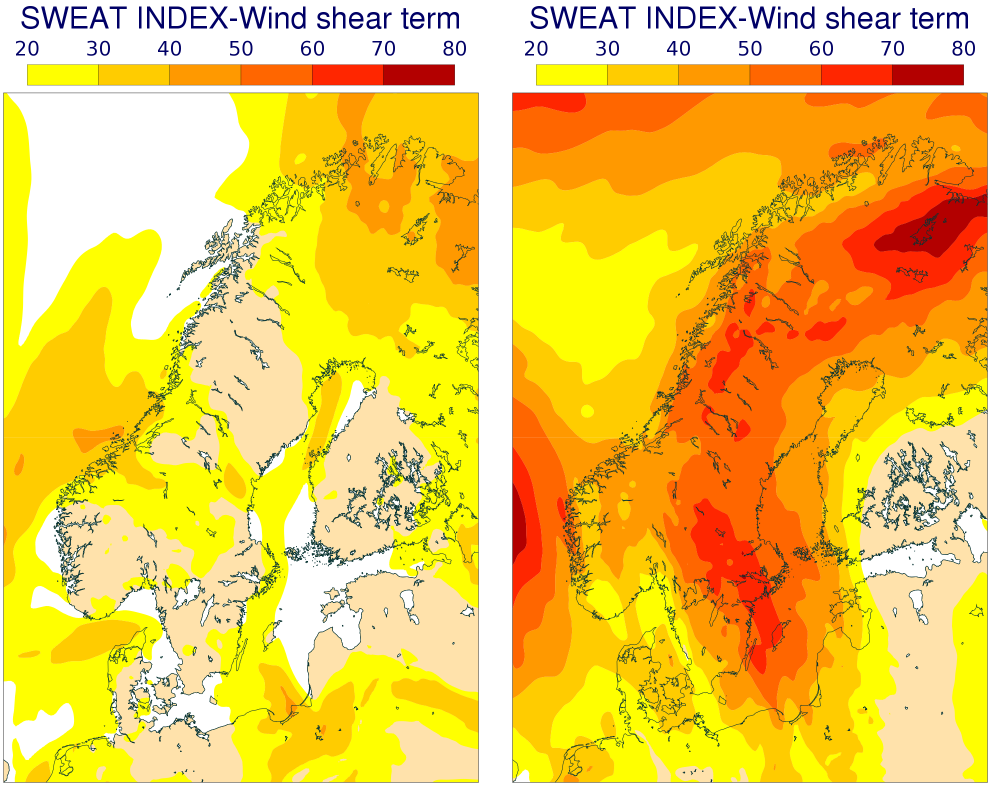

(a) 26th June 12UTC (b) 04th August 12UTC

Figure 3.44: SWEAT Index - $2f_{850} + f_{500}$ (in knots), the wind shear term, providing information about the wind speed change with height.

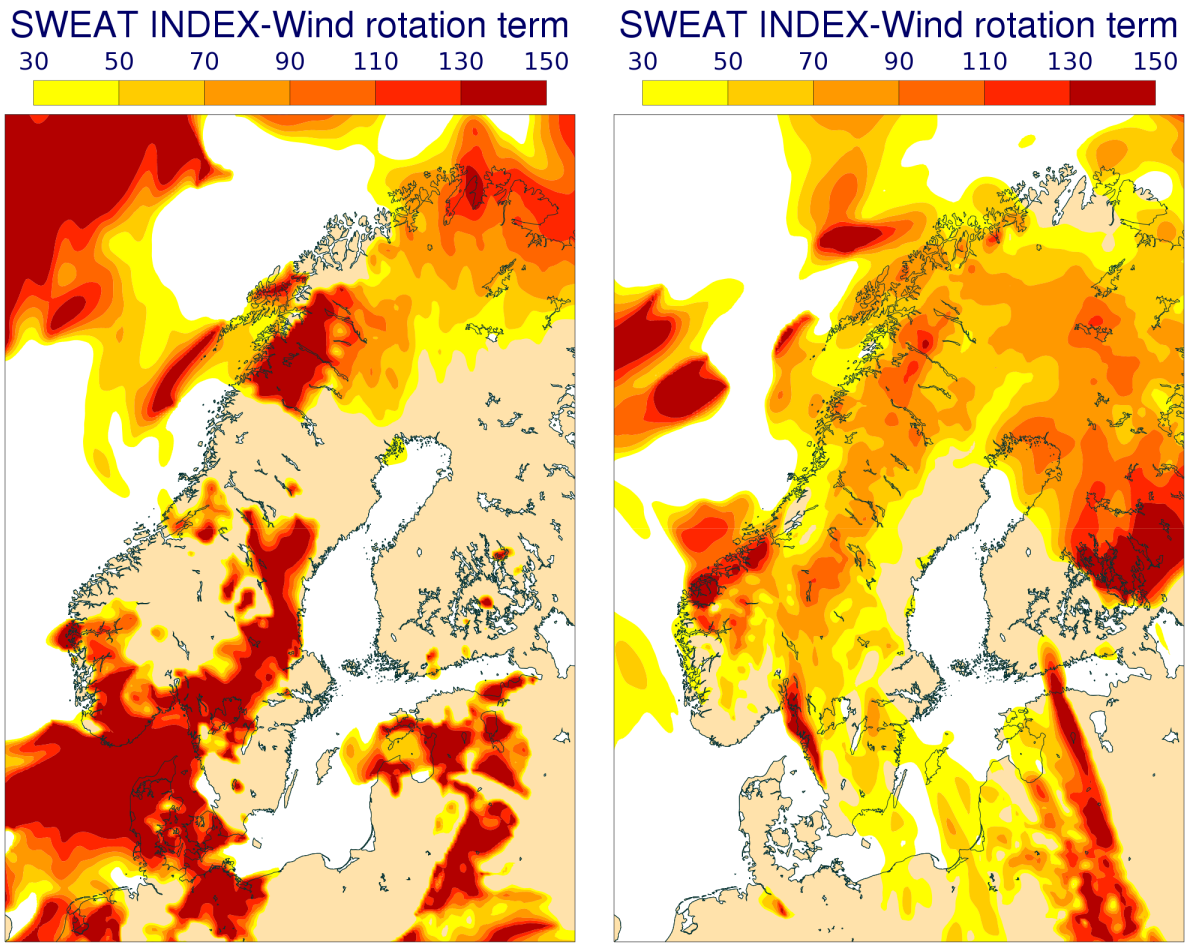

(a) 26th June 12UTC (b) 04th August 12UTC

Figure 3.45: Sweat Index - $125[sin(d_{500} - d_{850}) + 0.2]$, the wind shear rotation term, providing information about the change of the wind direction with height.

The term $125[sin(d_{500} - d_{850}) + 0.2]$ stands for the wind shear rotation. This term is important and needs to be large in order to have rotating updrafts. In Figure 3.45 it is seen that the values for the June case in general are much larger than in August, with the exception of the western Swedish coast, south of Oslo. Large values are expected when there is strong warm advection (veering of the wind), which is the case on August the 4th. The high values for June the 26th are certainly surprising, since no rotation was spotted in the radar images. However, weak low level winds can make this term sensitive as direction can change a lot over short distances.

3.4 Sea surface temperature

3.4.1 June

For June the 26th, it is found that the sea surface temperatures (SSTs) were anomalously large around Great Britain, Iceland up to Svalbard. West of Svalbard, where the trajectories closest to the area of deep convection originated, the sea is warmer than normal as well, but the anomaly is not as large. The trajectories then followed a path along the Norwegian coast, where the SST is at normal or lower than normal values. Finally, some of the trajectories had their paths over Skagerrak sea, which is more than 2°C warmer than normal. The Oslofjord's SST anomaly is 2°C above the mean. So if the SST did play any role in the thunderstorm formation, then it would be Skagerrak and the Oslofjord since both were warmer than normal and the trajectories did not get wetter until the last 48 hours.

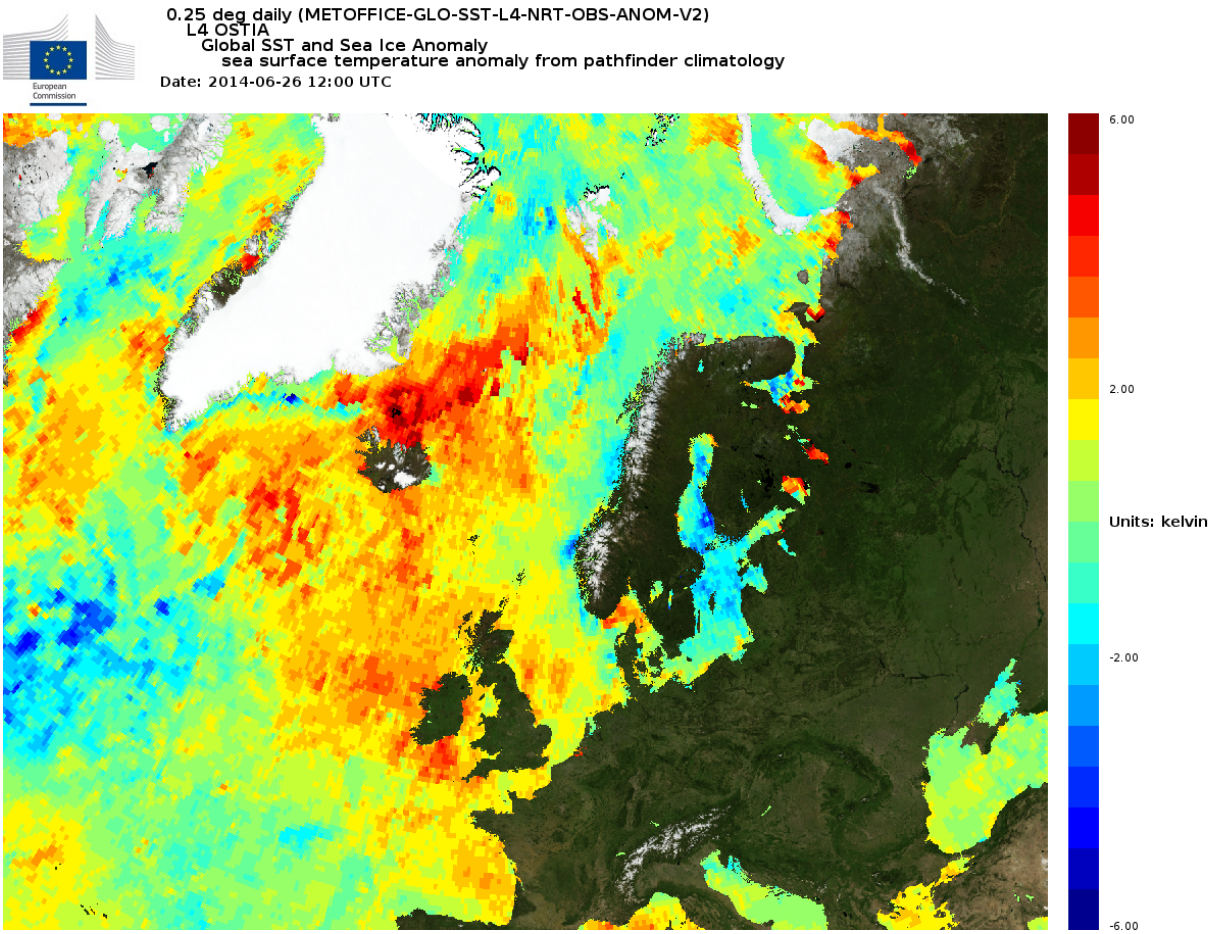

Figure 3.46: Sea surface temperature anomaly for 12 UTC 26 June 2014 compared to the same date in the period of 1985-2001.

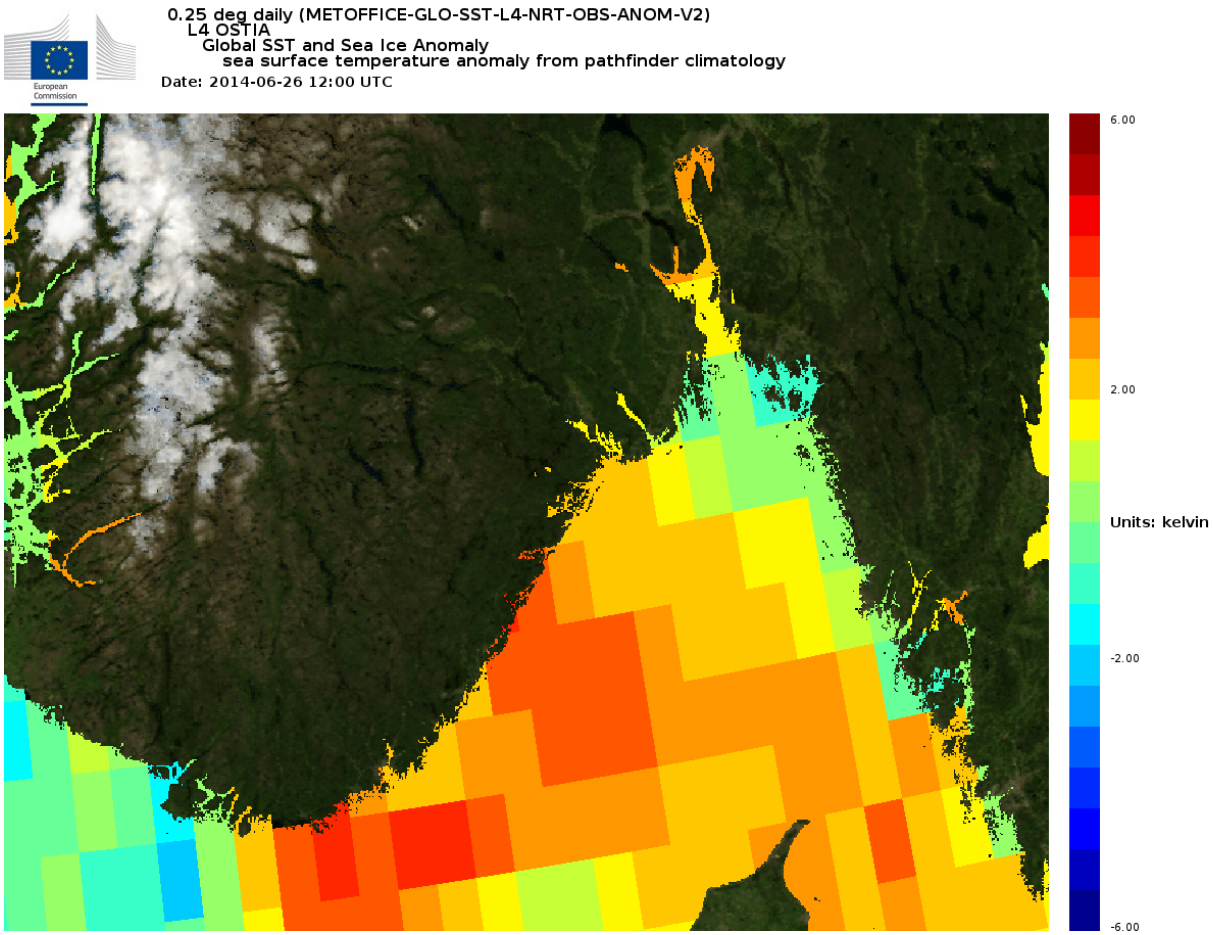

Figure 3.47: Sea surface temperature anomaly for 12 UTC 26 June 2014 compared to the same date in the period of 1985-2001.

3.4.2 August

The consistent days with extremely high temperatures in northern Europe during July led to large SST anomaly values in all seas around those regions. The SST anomaly on August the 4th is much higher than on June the 26th and there are values in the Baltic sea that even exceed 6°C as seen in Figure 3.48. Skagerrak is also abnormally warm, with SST anomaly reaching 4°C above normal. In this case, the SST must have played a bigger role than in June as the trajectories that perform a loop over the Baltic sea in Figure 3.28, immediately become wetter. Even though the trajectories indicate moist air over continental Europe as well, the high SSTs helped to increase the moisture even more in Scandinavia.

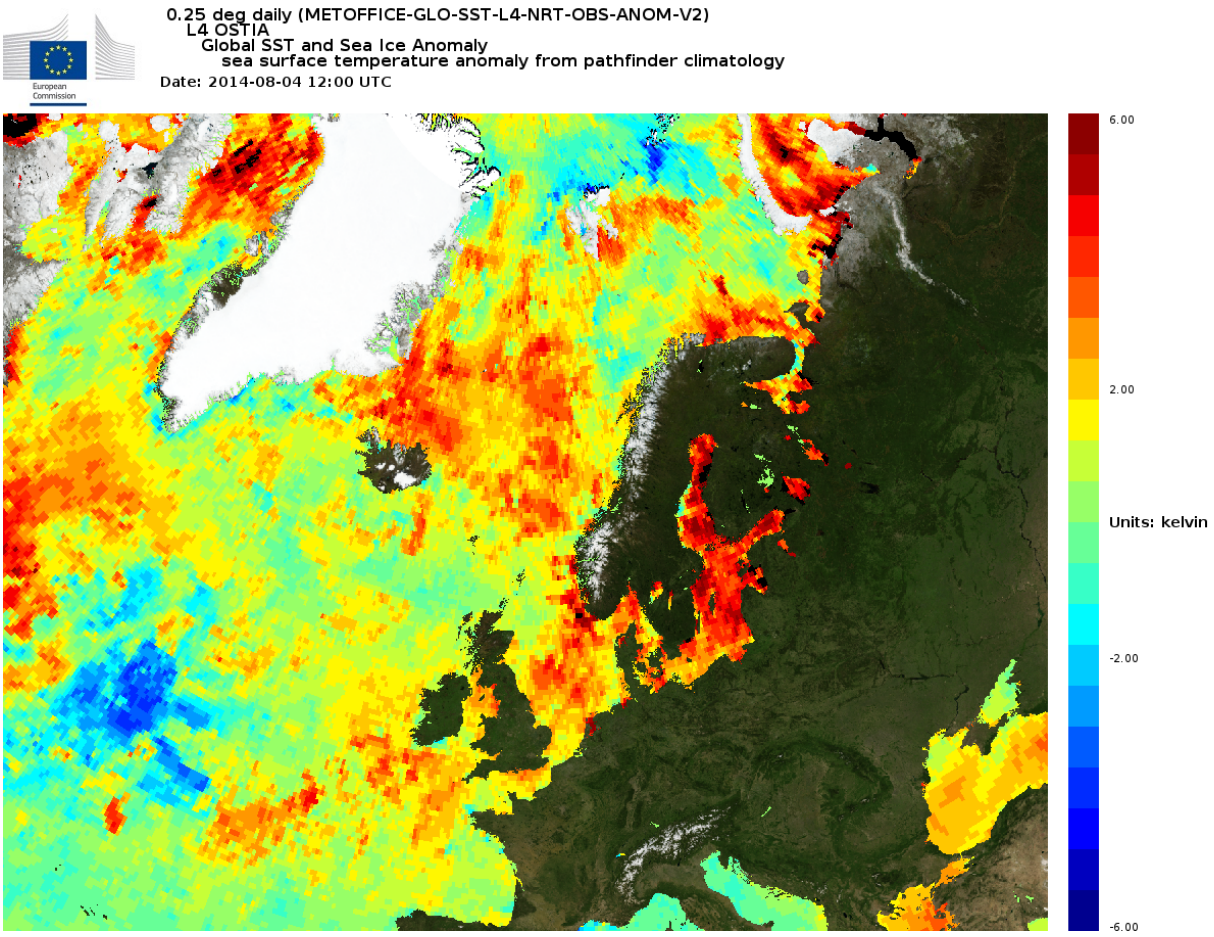

Figure 3.48: Sea surface temperature anomaly for 12 UTC 4 August 2014 compared to the same date in the period of 1985-2001.

Chapter 4

Summary and concluding remarks

4.1 June

4.1.1 Large scale flow

The main characteristic of the weather situation in the June case is the domination of low pressure east of Norway in combination with higher pressure to the west, a consistent pattern throughout the period. This pattern led to northerly winds and cold air advection over Norway through the depth of the troposphere. The result was a suppressed tropopause (cold anomaly) over Scandinavia on 26 June. In conjunction with surface heating, a large vertical temperature lapse rate in the region of observed deep convection emerged, providing large amounts of available potential energy for deep convection. These features are confirmed via a Lagrangian backward trajectory analysis, showing air parcels originating from the polar regions, moving southward and warming at low levels proceeding the event.

4.1.2 The necessary ingredients

As stated in the introduction, the necessary ingredients for deep convection can be succinctly defined as: i) a sufficiently moist and deep layer in the low or mid atmosphere, ii) conditional instability, and iii) a triggering mechanism to raise air parcels to the level of free convection. Given the analyses and results presented in Chapter 3, we can assess these ingredients for the 26 June case.

Moisture: The moisture content is relatively low for a case of extreme precipitation. With that said, there is a maximum of low level moisture in the region deep convection ensued. This can be seen in maps of low level specific humidity and in the analysis of the individual terms of the SWEAT index. In addition, the backward trajectories identified low-level moistening over the 24 hours before the event.

Conditional Instability: the stability indices examined confirm the existence of instability on the day of the event, all indicating the possibility for deep convection. The primary component leading to said instability appears to be a steep temperature lapse rate resulting from cold air aloft and surface heating, both serving to increase the environmental lapse rate.

Triggering Mechanism: There is no obvious large scale triggering mechanism (i.e. frontal boundary, orographic lifting, low-level convergence). In the absence of such features, all that remains is surface heating leading to a positively buoyant air parcel near the surface (i.e. a typical afternoon thunderstorm).

Given these facts, we hypothesize the combination of a local maximum in moisture content (albeit of small magnitude), a steep lapse rate and surface heating combined to generate positively buoyant air parcels throughout the depth of the troposphere (taking advantage of the large observed conditional instability).

4.2 August

4.2.1 Large scale flow

As previously stated, the large scale situation in the August case was significantly different than that for June. Surface temperatures were anomalously high over the period, and the synoptic scale flow pattern resulted in significant warm, moist air advection into the region of interest. Additionally, there was the presence of baroclinicity (i.e. a surface frontal boundary). The result was an elevated tropopause over Scandinavia and the presence of a low level thermal boundary. The Lagrangian backward trajectories confirm the significant warm, moist advection, identifying two distinct streams of air converging on the region of ensuing deep convection. One 'group' of trajectories originate over the Atlantic ocean and another with trajectories from central Europe, the Balkans and far east of Ukraine both of them carrying moisture towards Scandinavia.

4.2.2 The necessary ingredients

An assessment of the necessary ingredients for the August case follows.

Moisture: The moisture content is large over the area of interest, as observed in the TCWV and specific humidity fields.

Conditional Instability: as seen from the stability analysis, the conditional instability was extremely high for the August case. In contrast to June, it can be argued a main contributor to the conditional instability is the presence of a deep layer of enhanced moisture content.

Triggering Mechanism: The presence of a frontal boundary likely played an integral role in generating convective cells. However, it should be mentioned that the presence of deep convection prior to reaching the Oslo area and the long-lived nature of the organized convection (over 15 hours and larger than the south-north length of Norway) argues for mesoscale convective dynamics leading to the generation of new deep convective cells. The likelihood of these processes are emphasized via the stability indices analysis (particularly, the SWEAT index which includes wind field characteristics).

In contrast to the June case, the August event is fairly easily diagnosed via the above assessment. All criteria were met and were highly anomalous in terms of their magnitude.

4.3 The Utility of Stability Indices

The stability indices are used as thunderstorm predictors, but the predictability skill of each index can vary. In general, it is argued to not rely solely on any single index but many in conjunction, supplemented via a synoptic and mesoscale analysis of the weather situation (as the atmosphere will evolve over time).
CAPE proved to be a good predictor for both cases. A better predictor than CAPE itself for the two events proved to be the anomaly of CAPE. The maximum values of CAPE in both cases coincide with the locations of the strongest convective cells at that time. The utility of anomaly values has been shown in previous studies over Europe Graf *et al.*, 2011.
The K-index does capture the instability, but the regions with large values are almost too wide and K-index is not as successful in locating the regions with the most intense thunderstorms. It should be reminded though, that K-index is mostly suitable for identifying regions where heavy rainfalls are likely to occur rather than severe thunderstorms. The higher values in the August case are most likely due to the high values of moisture reaching higher up in the troposphere than in June. The Showalter index provided similar results .
As previously mentioned, the TT index is the only index found to be larger and for a wider region in the June case than in the August case. High temperature and dewpoint temperature result in a high TT like in August, but a major contribution is a low 500 hPa temperature as well. So with the temperature being almost twice as low at 500 hPa in the June case, the resulted TT is higher as well. It is a correct prediction by TT of higher instability in the June case than in the August case, but in this case higher TT did not mean more intense thunderstorms.
Finally, the SWEAT index also provided accurate thunderstorm prediction. On 26 June, the thunderstorms affected the area west and east of Oslo which is where the SWEAT index was at its maximum. The SWEAT index for the August case is even more accurate, with thunderstorms developing everywhere where the SWEAT index is above 150 and the most severe of them forming where the SWEAT index is the largest. Even the maximum values along the western Swedish coast coincide with the path of the cell that affected the eastern parts of Oslo that day.

To summarize, all stability indices had a predictive skill of the thunderstorm activity for both cases. Though out of all, the SWEAT index seems to be the best thunderstorm predictor. CAPE was also among the most successful indices and its anomaly proved an even better indication of the phenomena that occurred that day.

4.4 Concluding remarks

In a country where severe thunderstorms are rare, 2014 was a record breaking year with thunderstorm activity that not only was frequent, but lasted from spring to mid autumn. The thunderstorm season of 2014 was more reminiscent of the convective storm season in the southern parts of Europe in terms of intensity, longevity and frequency.

This study focused on two storms that impacted the greater Oslo area. While both were intense, their characteristics were found to be drastically different in terms of the large scale patterns that preconditioned the environment for deep convection and the time and spatial scales of the convective systems themselves. Yet, even given their differences, the combination of a synoptic scale analysis, the calculation of Lagrangian trajectories and an examination of local scale convective stability indices provided great insight into not only their formation but their observed structure

and evolution.

Understanding the dynamical processes leading to deep convection at high latitudes is integral to accurate prediction and damage mitigation. It is hoped this study provides a modicum of insight and useful knowledge on a topic that is of great interest to a wide spectrum of parties, including academics, operational forecasters, community managers and the general public who ultimately feels the brunt of damaging storms.

4.5 Future work

While admittedly limited in scope, it is believed the study results provide a foundation for significant future work.

A study of larger scope in terms of the study period and number of events would be advantageous. For example, the stability index analyses contained herein provided illuminating information regarding the formation and evolution of the events. Would these results prove to be robust in a more typical year?

An obvious extension is the use of a high-resolution numerical weather prediction model to simulate events. Such data would be invaluable to a better understanding of the importance of small scale dynamical processes. In addition, the successful simulation of observed events allows for so-called sensitivity studies wherein environmental characteristics such as SSTs, moisture content and baroclinicity can be modified to quantify impacts.

Finally, it is accepted that the climate is warming and that the largest warming is occurring at high latitudes. What would be the effect on the formation and characteristics of deep convection at these latitudes to warmer temperatures, higher SSTs and larger amounts of moisture? It is a fascinating question to ponder.

Bibliography

Berrisford, P, Dee, D, Poli, P, Brugge, R, Fielding, K, Fuentes, M, Kallberg, P, Kobayashi, S, Uppala, S, & Simmons, A. 2011. The ERA-Interim archive Version 2.0, ERA Report Series 1, ECMWF, Shinfield Park. *Reading, UK*, **13177**.

Brooks, Harold E. 2009. Proximity soundings for severe convection for Europe and the United States from reanalysis data. *Atmospheric Research*, **93**(1), 546–553.

Danevig, Petter. 1969. *Flymeteorologi*. H. Aschehoug & co (W. Nygaard).

Dee, DP, Uppala, SM, Simmons, AJ, Berrisford, Paul, Poli, P, Kobayashi, S, Andrae, U, Balmaseda, MA, Balsamo, G, Bauer, P, *et al.* 2011. The ERA-Interim reanalysis: Configuration and performance of the data assimilation system. *Quarterly Journal of the royal meteorological society*, **137**(656), 553–597.

Donlon, Craig J, Martin, Matthew, Stark, John, Roberts-Jones, Jonah, Fiedler, Emma, & Wimmer, Werenfrid. 2012. The operational sea surface temperature and sea ice analysis (OSTIA) system. *Remote Sensing of Environment*, **116**, 140–158.

Doswell III, CHARLES A, & Schultz, David M. 2006. On the use of indices and parameters in forecasting severe storms. *Electronic J. Severe Storms Meteor*, **1**(3), 1–22.

EUMETSAT. 2015a. *The 0 degree image service is the main mission of Meteosat Second Generation (MSG)*. `http://www.eumetsat.int/website/home/Data/MeteosatServices/0DegreeService/index.html`.

EUMETSAT. 2015b. *Meteosat Second Generation (MSG) provides images of the full Earth disc, and data for weather forecasts*. `http://www.eumetsat.int/website/home/Satellites/CurrentSatellites/Meteosat/index.html`.

George, J. J. 1960. *1960: Weather Forecasting for Aeronautics*.

Graf, Michael A, Sprenger, Michael, & Moore, Richard W. 2011. Central European tornado environments as viewed from a potential vorticity and Lagrangian perspective. *Atmospheric Research*, **101**(1), 31–45.

Haklander, Alwin J, & Van Delden, Aarnout. 2003. Thunderstorm predictors and their forecast skill for the Netherlands. *Atmospheric Research*, **67**, 273–299.

Huntrieser, H, Schiesser, HH, Schmid, W, & Waldvogel, A. 1997. Comparison of traditional and newly developed thunderstorm indices for Switzerland. *Weather and Forecasting*, **12**(1), 108–125.

Information, E.U. Copernicus Marine Service. 2012. *GLOBAL OCEAN OSTIA SEA SURFACE TEMPERATURE AND SEA ICE ANALYSIS.* http://marine.copernicus.eu/services-portfolio/access-to-products/?option=com_csw&view=details&product_id=SST_GLO_SST_L4_NRT_OBSERVATIONS_010_001.

Johns, Robert H, & Doswell III, Charles A. 1992. Severe local storms forecasting. *Weather and Forecasting*, **7**(4), 588–612.

Kaltenböck, Rudolf, Diendorfer, Gerhard, & Dotzek, Nikolai. 2009. Evaluation of thunderstorm indices from ECMWF analyses, lightning data and severe storm reports. *Atmospheric Research*, **93**(1), 381–396.

Lawrence, Mark G. 2005. The relationship between relative humidity and the dewpoint temperature in moist air: A simple conversion and applications. *Bulletin of the American Meteorological Society*, **86**(2), 225–233.

Lindgren, Hilde Martine, Boyesen, Britt, Rivrud, Kristin, & Olsson, Svein Vestrum. 2014 (October 10). *Mange branner etter lynnedslag i natt.* NRK. https://www.nrk.no/telemark/branner-og-strombrudd-etter-uvaer-1.11978322.

López, Laura, Marcos, José Luis, Sanchez, Jose Luis, Castro, Amaya, & Fraile, Roberto. 2001. CAPE values and hailstorms on northwestern Spain. *Atmospheric research*, **56**(1), 147–160.

McLaren, A, Fiedler, E, Roberts-Jones, J, Martin, M, Mao, C, & Good, S. 2016. QUALITY INFORMATION DOCUMENT Global Ocean OSTIA Near Real Time Level 4 Sea Surface Temperature Product.

MetEd. 2014. *Skew-T Mastery.* https://www.meted.ucar.edu/mesoprim/skewt/navmenu.php?tab=2&page=1.0.0.

Miller, Robert C. 1967. *Notes on analysis and severe-storm forecasting procedures of the Military Weather Warning Center.* Air Weather Service (MAC), United States Air Force.

Miller, Robert C, Bidner, A, & Maddox, RA. 1971. The use of computer products in severe weather forecasting (the SWEAT index). *Pages 1–6 of: Preprints 7th Conf. Severe Local Storms.*

Müller, Malte, Homleid, Mariken, Ivarsson, Karl-Ivar, Køltzow, Morten AØ, Lindskog, Magnus, Midtbø, Knut Helge, Andrae, Ulf, Aspelien, Trygve, Berggren, Lars, Bjørge, Dag, *et al.* 2017. AROME-MetCoOp: A Nordic Convective-Scale Operational Weather Prediction Model. *Weather and Forecasting*, **32**(2), 609–627.

Olsson, Svein Vestrum, & Stensholt, Anette Dotseth. 2014 (October 10). *Meteorolog: – Lynnedslagene et klimasignal.* NRK. https://www.nrk.no/norge/meteorolog_-_-lynene-et-klimasignal-1.11978609.

Peppler, Randy A. 1988. *A review of static stability indices and related thermodynamic parameters.* Tech. rept. Illinois State Water Survey.

Reitan, Harald. 2005. *Været i Norge.* Tun Forlag AS.

Riemann-Campe, Kathrin, Fraedrich, Klaus, & Lunkeit, Frank. 2009. Global climatology of convective available potential energy (CAPE) and convective inhibition (CIN) in ERA-40 reanalysis. *Atmospheric Research*, **93**(1), 534–545.

Romero, Romualdo, Gayà, Miquel, & Doswell, Charles A. 2007. European climatology of severe convective storm environmental parameters: A test for significant tornado events. *Atmospheric Research*, **83**(2), 389–404.

Sánchez, José Luis, Marcos, José Luis, Dessens, Jean, López, Laura, Bustos, Carlos, & García-Ortega, Eduardo. 2009. Assessing sounding-derived parameters as storm predictors in different latitudes. *Atmospheric Research*, **93**(1), 446–456.

Schultz, Paul. 1989. Relationships of several stability indices to convective weather events in northeast Colorado. *Weather and forecasting*, **4**(1), 73–80.

Showalter, Albert Kenneth. 1953. A stability index for thunderstorm forecasting. *Bull. Amer. Meteor. Soc*, **34**(6), 250–252.

SINTEF. 2014 (November 10). *Rekordår for lynregistreringen.* `http://www.sintef.no/siste-nytt/rekordar-for-lynregistreringen1/`.

SINTEF. 2015 (January 27). *Nok en lynrekord.* `http://www.sintef.no/siste-nytt/nok-en-lynrekord/`.

Sprenger, Michael, & Wernli, H. 2015. The LAGRANTO Lagrangian analysis tool–version 2.0. *Geoscientific Model Development*, **8**(8), 2569–2586.

Van Zomeren, Jeroen, & Van Delden, Aarnout. 2007. Vertically integrated moisture flux convergence as a predictor of thunderstorms. *Atmospheric research*, **83**(2), 435–445.

Wallace, John M, & Hobbs, Peter V. 2006. *Atmospheric science: an introductory survey.* Vol. 92. Academic press.